The Processing of Aerosol Particles and Soluble Trace Gases by Radiation Dogs in Fresno, California

by
Sarah B. Youngster

Department of Atmospheric Science
Colorado State University
Fort Collins, Colorado

August 2005

Colorado State University

Department of Atmospheric Science

Paper No. 760

Abstract

THE PROCESSING OF AEROSOL PARTICLES AND SOLUBLE TRACE GASES BY RADIATION FOGS IN FRESNO, CALIFORNIA

A radiation fog field campaign was conducted during the winter of 2003-2004 in Fresno, California. The purpose of this study was to gain more information about the chemical composition of these fogs, as well as their role in processing atmospheric aerosol in California's San Joaquin Valley (SJV).

These SJV radiation fogs had high pH values, above 6, due to large atmospheric concentrations of water-soluble ammonia. The dominant contributors to SJV fog composition include ammonium, nitrate, sulfate, nitrite, acetate, formate, formaldehyde, glyoxal, and methyl glyoxal. Significant differences were observed between the composition of small and large fog drops. The pH values were higher in the large drops. Small drops contain higher concentrations of ammonium, sulfate, nitrate, and organic carbon, but the large drops contain higher concentrations of nitrite.

Scavenging of atmospheric fine particles and soluble trace gases by fog droplets, followed by drop deposition to the ground, removes large amounts of ammonium, nitrate, sulfate, and organic carbon from the atmosphere. Deposition velocities for ammonium, nitrate, sulfate, nitrite, and organic carbon were observed to be on the order of 3 cm s^{-1}. The deposition velocities of these solutes were observed to be slightly lower than the deposition velocity of fog water itself. This pattern results from enrichment of these

species in smaller fog drops that settle more slowly and the dominance of sedimentation as a drop deposition mechanism in environments with low wind speeds and low surface roughness. The deposition velocity of nitrite was typically higher than fog water, due to its enrichment in larger, faster settling droplets. Wet deposition by fog water may deposit solute species 10 to 100 times more quickly than dry deposition alone. Typical reductions in boundary layer concentrations of organic carbon, nitrate, sulfate, and ammonium due to fog deposition were estimated to be of the order of 1 $\mu g\ m^{-3}\ hr^{-1}$.

ACKNOWLEDGMENTS

I would like to thank my advisor, Dr. Jeffrey L. Collett, Jr., for his constant guidance and assistance throughout the course of this project.

I am also grateful to my other committee members, Dr. Sonia M. Kreidenweis and Dr. John Volckens, for asking the tough questions and providing insightful comments for this work.

I would like to thank Dr. Pierre Herckes and Taehyoung Lee for their extensive contributions during the field campaign and the subsequent sample analysis. Further support was given by Andy Simpson during the field project and Hui Chang, Guenter Engling, and Courtney Gorin during sample analysis.

I would also like to thank my friends and family, especially Kyle, who offered invaluable support as I trudged through the writing process.

Funding for this project was provided by the National Science Foundation (ATM-0222607).

TABLE OF CONTENTS

LIST OF FIGURES

LIST OF TABLES

List of Symbols

(includes regularly used acronyms and notation)

Symbol	meaning
CAC	combined amino compounds
CASCC	Caltech Active Strand Cloudwater Collector
CCN	cloud condensation nuclei
CRPAQS	California Regional Particulate Air Quality Study
Da	Daltons (i.e., g mol^{-1})
D_{eff}	effective diameter (μm)
DI	deionized
DNPH	2,4-dinitrophenylhydrazine
DOC	dissolved organic carbon
DON	dissolved organic nitrogen
FAC	free amino compounds
HCHO	formaldehyde
Hi-Vol	high-volume aerosol sampler
HMS	hydroxymethanesulfonate

HONO	nitrous acid
HPAEC-PAD	high performance anion exchange chromatography with pulsed amperometric detection
HPLC	high performance liquid chromatography
IC	ion chromatography
IMS95	1995 Integrate Monitoring Study
LWC	liquid water content
MDL	minimum detection level
MW	molecular weight
NIST	National Institute of Standards and Technology
PAH	polyaromatic hydrocarbons
Ppm	parts per million (i.e., mg L^{-1})
PSA	particle surface area
PVM	Particulate Volume Monitor
RSD	relative standard deviation
ss-CASCC	stainless steel Caltech Active Strand Cloudwater Collector

S(IV)	$SO_2 \cdot H_2O + HSO_3^- + SO_3^{2-}$
SJV	San Joaquin Valley
SOA	secondary organic aerosol
ss-sf-CASCC	stainless steel size-fractioning Caltech Active Strand Cloudwater Collector
ss-xl-CACC	stainless steel extra-large Caltech Active Strand Cloudwater Collector
TC	total carbon
TDIN	total dissolved inorganic nitrogen
TOC	total organic carbon
TOM	total organic matter
VOC	volative organic compounds
WSOC	water-soluble organic carbon

1. Review of Fog Chemistry

1.1 Fog Formation

The word "fog" is a loose term applied to visible liquid aerosols, usually composed of water or ice, suspended close to the ground. Fogs are created during cooling of air next to the Earth's surface usually either by radiation to space (radiation fogs) or by contact with a cooler surface (advection fogs). Fogs have a microphysical structure similar to clouds. Some define a fog as any cloud that has come into contact with the surface. Typical fog liquid water contents vary from 0.02 to 0.5 g m^{-3}, and fog droplets have sizes ranging from a few micrometers (μm) to 40 μm (Seinfeld and Pandis, 1998). Fog droplets form as water vapor condenses onto aerosol nuclei. If the atmospheric relative humidity exceeds 100%, some aerosol particles will be activated to form fog droplets through the process of heterogeneous nucleation. The ability of an aerosol to become activated depends on its size and chemical composition, and on the maximum supersaturation experienced by the particle. The first particles to activate are usually larger in size and contain a large fraction of soluble material. As the supersaturation of the air mass increases, additional particles can also activate to form new drops. Activation of new drops will continue until a peak supersaturation is reached.

1.2 Terrain and meterological conditions in CA's Central Valley

California's Central Valley, is encompassed by the Sierra Nevada, Cascade, and Coastal Mountain Ranges. The valley is roughly 450 miles long, and home to the San Joaquin and Sacramento Rivers. The Central Valley is home to several cities and numerous agricultural operations, making the study of air quality and pollutant deposition very important.

During the winter, high-inversion fogs form in the valley and may last for days at a time. High-inversion fog is a radiation fog that forms when polar maritime air stagnates in a valley under the dominance of a persistent high pressure system (Holets and Swanson, 1981). A strong subsidence inversion associated with the high traps the cool, moist air in the valley. On clear nights, longwave radiation from the surface cools the air. As the air temperature approaches the dewpoint temperature (the temperature to which water must cool to condense), water begins to condense on condensation nuclei. Slight breezes cause more contact between the ground and the moist air, increasing the transfer of heat.

Holets and Swanson (1981) summarized the typical meteorological conditions during a fog event: wind speeds are less than 3.5 m s^{-1}, surface temperature was about 2° C, the fog layer had a near moist adiabatic lapse rate and a fog layer thickness of 130 m to 530 m. They found that, in general, high-inversion fog episodes are characterized by spatially and temporarily uniform meteorological conditions in the Central Valley.

1.3 Fog scavenging of gases

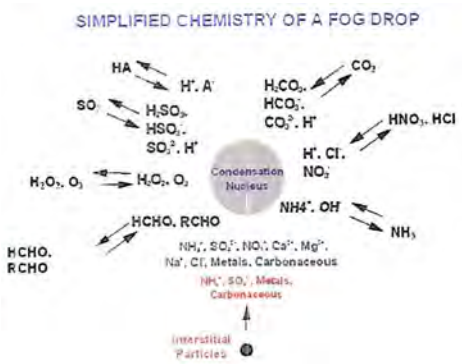

Figure 1-1. Simplified chemistry of a cloud/fog water droplet.

The pollution scavenging role of fog water droplets has been the focus of many studies in the past (e.g., Jacob, 1986; Laj et al., 1997). As shown in Figure 1-4, major chemical species of interest include SO_2, CO_2, nitrogen species (e.g., NO, NO_2, NO_3, NH_3, NH_4^+), other inorganic species (e.g., SO_4^{2-}, Ca^{2+}, Mg^{2+}, etc), oxidants (e.g., H_2O_2, other organic peroxides, O_3), and a large variety of organic compounds (e.g., formaldehyde and other aldehydes, low molecular weight carboxylic acids, phenols). The initial chemical composition of a fog droplet is controlled by the composition of the corresponding fog condensation nuclei. Uptake of soluble gases and chemical reactions within the droplets further alter their composition.

Soluble gas uptake also plays an important role in determining the pH of fog. In remote environments, for example, pH is determined largely by uptake of CO_2 along with formic and acetic acids. In more polluted environments, uptake of gaseous acids (e.g., HNO_3) and bases (e.g., NH_3) exerts significant control on drop acidity. Several patterns in fog composition have become apparent during studies of Central Valley fogs. The pH

of the fog water samples was usually close to neutral or slightly basic. Pure fog droplets will have a pH of 5.6 at an ambient CO_2 mixing ratio of 350 ppm at 298K. Jacob et al. (1986) reports a pH range of 5.10 to 6.92 in Bakersfield, and 5.51 to 7.23 in Visalia. Collett et al. (1999a) found a pH range of 4.97 to 7.43 in San Joaquin Valley (SVJ) fogs. Collett et al. (2001) measured pH between 6 and 7 in fog waters collected in Davis, CA. Large inputs of NH_3 from surrounding agricultural activities can contribute to the high values of pH.

In most of these analyses, the inorganic composition was dominated by NH_4^+, NO_3^-, and SO_4^{2-}. These compounds can be attributed in part to agricultural activity, oil recovery processes and vehicle emissions (Jacob et al., 1984). Jacob et al. (1984) also determined that $NH_3(g)$ was the most important alkaline component in the valley. $NH_3(g)$, and other alkaline compounds, act to neutralize strong acids, so that the acidity of the fog droplets is limited by its availability. In other words, high NH_3 concentrations in the Central Valley neutralize fog water, leading to high pH values. Collett et al. (2002) also showed that the balance of ammonia and strong acids in different environments is the primary determinant of fog pH.

In addition to NH_3 acting as a buffer, Collett et al. (1999b) found that acid titrations of samples with high pH revealed the presence of considerable internal acid buffering, which was found to correlate strongly with the sum of dissolved acetate and formate compounds. This suggests that unmeasured organic species may also be important contributors including, perhaps, humic-like substances (HULIS).

1.4 Aqueous phase reactions

1.4.1 Aqueous phase reactions of SO_2

Considerable attention has been given to the aqueous oxidation of dissolved sulfur dioxide to sulfate because sulfate comprises a significant fraction of the atmospheric aerosol and contributes greatly to issues such as acid deposition and visibility degradation. Munger et al. (1983) measured unusually high concentrations of sulfate, especially after a fog event that was preceded by a smoggy period. They noticed that the radiation fogs formed more readily in a particle-laden atmosphere, and that they appeared to accelerate and enhance smog production, visibility reduction, and particulate sulfate levels during the following day. They dubbed this relationship the smog-fog-smog cycle.

Oxidation of sulfur dioxide occurs much more quickly in the aqueous phase than in the gas phase. Because dissolved SO_2 can have different forms in the solution, the oxidation state (+4) is used to represent all the forms:

$$S\ (IV) = SO_2 \cdot H_2O + HSO_3^- + SO_3^{2-} \qquad (1\text{-}1)$$

and the final oxidized state (+6) of sulfate, bisulfate, or sulfuric acid is referred to as S(VI).

1.4.1.1 S(IV) oxidation by O_3

Ozone reacts very slowly with SO_2 in the gas phase, however, the aqueous phase reaction,

$$S(IV) + O_3 \leftrightarrow S(VI) + O_2 \quad (1\text{-}2)$$

is rapid. The various forms of S(IV) can react with ozone separately with a unique mechanism and rate constant. The total oxidation rate can be written as:

$$-\frac{d[S(IV)]}{dt} = (k_1[SO_2 \cdot H_2O] + k_2[HSO_3^-] + k_3[SO_3^{2-}])[O_3] \quad (1\text{-}3)$$

where k_1, k_2, and k_3 are the rate constants.

Because the effective solubility of sulfur dioxide increases with pH, and because sulfite is oxidized faster than bisulfite, which is oxidized faster than sulfurous acid, the reaction rate of sulfate production by this pathway increases strongly with increasing pH. However, as more sulfate is formed, the pH decreases and the reaction rate slows, so this reaction is self-limiting. Therefore, S(IV) oxidation by ozone is most important at high pH.

1.4.1.2 S(IV) oxidation by hydrogen peroxide

The oxidation of S(IV) by hydrogen peroxide, H_2O_2, is typically considered to be the most efficient in acidic environments. H_2O_2 is very soluble in water and typically exists in concentrations about six orders of magnitude greater than that of dissolved ozone (Seinfeld and Pandis, 1998). Hydrogen peroxide can react with bisulfite to produce peroxymonosulfurous acid, SO_2OOH^-,

$$HSO_3^- + H_2O_2 \leftrightarrow SO_2OOH^- + H_2O \quad (1\text{-}4)$$

The peroxymonosulfurous acid, SO_2OOH^-, reacts with a proton to produce sulfuric acid,

$$SO_2OOH^- + H^+ \leftrightarrow H_2SO_4 \quad (1\text{-}5)$$

This reaction becomes faster as the droplets become more acidic, which is why S(IV) oxidation by hydrogen peroxide is viewed as the most effective reaction at low pH values.

1.4.1.3 S(IV) oxidation by oxygen

S(IV) oxidation by oxygen is very slow except in the presence of catalysts such as Fe(III) and Mn(II). If fog water, these two trace metals can be relatively abundant because they are because they are common components of aerosol originating from crustal erosion. The catalyzed auto-oxidation mechanism and its kinetics are very complex. Although an accurate measurement of the iron and manganese oxidation states is difficult in the field, an upper bound to S(IV) oxidation by O_2 can be determined by using the total Fe and Mn concentrations. In general, since S(IV) oxidation by O_2 is only significant when the pH value is neutral, and at this pH, formation of HMS and S(IV) oxidation by ozone can be even faster, metal-catalyzed S(IV) oxidation typically doesn't play a large role in the overall sulfate production in fogs (Rao and Collett, 1998).

1.4.2 Aqueous phase reactions of organics

A variety of aqueous phase reactions also involve organic compounds. Several researchers have suggested that a significant portion of secondary organic aerosol (SOA)

formation takes place in cloud and fog droplets (Strader et al., 1999; Blando et al., 2000). Aqueous phase oxidation processes can enhance the solubility of organic aerosol by introducing polar functional groups into the molecular structure, such as mono- and dicarboxylic acids, aldehydes, alcohols, and ketones, which are fairly abundant in fog water (Facchini et al., 1999; Blando and Turpin, 2000). Blando and Turpin (2000) identified potential precursors that include aldehydes, acetone, alcohols, monocarboxylic acids (e.g., formic and acetic acid), and organic peroxides. Carboxylic acids, glyoxal, esters, organosulfur compounds, polyols, amines, and amino acids were identified as potential products of cloud and fog processing.

1.5 Drop size-dependence of fog composition

One topic to receive an increase in attention in recent years is the variation of solute concentrations across the fog drop size spectrum. Several factors contribute to this variation, including the size-dependent composition of CCN, faster dilution of small droplets by condensational growth, and faster uptake of soluble gases by smaller fog drops. Initial differences in fog drop composition with drop size can be further enhanced by differing rates of aqueous phase reactions (due to the reaction rate dependence on reactant concentrations).

Several studies have shown that fog drop composition can vary with drop size (Munger et al., 1989; Schell et al., 1996; Vong et al., 1997; Collett et al., 1999a; Reilly et al., 2001; Moore et al., 2004). Studies of radiation fogs have often revealed that small drops are more acidic than large drops, and that most of the major solutes are

concentrated more in the small drops. Collett et al. (2001) found that nitrate had the strongest enrichment, followed by sulfate, and ammonium had the smallest small: large droplet ratio. Herckes et al. (2002b) found that the TOC concentrations were also enriched in small droplets. These studies have also shown that NO_2^- is enriched in larger drops, apparently because of increased HONO solubility at higher pH.

Because drop sedimentation is a strong function of drop size, size-dependent fog drop composition can also give rise to enhanced deposition velocities for species enriched in the large fog droplets and reduced deposition velocities for species enriched in the small drops. The deposition velocities of these species are a function of their size distribution. Collett et al. (1999a, 2001) found that species enriched in the small drops had smaller deposition velocities. Nitrate, which had the strongest enrichment, also had the smallest deposition velocity, followed by sulfate, and ammonium had the largest deposition velocity. TOC enriched in the small drop size-fraction was also found to have deposition velocities smaller than that of the fog water (Herckes et al., 2002b). Nitrite, enriched in larger droplets, had a deposition velocity higher than fog water.

1.6 Organic composition of fog water

Work has also been done to look at the organic carbon compounds found in Central Valley fog waters (Herckes et al., 2002a, b). Herckes et al. (2002a) identified numerous organic compounds, including various alkanes, polycylic aromatic hydrocarbons (PAH), and alkanoic acids. High molecular weight, less polar compounds, were found more in the insoluble phase, while lower MW, more polar compounds were

found primarily dissolved in the fog water. They were able to speciate on average less than 20% of the fog water total organic carbon compounds. Herckes et al. (2002b) found that approximately 23% of the organic carbon was not dissolved inside the droplets. They also determined that as much as half of the dissolved organic carbon was comprised of compounds with molecular weights greater than 500 Daltons.

1.7 Major research goals

This study is part of an ongoing investigation of the organic composition of fogs and clouds and how that composition is related to fog water processing of carbonaceous aerosol particles and soluble trace gases. Several different analyses will be utilized to study the chemical composition of fog water sampled in Fresno, CA., including analysis by high-performance liquid chromatography (HPLC), ion chromatography (IC), total organic carbon (TOC), fluorometry, and ultrafiltration. The methods employed to study samples taken during this project will help to further characterize organic and inorganic material found in Central Valley fog droplets, which will lead to a better understanding of the role that fog water scavenging plays in the removal of atmospheric aerosol via deposition.

This project will also attempt to better characterize organic matter found in fog water. More investigation into the prevalence of organic carbon will be made. A number of organic acids and carbonyl compounds will be speciated in the dissolved organic carbon fraction of the samples. Ultrafiltration will be used to determine a rough molecular weight distribution of organic carbon also.

More observations of fog solute deposition fluxes and deposition velocities are needed to evaluate the role of these fogs as atmospheric cleansers. Deposition plates will be used to study how fog solutes are deposited onto the ground during a fog event. Because drop sedimentation is a strong function of drop size, in order to better understand deposition of individual species, it is important to understand the size-dependence of fog solutes. Size-fractionated samples will therefore be taken to study the drop size-dependence of fog water solutes.

2. Methodology

Field work for this study was carried out during December 2003 through January 2004. Cloud collectors, along with several other instruments, were used to collect fog samples. Laboratory work was done in the field as well as at Colorado State University (CSU).

2.1 Site

The Fresno, California (36° N, 119.72° W) site was located on agricultural land on the California State University-Fresno campus, located within the Fresno urban area. The San Joaquin Valley (SJV) is known for its prevalent winter radiation fogs. Located about 100 yards south from the site was the university's beef/cattle unit, so animal waste was expected to have an influence on the samples collected. The operations here are similar to many throughout the SJV. Cloud collectors and a Particulate Volume Monitor (PVM) were mounted on poles roughly 10 feet high in an open field. The cloud collectors were situated to form a box with about 30 feet in between each other, while the PVM was placed in the middle.

2.2 Sampling Instruments

2.2.1 Fog/Cloud Collectors

Four different versions of the Caltech Active Strand Cloudwater Collector (CASCC) were used to collect fog water. The following four sections will describe each of these collectors in more detail.

2.2.1.1 Plastic CASCC

This collector uses a fan that draws fog droplets through its plastic body, which then inertially impact on three inclined sets of Teflon strands (508 μm). The impacted droplets are pulled by gravity and aerodynamic drag down the strands into a Teflon collector trough, where they then run through a Teflon tube and are collected in a polyethylene bottle. Theoretically, the 50% size cut of the CASCC is 3.5 μm given a sampling velocity of 8.5 m/s (Demoz et al., 1996). Samples from the CASCC were used to measure ionic species (Cl^-, NO_2^-, NO_3^-, SO_4^{2-}, Na^+, NH_4^+, K^+, Mg^{2+}, and Ca^{2+}). Figure 2-1 (below) is a picture of the CASCC collector. The fan can be seen on the left side of the collector, and the strands can be seen on the right side.

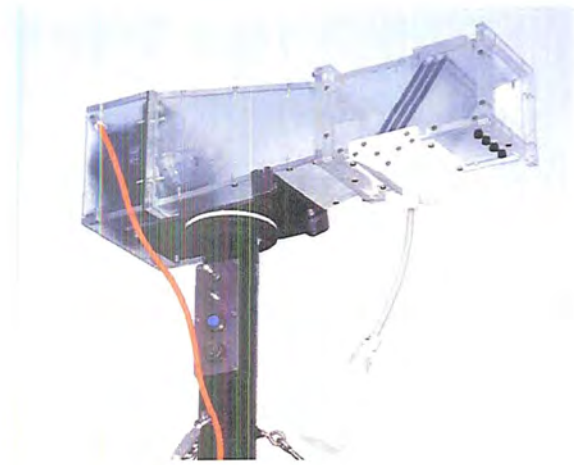

Figure 2-1. Picture of the CASCC collector.

2.2.1.2 Stainless Steel CASCC

The second collector used was the stainless steel CASCC (ss-CASCC), designed by Herckes et al. (2002). This collector also has a theoretical size cut of 3.5 μm. Its structure is very similar to that of the plastic CASCC, but it is made of stainless steel instead. The ss-CASCC draws foggy air through three sets of stainless steel strands. The fog droplets inertially impact the strands and are collected in a stainless steel trough. The water then runs through a stainless steel tube and into a pre-fired amber glass collection bottle. The ss-CASCC was used to measure bulk organics and study particulate scavenging by fog water. Figure 2-2 shows the ss-CASCC collector. The fan is in the left side of the collector, and air is drawn through from right to left.

Figure 2-2. Picture of the ss-CASCC collector.

2.2.1.3 Size-fractioning Stainless Steel Collector

The third collector we used was the size-fractioning stainless steel collector (sf-ss-CASCC). The sf-ss-CASCC was designed to simultaneously collect samples representing two portions of the cloud drop spectrum. The collector is similar to the sf-CASCC described by Demoz et al. (1996), but is twice as large in cross section and uses two fans (side-by-side) to draw foggy air through the collector. The larger droplets first impact three rows of stainless steel rods (diameter = 12.7 mm; theoretical 50% size cut = 23 μm). The remaining droplets are collected on three rows of stainless steel strands (diameter = 508 μm; theoretical 50% size cut = 4 μm). The collection efficiency of a multi-stage collector is difficult to perfect, however. The efficiency curves for the large sampling rods required to achieve a 50% size cut near 20 μm are inherently not very sharp (Demoz et al, 1996). Also, the incomplete sampling of air transiting the rods allows some large drops to make it through the inlet and "contaminate" the small drop fraction. The sf-ss-CASCC was used to study the drop-size dependence of organic compounds. Figure 2-3 shows the ss-sf-CASCC collector. The collection bottle on the right is collection the large droplet fraction, the bottle on the right is collection the small droplet fraction.

Figure 2-3. Picture of the ss-sf-CASCC.

2.2.1.4 Extra Large Stainless Steel Collector

The fourth collector used was the extra large stainless steel collector (xl-ss-CASCC). This collector uses two fans to pull in foggy air, so its sampling volume is roughly twice that of the ss-CASCC. This collector uses three rows of stainless steel strands (diameter = 508 μm; theoretical 50% size cut = 4 μm) to collect fog droplets. This collector was used to collect large volumes of fog water to be analyzed for organic compounds at the U.S. Geological Survey.

2.2.2 Other Instruments

2.2.2.1 Particulate Volume Monitor

In addition to the cloud collectors, a Gerber Scientific Particulate Volume Monitor (model PVM-100) was used to continuously measure the liquid water content of the air, as well as the fog droplet particle surface area. The PVM measures droplets in the range of 3 – 50 μm, and has a measurement accuracy (as determined by the manufacturer) of 5%, and a measurement precision of 2%. The PVM was connected to a modem, which

was programmed to call a cell phone when the liquid water content remained above 60 mg/m^3 for more than 300 sec.

Light from a 780 nm laser diode is scattered by the fog droplets into the forward direction and collected by a lens. The lens focuses the light onto two spatial filter/ silicon photo-diode sensor combinations. One filter weights the scattered light to produce an output of Liquid Water Content, given by the following equation,

$$LWC\ [g/m^3] = \frac{4\pi\rho}{3}\sum r^3 n(r)\Delta r \tag{2.1}$$

where r (units: cm) is the droplet radius, $\rho = 1.0$ [g/cm^3] is the droplet density, and $n(r)$ (units: $number/m^3$) is the droplet size distribution.

The second filter weights the scattered light to produce an output of Integrated Particle Surface Area, as given by the following equation,

$$PSA\ [cm^2/m^3] = 4\pi\sum r^2 n(r)\Delta r \tag{2.2}$$

The third channel of the PVM divides the LWC output by the PSA output and multiplies the ratio by a constant. This ratio is related to the droplet effective radius,

$$R_e\ [cm] = \frac{\sum r^3 n(r)\Delta r}{\sum r^2 n(r)\Delta r} \tag{2.3}$$

Combining equations (2.1), (2.2), and (2.3) yields,

$$R_e\ [cm] = 30{,}000\frac{LWC[g/m^3]}{PSA[cm^2/m^3]} \tag{2.4}$$

The PVM is manually calibrated in two different ways. First, the laser beam is blocked with an opaque object, and the zero potentiometers on the base plate of the instrument are adjusted so that the voltage outputs for the LWC and PSA channels are close to 0. This procedure removes the electronic offset in the voltage output of each

channel. Then a light-diffusing disk is placed against the opening on the receiver arm. The span controls on the base plate are adjusted to the calibrated voltages unique to the disk, given by the manufacturer. The calibration voltage for the PSA channel was 2115 V and the calibration voltage for the LWC channel was 117 V. These two steps are repeated several times to achieve the most accurate calibration possible. According to the manufacturer, however, typical offset voltages of 10 – 20 mV will still remain. This calibration was performed every couple of days.

2.2.2.2 High-Volume Aerosol Sampler

A Thermo Anderson high-volume aerosol sampler (Hi-Vol; model GS2310) was used before, during, and after fog events to collect aerosol particles to determine the scavenging efficiency of the fogs. The Hi-Vol uses a pump to draw air into the instrument, where aerosol particles are collected on a pre-fired quartz filter. The Hi-Vol was equipped with a Tisch Series 230 PM2.5 impactor to give a nominal size cut of 2.5 μm aerodynamic particle diameter. The flow rate was maintained at 1.13 m^3/min, and this was checked every day. Calibration of the flow rate was completed every few days to maintain a constant rate. Sample filters were placed in aluminum jackets to prevent contamination and frozen until analysis in the lab at CSU.

2.2.2.3 Deposition Plates

Two Teflon deposition plates (Collett et al., 2001) were placed on the ground, side by side, to measure deposition fluxes and velocities. Fog deposited on these two 0.30 m^2

plates, where it was collected with pipettes and stored in polyethylene bottles. These samples were then analyzed in the lab for TOC and ion species.

2.3 Fog Aliquots and Analysis

2.3.1 On-site Procedures

Depending on the liquid water content (LWC) of the air, sampling bottles on the fog collectors were changed every 2 to 4 hours. The bottles were weighed prior to and immediately after sample collection and the sample weight was recorded. A 1 mL aliquot of sample was taken after the sample weight had been recorded and placed in a 2 mL cryogenic vial. The pH of this sample was immediately measured with a Model 290A pH meter and a Microelectrodes, Inc. Model MI-710 pH combination electrode. The pH meter was calibrated with pH 4 and 7 standards before the samples were measured. Aliquots for various measurements, including inorganic ions, total organic carbon (TOC), organic acids, formaldehyde, and carbonyls, were taken after the pH of the sample was measured. Table 2-1 reports the volume of aliquot taken, the type of container it was stored in, and the type and volume of preservation chemical added, if any.

Chloroform was added to the organic acid aliquots to kill any bacteria in the sample. A buffered formaldehyde preservation solution containing bisulfite (20 mM NaOH, 10 mM CDTA, 3 mM $NaHSO_3$) was added to the formaldehyde aliquot to form stable hydroxymethanesulfonate (HMS). A procedure for the preparation of the preservation solution can be found in Appendix A.

If there was enough sample volume left over from the ss-CASCC and sf-ss-CASCC collectors, it was filtered through a pre-fired quartz filter [GelmanSciences PALLFLEX Membrane Filters, 44mm], and aliquots of the filtered sample were taken for analysis of dissolved organic carbon (DOC) and dissolved organic nitrogen (DON). All aliquots were stored in a refrigerator for transport back to the lab for analysis.

The carbonyl aliquots need to be derivatized as shortly after collection as possible, and not more than 3 days afterwards. Derivatizations were carried out in a lab on the campus of CSUF in accordance with a revised version of the U.S. EPA Method 8315(A). This 2,4-dinitrophenylhydrazine (DNPH) method is based on the acid-catalyzed derivatization of carbonyls by nucleophilic addition of DNPH to a C=O bond, followed by 1,2-elimination of water to form 2,4-dinitrophenylhydrazone. A 20 mL aliquot of fog water is put into an Erlenmeyer flask, along with 4 mL of citrate buffer (80 mL of 1 M citric acid solution + 20 mL of 1 M sodium citrate solution), and 6 mL of DNPH reagent. The DNPH reagent is a 3 mg/mL solution prepared by dissolving 428.7 mg of 70% (w/w) DNPH crystals in 100 mL of acetonitrile. The procedure for the preparation of the DNPH crystals can be found in Appendix B. The pH was adjusted to 3.0 ± 0.1 with 6 M HCl or NaOH. The flask is sealed and placed on a heated (40° C) stirring plate for approximately two hours. The agitation is adjusted to produce a gentle swirling of the reaction solution. The derivatized solution is then serially extracted with three 20 mL portions of methylene chloride using a 125 or 250 mL separatory funnel. The extracted solution is stored in a 40 mL amber glass bottle for further analysis in the CSU lab.

Sampler	Aliquot Type	Container	Aliquot Volume	Solution added
CASCC	pH	2 mL cryogenic vial	1 mL	-----
	IC	IC plastic vial	600 µL	-----
	TOC	16 mL glass vial with Teflon-lined cap	15 mL	-----
ss-CASCC	pH	2 mL cryogenic vial	1 mL	-----
	IC	IC plastic vial	600 µL	-----
	HCHO	1.5 mL glass vial with Teflon-lined cap	1 mL	100 µL HCHO Preservir Solution
	Organic Acids	1.5 mL glass autosampler vial with Teflon-lined cap	1.4 mL	50 µL Chloroform
	TOC	16 mL glass vial with Teflon-lined cap	15 mL	-----
	DOC	16 mL glass vial with Teflon-lined cap	15 mL	-----
	Carbonyls	40 mL amber glass vial	20 mL	-----
	DON	30 mL amber plastic bottle	10 mL	-----
sf-ss-CASCC	pH	2 mL cryogenic vial	1 mL	-----
	IC	IC plastic vial	600 µL	-----
	HCHO	1.5 mL glass vial with Teflon-lined cap	1 mL	100 µL HCHO Preservir Solution
	Organic Acids	1.5 mL glass autosampler vial with Teflon-lined cap	1.4 mL	50 µL Chloroform
	TOC	16 mL glass vial with Teflon-lined cap	15 mL	-----
	DOC	16 mL glass vial with Teflon-lined cap	15 mL	-----
	Carbonyls	40 mL amber glass vial	20 mL	-----
	DON	30 mL amber plastic bottle	10 mL	-----
xl-ss-CASCC	TOC	16 mL glass vial with Teflon-lined cap	15 mL	-----
	USGS	Plastic carboys	Remainder of sample	Preservative added to cart
Deposition Plates	IC	IC plastic vial	600 µL	-----
	TOC	16 mL glass vial with Teflon-lined cap	15 mL	-----

Table 2-1. Summary of aliquots taken from each collector.

2.3.2 Laboratory analysis

2.3.2.1 Inorganic ion analysis

Inorganic anion (NO_3^-, NO_2^-, SO_4^{2-}, and Cl^-) concentrations were measured using a Dionex DX-500 ion chromatograph equipped with an AS3500 auto-sampler, an AG4A-SC guard column, AS4A-SC separation column, suppressed by Dionex Anion Self-Regenerating Suppressor (ASRS), and detected by conductivity detection. Separation was achieved using a 1.8 mM Na_2CO_3/1.7 mM $NaHCO_3$ eluent at a flow rate of 2.0 mL/min. Inorganic cation (Na^+, NH_4^+, K^+, Mg^{2+}, and Ca^{2+}) concentrations were measured using another DX-500 ion chromatograph equipped with an AS3500 auto-sampler, CG-12 and CS-12 guard and separation columns, suppressed by a Dionex Cation Self-Regenerating Suppressor (CSRS) and detected by conductivity detection. Separation was achieved by using a 20 mM methanesulfonic acid eluent at a flow rate of 1.0 mL/min. Both IC systems were calibrated daily using ion standards prepared in the lab. Calibration accuracy was monitored by injection of independent, NIST traceable standards, and the calibration stability was monitored during each day's analysis by periodic injection of a standard solution.

2.3.2.2 TOC/DOC Analysis

TOC and DOC were measured with a Shimadzu TOC-5000A analyzer. The instrument vaporizes and oxidizes the sample on a platinum catalyst in a 680°

furnace. The produced carbon dioxide is then measured in a non-dispersive infrared (NDIR) detector. This gives a measurement of total carbon (TC). To measure the inorganic carbon (IC) in the sample (carbonate) the instrument reacts the sample with 25% phosphoric acid, thereby converting the carbonate to carbon dioxide, which is then measured with the NDIR detector. Because the TOC analyzer is calibrated with lab-prepared standards of known concentrations, the instrument provides the TC and IC concentrations in parts per million (ppm). The TOC is determined as TC minus IC.

2.3.2.3 Organic acid analysis

C1-C3 carboxylic acids were analyzed using the anion Dionex IC. The organic acid column used was a Dionex AS-11 separation column with an AG-11 guard column. Separation was achieved using a 0.5 mM NaOH eluent at a flow rate of 2.0 mL/min. The IC was calibrated daily using a series of lab-prepared standards. Calibration stability during each day's analysis was monitored by periodic injections of a standard solution.

2.3.2.4 Formaldehyde analysis

The samples were analyzed by a Hach DR/4000 fluorescence spectrophotometer utilizing the method of Dong and Dasgupta (1987). This method measures total formaldehyde, which is defined as the sum of free

formaldehyde and any hydroxymethanesulfonate (HMS) that existed in the sample before preservation.

2.3.2.5 Carbonyl analysis

About 5.0 grams of anhydrous sodium sulfate are added to the extracted solution to remove any traces of water. The methylene chloride extracts are then transferred to a clean beaker carefully to minimize transfer of the sodium sulfate crystals. The crystals were washed with 3-4 mL of methylene chloride three times to ensure that the entire sample was transferred. The extracts were then allowed to evaporate in a fume hood until approximately 1 mL of solution was left and the remaining sample was taken back up in acetonitrile. The sample is then analyzed by high performance liquid chromatography (HPLC) with ultraviolet (UV) detection. The following conditions were applied:

- Column: Supelco C18, 25 cm x 4.6 mm, 5 μm particle size
- Mobile Phase Gradient: 50/50 acetonitrile/water (v/v), hold for 20 min. 50/50 acetonitrile/water to 95% acetonitrile in 15 min., 95% acetonitrile for 5 min. Total of 40 minutes plus 6 minutes of flush time.
- Temperature: 40.0° C
- Flow Rate: 1.5 mL/min.
- Detector: Ultraviolet absorption, monitored at 360 nm for monocarbonyls, 430 nm for dicarbonyls
- Injection Volume: 20 μL

The HPLC was calibrated with a Supelco standard mixture of monocarbonyls containing 15 μg/mL of the following: formaldehyde, acetaldehyde, acrolein, acetone, propionaldehyde, crotonaldehyde, butyraldehyde, benzaldehyde, isovaleraldehyde, valeraldehyde, o-tolualdehyde, m-tolualdehyde, p-tolualdehyde, hexaldehyde, and 2,5-dimethylbenzaldehyde, and a different Supelco standard containing methyl glyoxal and glyoxal.

2.3.2.6 DON analysis

The samples were acidified with diluted (20:1) sulfuric acid (H_2SO_4) to a pH of 3. The samples were then photolyzed with UV radiation for 24 hours in a Rayonet photolysis chamber. Ion chromatography was performed on the samples before photolysis to determine the amount of inorganic nitrogen present in the samples. Photolysis breaks O-N bonds in organic nitrogen compounds. The resulting "free" nitrogen atoms then combine with other molecules to form inorganic nitrogen species. IC is performed on the samples after photolysis to determine (by difference) how much inorganic nitrogen was produced during photolysis. Therefore, the amount of inorganic nitrogen measured after photolysis minus the amount measured before photolysis yields the amount of DON present in the samples.

2.3.2.7 Ultrafiltration

Ultrafiltration was performed on remaining fog water samples to study the approximate molecular weight distribution of organic compounds. The procedure was adapted from Likens et al. (1983). Separation of DOC was made in a pressurized (~50 psi) and stirred ultrafiltration cell (Amicon model 8050), using two different Millipore ultrafiltration membranes- YM1 (nominal size cut of 1000 Daltons) and YC05 (nominal size cut of 500 Daltons). Figure 2-4 describes the sampling fractionation.

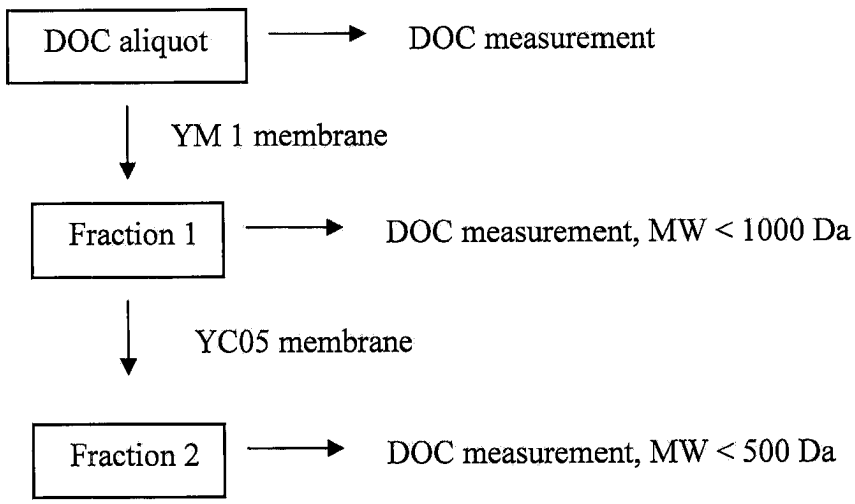

Figure 2-4. Schematic diagram of ultrafiltration fractionation.

Filter efficiencies were tested with three different standards, each with a molecular weight that falls into one of the three molecular weight fractions separated by the ultrafiltration procedure. The three standards used were oxalic acid (MW=126.07 g/mol), naringin hydrate (MW=580.55), and β-cyclodextrin hydrate (MW=1134.98 g/mol). The oxalic acid should pass through both filters, the naringin hydrate should be mostly filtered out by the 500 Da filter but pass

through the 1000 Da filter, and the β-cyclodextrin hydrate should be removed by both filters. The carbon concentrations of these standard solutions were measured, and then all three were filtered through the 500 Da filter, and the oxalic acid and β-cyclodextrin hydrate was filtered through the 1000 Da filter. The carbon concentration of the filtrate was measured to determine the efficiencies of the filters.

To minimize contamination of the samples by the filters, new filters were sonicated in deionized water for approximately two hours. The filters were sonicated in fresh DI water for one hour in between samples. DI water blanks were taken before every sample to ensure that the filters were clean and functioning properly.

2.3.2.8 Levoglucosan Analysis

Fog water samples were analyzed for anhydrosugars, more specifically levoglucosan, by high performance anion exchange chromatography with pulsed amperometric detection (HPAEC-PAD). This approach is based on liquid chromatographic (LC) separation of the non-derivatized anhydrosugars, using an anion exchange stationary phase, and their detection by an electrochemical method, using a pulsed amperometric technique. Carbohydrates are suitable for HPAEC due to their weak acidic nature. The detection method is based on the application of a constant potential (voltage) and measurement of the electrical current that is generated by the oxidation of the analytes at the surface of an electrode. The desired selectivity and sensitivity for carbohydrates is an intrinsic

characteristic of HPAEC-PAD, because the detector responds to only those compounds with functional groups that are oxidizable at the set voltage. The generated current is proportional to the amount of the analytes and can therefore be used for direct quantification.

Levoglucosan analysis in the Fresno fog samples was carried out on a Dionex DX-500 series ion chromatograph, consisting of a Dionex LC25 Chromatography Oven, Dionex GP50 Gradient Pump, and Dionex ED50 Electrochemical Detector. The electrochemical detector was equipped with a Dionex ED50/ED50A Electrochemical Cell, utilizing disposable gold electrodes and was operated in integrating amperometric mode. Separation of the individual anhydrosugars was achieved using a Dionex CarboPac PA 10 Analytical Column (4 x 250 mm) with an 18 mM aqueous sodium hydroxide (NaOH) eluent (at a flow rate of 0.5 mL/min). With no prior chemical derivatization or concentration, 100 μL of a fog sample was injected, using a SpectraSYSTEM AS3000 autosampler.

Analyses were conducted on organic acid fog water aliquots, which contained chloroform. Subsequent to analysis, separate tests in our laboratory indicated the presence of the chloroform depresses the detector response to levoglucosan in the sample in a manner which cannot be readily quantified. Reported levoglucosan concentrations, therefore, should be considered conservative estimates of amounts actually contained in the samples. While direct analysis of fog water by the HPAEC-PAD technique is also possible, tests have shown that levoglucosan

concentrations decline rather rapidly in unpreserved samples, presumably due to microbial activity.

2.3.2.9 Filter analysis

Filters taken from the Hi-Vol sampler were first cut into 8 equal-sized pieces. An individual fraction of each filter was then placed in a beaker along with 15 mL of DI water. The filters were then sonicated for approximately 30 minutes. The water was extracted from the beaker and stored in a clean glass vial. The filter was then sonicated again for 30 minutes in a clean 10 mL DI water aliquot. The water was again extracted and combined with the previous filtrate. The total DI water extract solution was then filtered through a pre-fired quartz filter. The remaining filtrate was analyzed by the TOC analyzer, explained in Section 2.3.2.2.

2.4 Quality Assurance and Control

Several different quality control measures were taken throughout the field campaign and during the chemical analysis of the samples to ensure that the samples were not contaminated, and were accurately and precisely analyzed. These measures thoroughly cleaning the collection bottles before sample collection, included washing the cloud collectors after each fog event, covering them between events to minimize particle deposition, taking blanks, measuring sample replicates and duplicates, and careful instrument calibrations.

2.4.1 Bottle cleaning

The amber glass sample collection bottles were first cleaned with Alconox detergent and rinsed thoroughly with tap water. They were then rinsed with DI water and allowed to dry. After drying, they were then rinsed with isopropyl alcohol and allowed to dry again. They were then covered with aluminum foil and baked in an oven at 450°C for 5-6 hours. Their Teflon-lined caps were also cleaned thoroughly with isopropyl alcohol. The polyethylene sample collection bottles were cleaned with a diluted Triton solution and then thoroughly rinsed with DI water.

2.4.2 Collector Cleaning and Blanks

Shortly after the collectors were set up at the site, they were cleaned with DI water and blanks were taken. Cleaning the collectors involves spraying the collection surfaces (Teflon and stainless steel strands and rods) and the insides of the collectors with ample amounts of water. A blank is then collected by spraying clean water onto the collection surfaces and collecting it through the normal sample collection path into the appropriate bottle type. This same process occurs after every fog event. If the fog event happened to be particularly dirty, the collectors may have been scrubbed with Kimwipes and Triton-X100 and then rinsed with DI water again. DI water blanks from the spray packs were also taken. The collectors were then covered with plastic to prevent contamination between fog episodes.

where t is the value at the 95% confidence level for the appropriate number of degrees of freedom, s_b is the blank standard deviation, N_i is the number of sample measurements (for single analysis, $N_i = 1$), and N_b is the number of analyzed blanks. The subscript b refers to the blank determination.

2.4.3.1 Ions

Table 2-2 lists the RSD, MDL, and average concentrations of the ions over the total study taken from the CASCC. The RSD was measured using replicate samples, while the MDL were calculated using blanks from all the collectors. All RSD values are below 10%. The MDL values of NO_3^- and NH_4^+ seem a bit high compared to the other species, but they are still below the sample averages.

	Cl^-	NO_2^-	NO_3^-	SO_4^{2-}	Na^+	NH_4^+	K^+	Mg^{2+}	Ca^{2+}
RSD(%)	1.12	1.42	1.54	2.15	5.86	1.13	6.70	4.87	5.47
MDL (95% CL) (μN)	4.85	1.07	12.26	4.53	7.39	14.72	2.03	2.52	8.71
Average (μN)	25.79	132.11	585.13	141.44	16.67	1108.09	7.17	4.20	23.04

Table 2-2. RSD and MDL summary for fog ions.

2.4.3.2 Organic Acids

Table 2-3 lists the RSD, MDL, and average concentrations of the organic acids over the total study taken from the ss-CASCC. The RSD values of all species except for glutarate fell below 10%. The MDL of pyruvate is the only value that is greater than the measured average value of the species. The one sample taken the night of Dec. 31 from the ss-CASCC had a pyruvate

concentration of 0 μM. If you ignore this sampling night when calculating the average, then the total average concentration of pyruvate is 0.67 μM, slightly above the MDL.

	Acetate	Propionate*	Formate	Pyruvate*	Glutarate*	Succinate*
RSD(%)	1.33	3.08	3.36	7.04	32.11	4.98
MDL (95% CL) (μM)	5.25	0.65	7.33	0.64	1.81	3.07
Average (μM)	143.97	8.58	76.76	0.45	1.48	3.12
	Malonate*	Oxalate	Lactic	Butyric	MSA	Pinic
RSD(%)	9.52	2.60	0.59	5.01	1.49	9.00
MDL (95% CL) (μM)	1.36	2.09	8.80	N/A	N/A	N/A
Average (μM)	2.69	20.74	2.53	2.19	2.44	2.63

Table 2-3. RSD and MDL summary for fog organic acids.

***MDL values were calculated from standard replicates.**

2.4.3.3 Carbonyls

Table 2-4 gives the RSD, MDL, and average concentrations of carbonyls measured in the samples. All RSD values fall below 10% except for acetone/acrolein. MDL values of m-tolualdehyde, p-tolualdehyde, hexaldehyde, and glyoxal are not available because they were not measured in the blanks and replicate standards were not measured. The MDLs for the other species are still far below their average concentrations.

	Formaldehyde	Acetaldehyde	Acetone/Acrolein	Isovaleraldehyde	m-Tolualdehyde
RSD (%)	1.48	6.65	12.65	2.27	9.08
MDL (95% CL) (μN)	0.96	3.23	0.39	0.98	N/A
Average (μN)	24.01	3.86	2.09	2.36	0.11
	p-Tolualdehyde	Hexaldehyde	Glyoxal	Methyl Glyoxal	
RSD (%)	6.94	6.31	4.13	3.60	
MDL (95% CL) (μN)	N/A	N/A	N/A	0.42	
Average (μN)	0.22	0.53	13.66	11.77	

Table 2-4. RSD and MDL summary for fog carbonyls.

2.4.3.4 Formaldehyde, TOC, DOC, DON

Table 2-5 gives the RSD, MDL, and average concentration of formaldehyde measured by the fluorometry procedure, TOC, DOC, and DON. The RSD is far below 10% except for DON, and the MDL is also far below the average measured concentrations. The replicate samples measured for DON had a high standard deviation. More method development may be required to decrease this number. The DOC MDL was determined to be somewhat larger than for TOC, in part because fewer replicate analyses were available to establish the DOC RSD.

	Formaldehyde	TOC	DOC	DON
RSD (%)	3.69	2.24	3.99	22.98
MDL (95% CL)	1.30 μM	0.73 ppm	1.88 ppm	24.62 μN
Average	41.08μM	18.38 ppm	13.87 ppm	202.83 μN

Table 2-5. RSD and MDL of fog formaldehyde, TOC, DOC, and DON.

3. Results and Discussion

3.1 Summary of Events

Fog samples were taken during four different events, though only the CASCC collector was run during the first and fourth events because the fog was not very dense. The first event occurred during the early morning of Dec. 31 (2:30 to 6:33 am), the second occurred during the night of Jan. 10-11 (9:30 pm to 11:40 am), the third began the following evening of Jan. 11-12 (6:30 pm to 10:00 am), and the fourth occurred during the morning of Jan. 13 (4:20 to 6:53 am). Table 3-1 gives a summary of the events. The LWC was highest during the second event, averaging 113.67 mg/m^3; however it was still not very dense. Figure 3-1 illustrates the LWC during the entire campaign. The four separate fog events are indicated on the graph. Most of the results in this chapter will focus on the two consecutive events of Jan. 10-11 and Jan. 11-12.

Event 1: Dec. 31, 2003 12/31/03 - 12/31/03 2:30 am – 6:30 am			**Event 2: Jan.10, 2003** 1/10/03 - 11/11/03 9:30 pm – 11:40 am		
LWC (mg/m^3)	Temperature (°C)	Pressure (mb)	LWC (mg/m^3)	Temperature (°C)	Pressure (mb)
111.42	7.8	1001.24	113.67	6.91	1004.96
Collector	No. of Samples	Average pH (max. pH-min pH)	Collector	No. of Samples	Average pH (max. pH-min pH)
CASCC	4	6.56 (6.41-6.66)	CASCC	7	6.68 (6.52-6.89)
ss-CASCC	0	N/A	ss-CASCC	4	6.82 (6.58-7.1)
xl-CASCC	3	N/A	xl-CASCC	6	N/A
Large-sf-ss-CASCC	0	N/A	Large-sf-ss-CASCC	4	6.87 (6.72-7.05)
Small-sf-ss-CASCC	0	N/A	Small-sf-ss-CASCC	4	6.80 (6.60-7.22)
Dep. plates	0	N/A	Dep. plates	7	N/A
Event 3: Jan. 11, 2003 1/11/03-1/12/03 6:00 pm-10:00 am			**Event 4: Jan. 13, 2003** 1/13/03-1/13/03 4:20 am-6:53 am		
LWC (mg/m^3)	Temperature (°C)	Pressure (mb)	LWC (mg/m^3)	Temperature (°C)	Pressure (mb)
105.16	6.1	1005.96	19.68	6.7	1012.41
Collector	No. of Samples	Average pH (max. pH-min pH)	Collector	No. of Samples	Average pH (max. pH-min pH)
CASCC	6	6.87 (6.38-7.15)	CASCC	8	N/A
ss-CASCC	3	7.11 (6.91-7.23)	ss-CASCC	0	N/A
xl-CASCC	4	N/A	xl-CASCC	0	N/A
Large-sf-ss-CASCC	3	7.07 (7.02-7.13)	Large-sf-ss-CASCC	0	N/A
Small-sf-ss-CASCC	3	6.59 (5.95-7)	Small-sf-ss-CASCC	0	N/A
Dep. plates	6	N/A	Dep. plates	0	N/A

Table 3-1. Summary of fog events. Liquid water content, temperature, and pressure averaged over sampling time. Temperature and pressure recorded at Fresno Yosemite International Airport, roughly 5 miles SSE of the site.

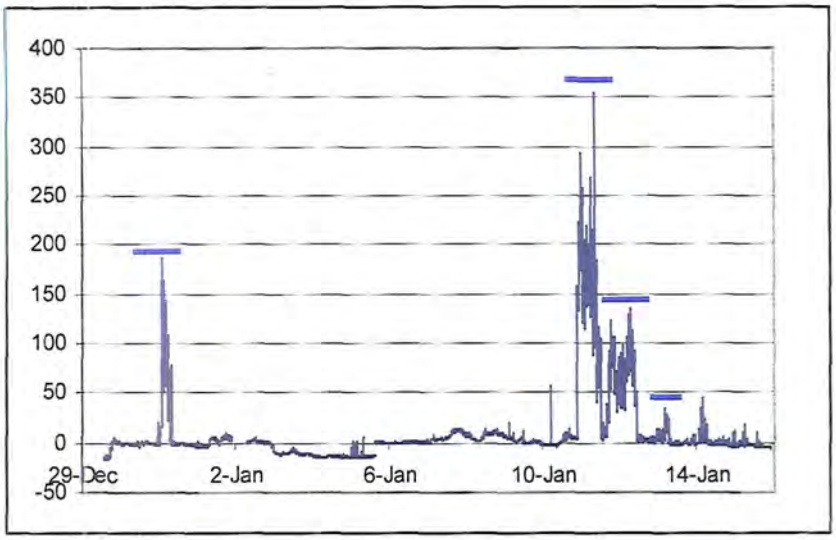

Figure 3-1. Temporal variation of LWC. The blue lines indicate the fog events. Negative LWC values indicate background concentrations.

For each fog event, the PVM recorded the total surface area of the droplets (S, unit: cm^2/m^3) as well as the LWC (mg/m^3). One can calculate the effective diameter (D_{eff}; unit: μm), proportional to the drop volume divided by the drop surface area, from these data. The equation is as follows:

$$D_{eff} = 60 \times \frac{LWC}{S} \tag{3-1}$$

Figures 3-2 to 3-3 show timelines of D_{eff} and LWC for the two consecutive fog events when most of the samples were taken.

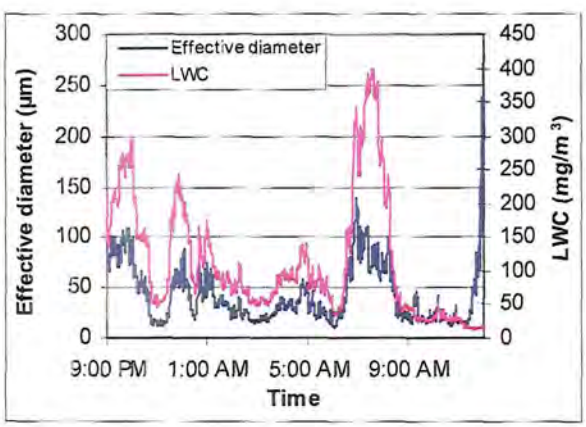

Figure 3-2. Effective diameter and LWC during Jan. 10-11,2004.

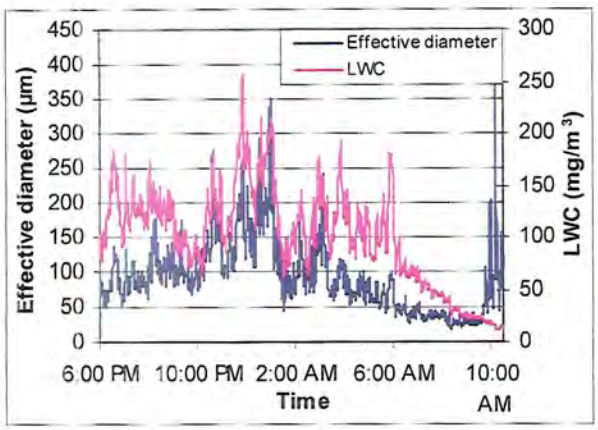

Figure 3-3. Effective diameter and LWC during Jan. 11-12, 2004.

The D_{eff} values indicate the characteristic drop sizes of the fog water. By plotting the temporal variations of the D_{eff}, one can get a sense of when the fog water samples are dominated by larger or smaller drops.

3.2 Fog pH

The pH of the samples taken from the CASCC collector on Dec. 31 ranged from 6.41 to 6.66, with an average of 6.56. The pH of the samples taken from the CASCC collector on Jan. 10-11 ranged from 6.52 to 6.89, with an average of 6.68. The pH of the samples taken from the CASCC collector on Jan. 11-12 ranged from 6.38 to 7.15, with an average of 6.87. pH measurements were not made for samples taken on Jan. 13. Figures 3-4 to 3-6 show the temporal variation of the pH and LWC.

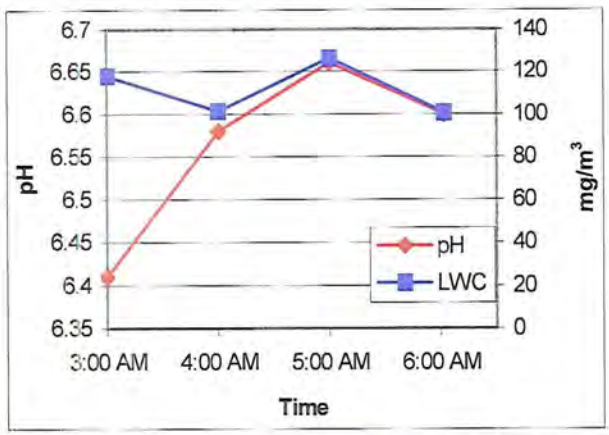

Figure 3-4. Temporal variation of pH during night of Dec. 31. LWC is shown on second y-axis.

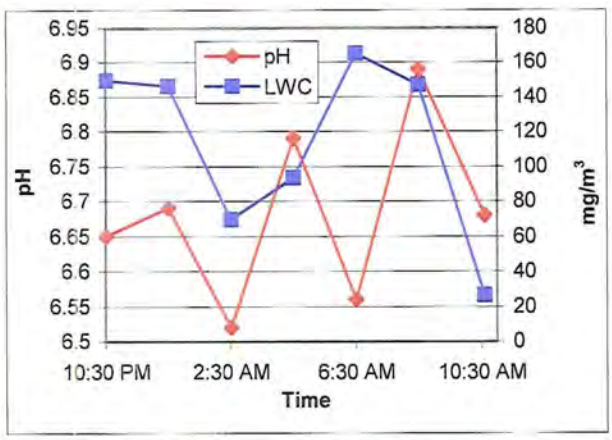

Figure 3-5.Temporal variation of pH during night of Jan. 10-11. LWC is shown on second y-axis.

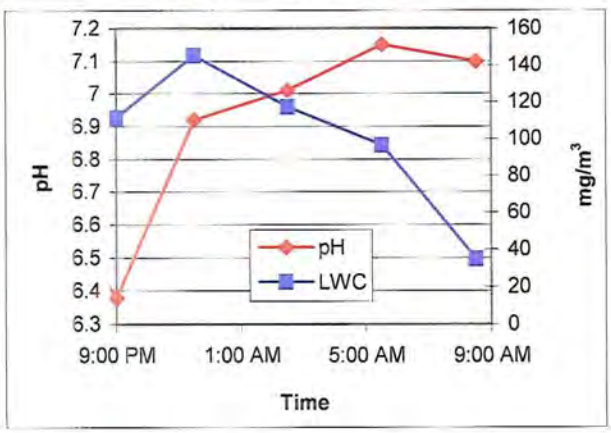

Figure 3-6. Temporal variation of pH during night of Jan. 11-12. LWC is shown on second y-axis.

It is important to also look at the differences in pH between the two different drop sizes. Figure 3-7 plots the pH of the small droplets versus the large droplets for the two nights the ss-sf-CASCC was run (Jan. 10-11 and 11-12). The pH of the larger drops is often slightly greater than that of the smaller drops. One possibility is the preferential uptake of nitric acid into the small droplets. Nitric

acid is very water soluble, and the small droplets have a large surface area-to-volume ratio, so gaseous nitric acid partitions to the small droplets much faster than to the large.

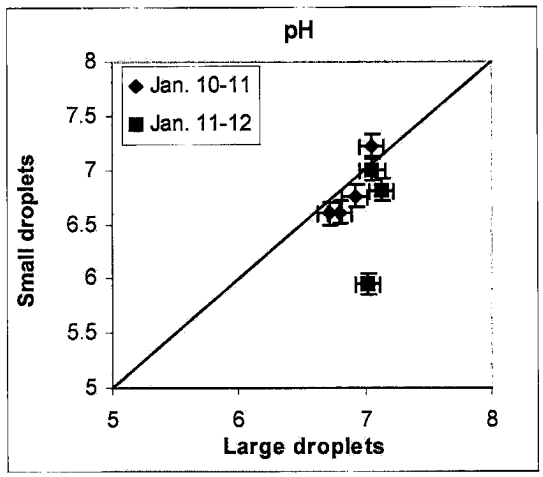

Figure 3-7. Drop size-dependence of pH. Standard deviation (± 0.1) taken from Collett et al. (1994).

3.3 Ion concentrations

Table 3-2 summarizes the fog water inorganic ion concentrations of the four sampling periods, taken from the CASCC collector.

	Cl^-	NO_2^-	NO_3^-	SO_4^{2-}	Na^+	NH_4^+	K^+	Mg^{2+}	Ca^{2+}
Dec. 31	12.5	130.9	231.4	60.6	5.4	761.3	6.7	3.2	13.0
Jan. 10-11	11.3	65.2	276.8	63.5	5.2	736.2	3.7	3.0	10.2
Jan.11-12	39.0	77.2	987.7	221.7	6.6	1902.2	9.3	3.1	16.2
Jan. 13	34.7	219.1	735.1	188.7	16.0	1599.4	15.8	8.8	50.4

Table 3-2. Summary of event-averaged inorganic ion concentrations. Values are in μN.

Figure 3-8 shows the composition of the inorganic ion species for each fog event. In all events, ammonium, nitrate, nitrite, and sulfate were the dominant

species, accounting for roughly 60%, 25%, 7%, and 6% of the total inorganic ion species, respectively.

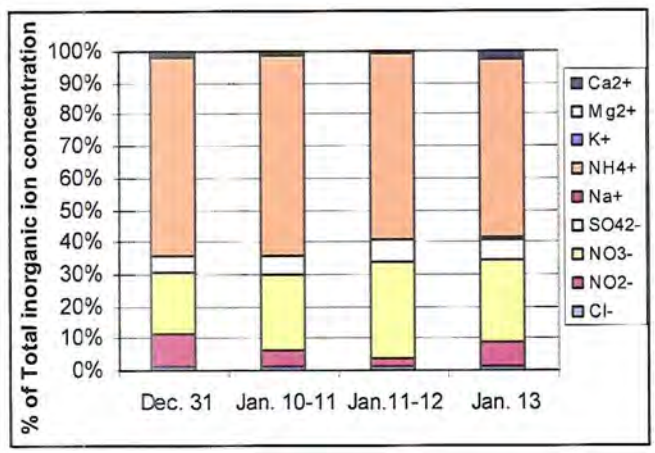

Figure 3-8. Composition of inorganic ion species. Values for each event averaged over total sampling period.

During December 1995-January 1996, Collett et al. (1999) sampled fog water in Fresno as part of the 1995 Integrated Monitoring Study (IMS95). Figure 3-9 shows a comparison between the most prevalent ionic species measured in both campaigns. The composition is remarkably similar, though the concentrations from the present study are slightly higher. NO_2^- is not compared because it was not analyzed during the IMS95 project.

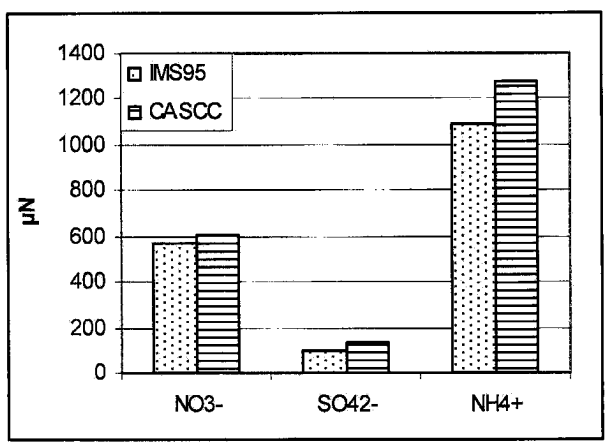

Figure 3-9. Comparison of Fresno and IMS95 averaged ion concentrations.

3.3.1 Temporal variations

Figures 3-10 to 3-13 show the temporal variations in the ion concentrations as well as LWC. All four figures were plotted using measurements from the CASCC collector. In Figures 3-10 and 3-11, as the fog evaporates, the ion species become more concentrated, as expected. However, this same trend is not present in Figures 3-12 and 3-13, perhaps reflecting depletion of water and solutes by ongoing deposition.

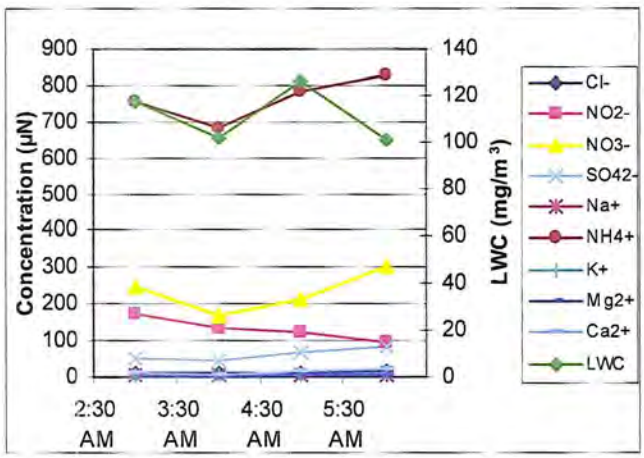

Figure 3-10. Temporal variations in ion concentrations during the night of Dec. 31, 2003.

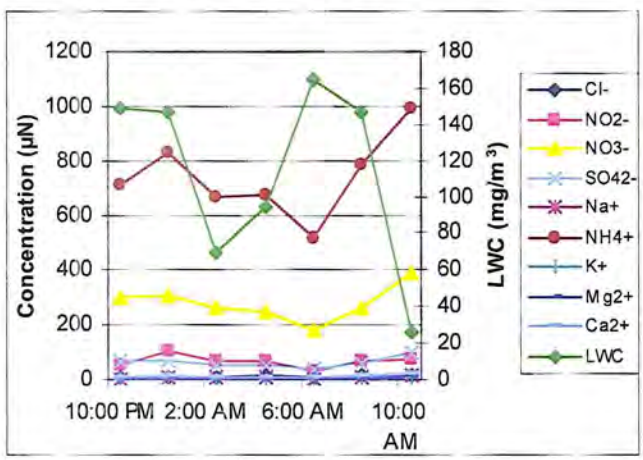

Figure 3-11. Temporal variations in ion concentrations during the night of Jan. 10-11.

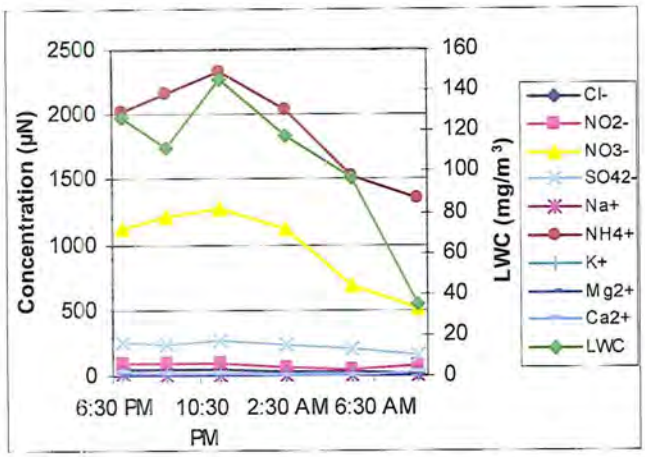

Figure 3-12. Temporal variations in ion concentrations during the night of Jan. 11-12.

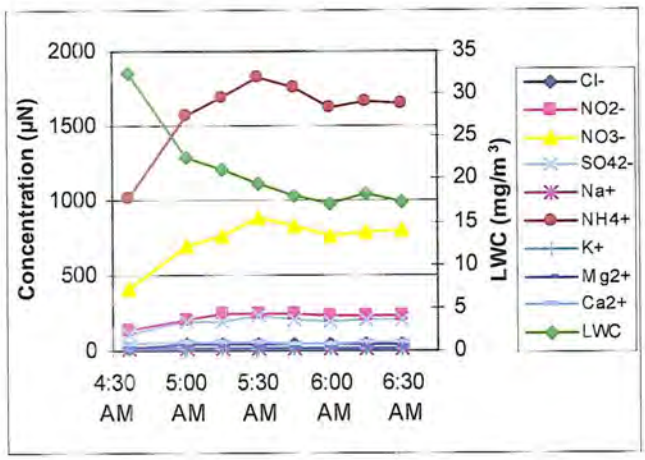

Figure 3-13. Temporal variations in ion concentrations during the morning of Jan. 13.

3.3.2 Drop size-dependence

It is useful to study the drop size-dependence of chemical species to determine how they partition to different droplet sizes and possible impacts of these patterns on pollutant deposition and drop chemistry. Figures 3-14 to 3-21 show the drop size-dependence of the ions, analyzed from samples taken from the size-fractionated collector (large drops: > 23 µm; small drops: 4 < µm < 23 µm). The diagonal lines represent the one-to-one line, where the concentrations in both size

drops would be equal. There is a significant enrichment of all the ionic species in the small drops except for NO_2^-.

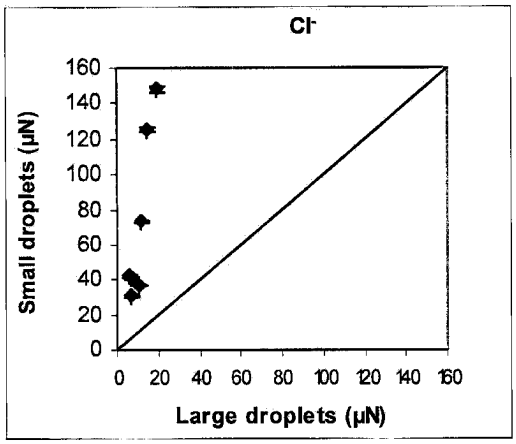

Figure 3-14. Drop size-dependence of Cl^- in large and small droplets. Error bars represent analytical RSD as reported in chapter 2.

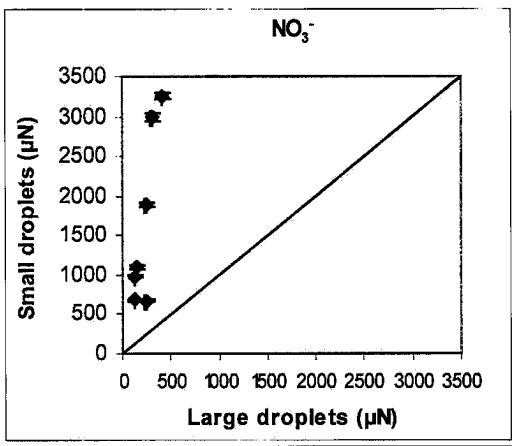

Figure 3-15. Drop size-dependence of NO_3^- in large and small drops. Error bars represent analytical RSD as reported in chapter 2.

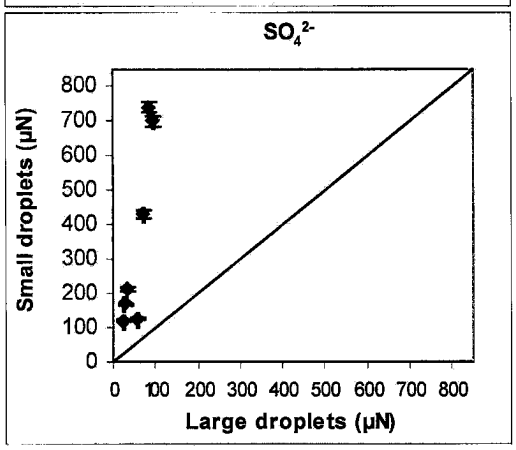

Figure 3-16. Drop size-dependence of SO_4^{2-} in large and small drops. Error bars represent analytical RSD as reported in Chapter 2.

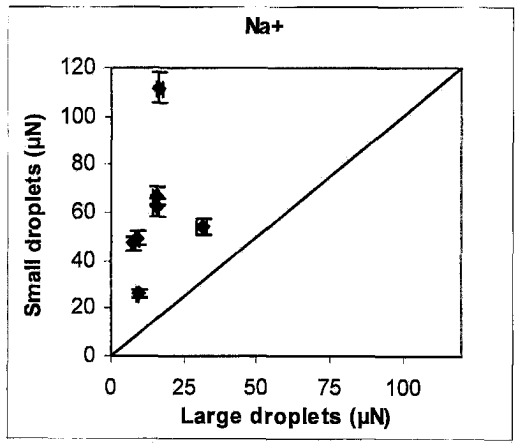

Figure 3-17. Drop size-dependence of Na^+ in large and small drops. Error bars represent analytical RSD as reported in Chapter 2.

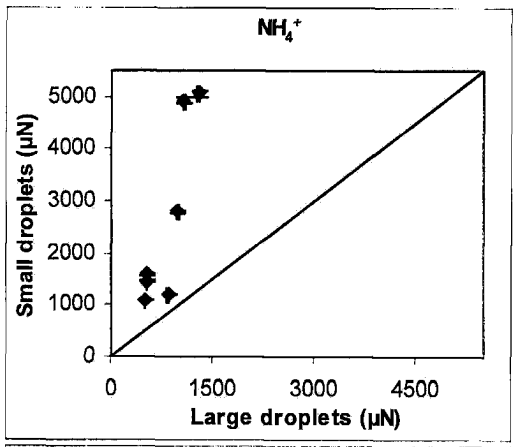

Figure 3-18. Drop size-dependence of NH_4^+ in large and small drops. Error bars represent analytical RSD as reported in Chapter 2.

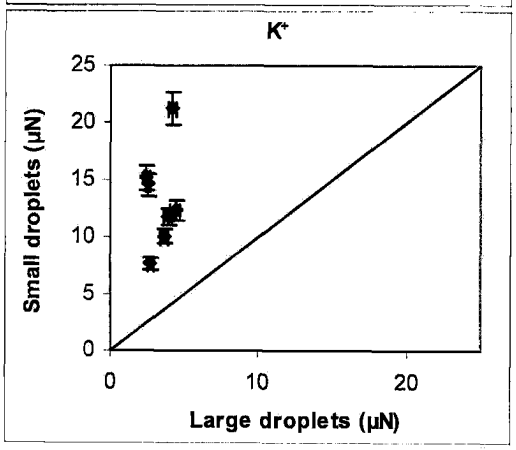

Figure 3-19. Drop size-dependence of K+ in large and small drops. Error bars represent analytical RSD as reported in Chapter 2.

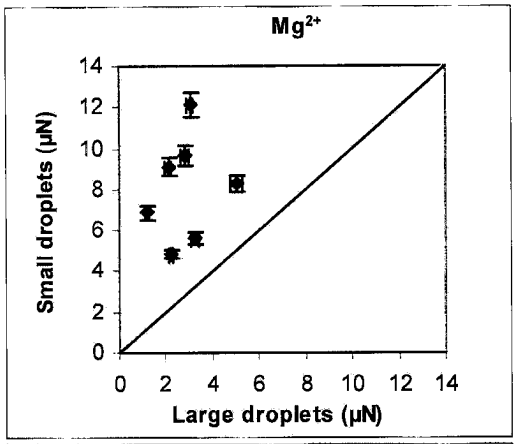

Figure 3-20. Drop size-dependence of Mg^{2+} in large and small drops. Error bars represent analytical RSD as reported in Chapter 2.

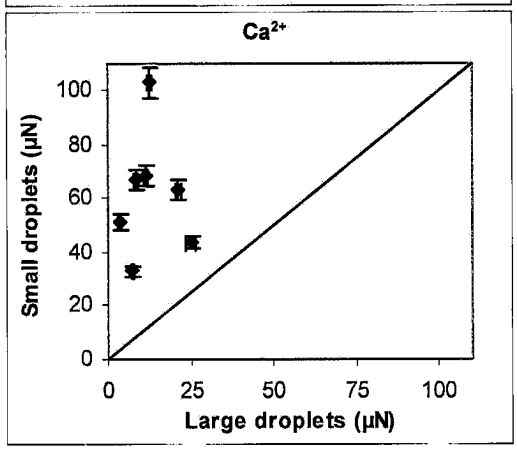

Figure 3-21. Drop size-dependence of Ca^{2+} in large and small drops. Error bars represent analytical RSD as reported in Chapter 2.

Drop size-dependence of inorganic compounds has been thought to be caused by the inhomogeneity of the aerosol population on which the droplets formed (Ogren and Charlson, 1992; Bator and Collett, 1997). Smaller CCN, which typically produce smaller drops, usually show higher concentrations of organic carbon, sulfate, and ammonium. Larger fog drops are likely to form on larger CCN, formed by mechanical processes, which might be enriched in sodium, chloride, and calcium. However, the species expected to be enriched in the large droplets (Na^+, Cl^-, Mg^{2+}, Ca^{2+}) were actually found to be enriched in the small drops. Clearly, other processes, whether during formation or in the fog droplets themselves, also influence drop size-dependence in these species.

The opposite effect is seen in the size-dependence of NO_2^-, however. NO_2^- is actually enriched in the large droplets. This is consistent with measurements made during the California Regional Particulate Air Quality Study (CRPAQS) (Chang, 2004). Moore (2002) also found an enrichment of NO_2^- in the large drop size-fractionated samples in Davis fog water. Figure 3-22 shows the drop size-dependence of NO_2^-.

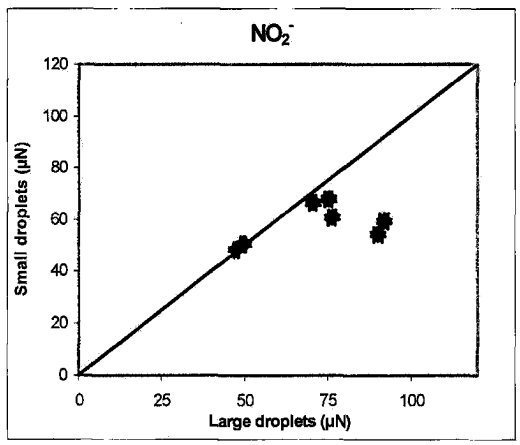

Figure 3-22. Drop size-dependence of NO_2^- in large and small drops. Error bars represent the analytical RSD as reported in chapter 2.

Nitrous acid, found in urban nighttime atmospheres, may play a part in aqueous NO_2^- formation. A suggested chemical pathway for the formation of NO_2^- is as follows:

$$HONO(g) \leftrightarrow HONO(aq) \leftrightarrow NO_2^- + H^+ \qquad (3\text{-}2)$$

If the pH of the droplets decreases (i.e., the H^+ concentration increases), Le Chatelier's principle states that the reaction will be driven to the left to restore equilibrium. Therefore, the concentration of NO_2^- will decrease. If the pH

increases (i.e., the H^+ concentration decreases), the reaction will be driven to the right to restore equilibrium so that the concentration of NO_2^- increases. As already shown in Figure 3-7, the pH of the large drops is typically greater than that of the small droplets. One would therefore expect an enrichment of NO_2^- in the large droplets.

3.4 Organic acid concentrations

Table 3-3 summarizes the organic acid concentrations measured during the first three sampling events by the CASCC and ss-CASCC. Small sample volumes precluded aliquots from being taken during the fourth event.

	Acetate	Propionate	Formate	Pyruvate	Glutarate	Succinate
Dec. 31*	126.93	8.01	66.52	0	0.52	1.28
Jan. 10-11	120.33	7.60	57.35	0.48	0.53	2.36
Jan. 11-12	184.64	10.14	106.41	0.86	3.39	5.71
	Malonate	Oxalate	Lactic	Butyric	MSA	Pinic
Dec. 31*	2.18	17.63	2.68	1.94	1.33	2.26
Jan. 10-11	1.24	12.47	1.69	2.23	1.86	1.75
Jan. 11-12	4.64	32.13	3.23	2.39	4.14	3.90

Table 3-3. Summary of fog water organic acids (units: μM). Values were averaged over total sampling period for each event.

***Samples taken from CASCC.**

Figure 3-23 shows the composition of the organic acid species for each fog event. In all events, acetate, formate, and oxalate were the dominant species, accounting for roughly 54%, 29%, and 8% of the total organic acid species, respectively.

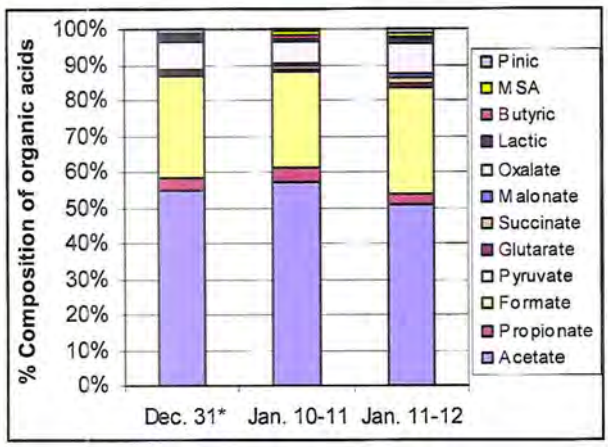

Figure 3-23. Composition of organic acids for each fog event. Values were averaged for each event over the total sampling period.

*** Samples taken from CASCC**

Figure 3-24 compares organic acid measurements made during the IMS95 project (Collett et al., 1999a) and the present project. Concentrations are again rather similar. The current Fresno study had slightly larger concentrations of acetate, formate, and propionate, while the IMS95 study had larger concentrations of pyruvate and oxalate. The concentrations presented here from the IMS95 project are averages of measurements taken at 3 different sites in the southern SJV- two urban and one rural.

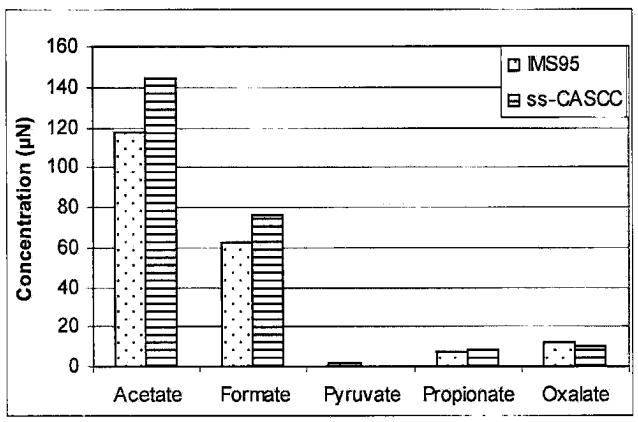

Figure 3-24. Comparison of organic acid concentrations from IMS95 and current project.

3.4.1 Temporal variations

Figures 3-25 to 3-27 show temporal variations of the organic acids and LWC. Figure 3-16 shows data taken from the CASCC collector the night of Dec. 31, 2003, while the other two figures show data taken from the ss-CASCC on the two consecutive sampling nights. Again, on the nights of Jan. 10-11 and Jan. 11-12, as the fog evaporates, the concentrations of the major organic acid species increase. No discernible trend was seen during the first night of sampling.

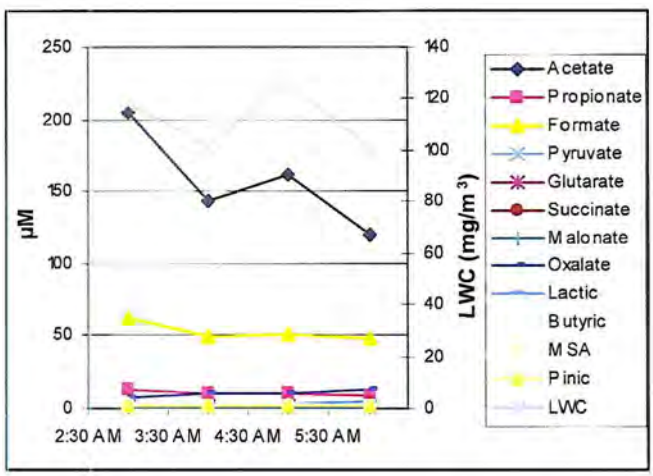

Figure 3-25. Temporal variation in organic acid concentrations on Dec. 31, 2003.

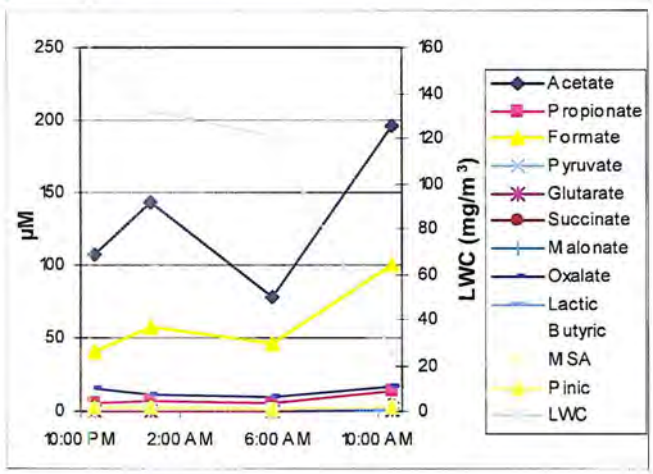

Figure 3-26. Temporal variation in organic acid concentrations on Jan. 10-11, 2004.

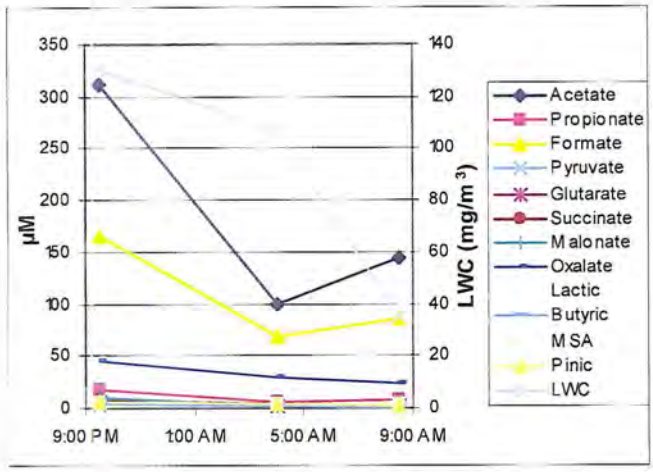

Figure 3-27. Temporal variation in organic acid concentrations on Jan. 11-12, 2004.

3.4.2 Drop size-dependence

Figures 3-28 to 3-39 show the drop size-dependence of organic acids. The diagonal line is the one-to-one line. Overall, the acids are more enriched in the small droplets than the large; some species more than others. Only pinic acid does not show such an obvious tendency.

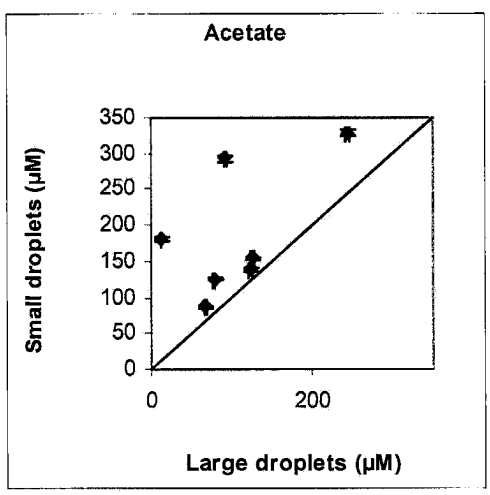

Figure 3-28. Drop size-dependence of acetate in large and small drops. Error bars represent analytical RSD as reported in Chapter 2.

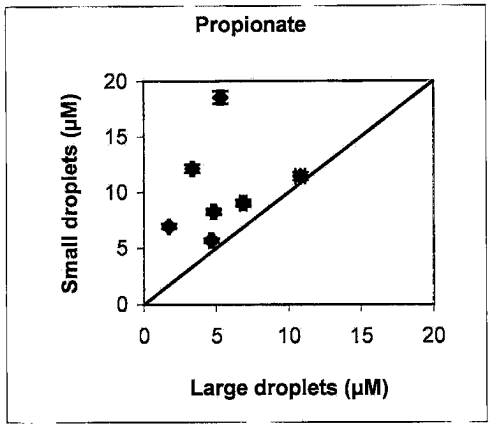

Figure 3-29. Drop size-dependence of propionate in large and small drops. Error bars represent analytical RSD as reported in Chapter 2.

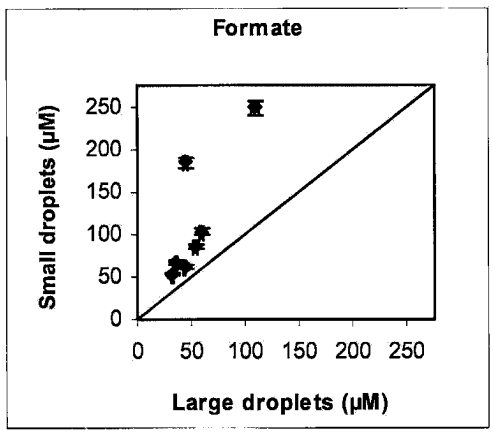

Figure 3-30. Drop size-dependence of formate in large and small drops. Error bars represent analytical RSD as reported in Chapter 2.

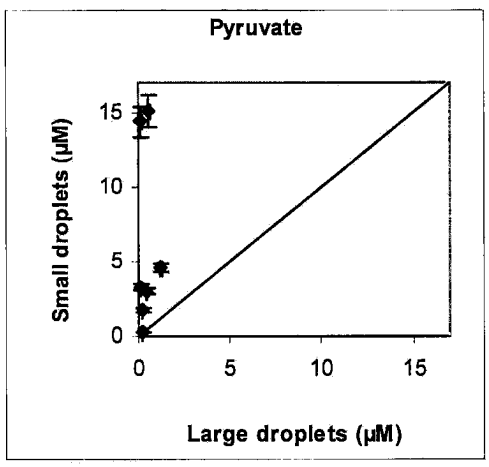

Figure 3-31. Drop size-dependence of pyruvate in large and small drops. Error bars represent analytical RSD as reported in Chapter 2.

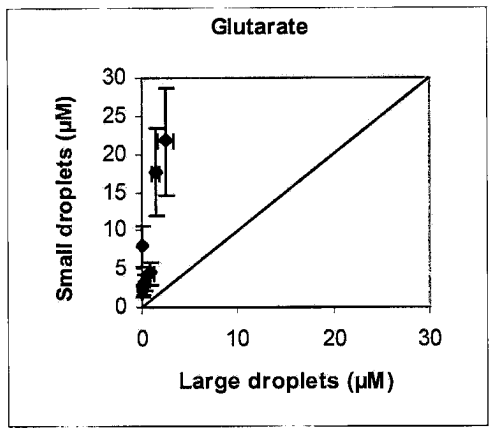

Figure 3-32. Drop size-dependence of glutarate in large and small drops. Error bars represent analytical RSD as reported in Chapter 2.

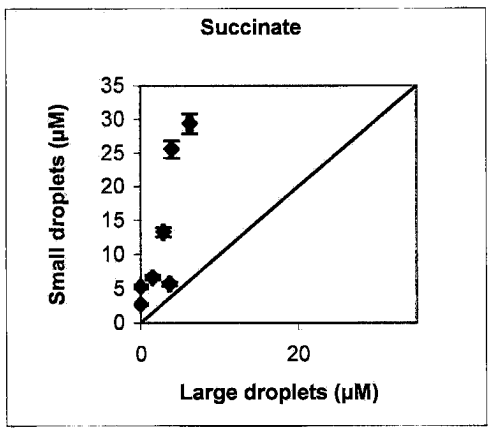

Figure 3-33. Drop size-dependence of succinate in large and small drops. Error bars represent analytical RSD as reported in Chapter 2.

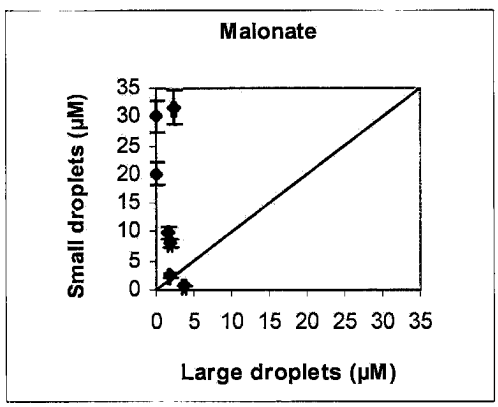

Figure 3-34. Drop size-dependence of malonate in large and small drops. Error bars represent analytical RSD as reported in Chapter 2.

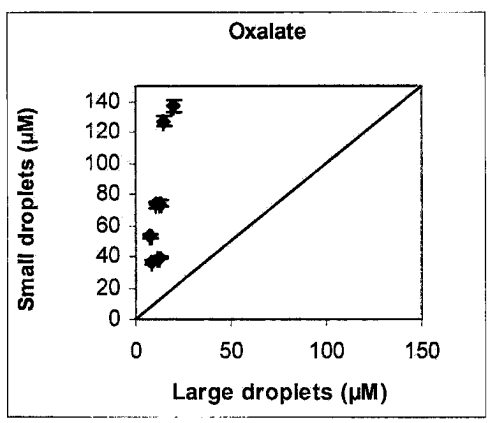

Figure 3-35. Drop size-dependence of oxalate in large and small drops. Error bars represent analytical RSD as reported in Chapter 2.

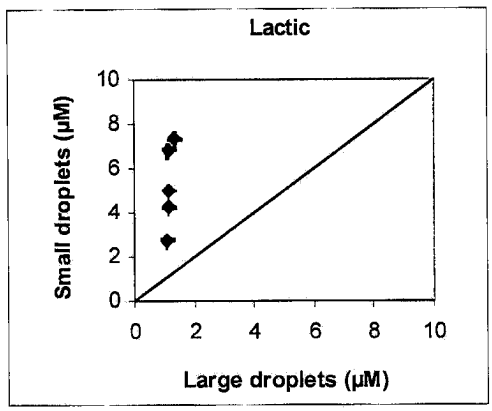

Figure 3-36. Drop size-dependence of lactic acid in large and small drops. Error bars represent analytical RSD as reported in Chapter 2.

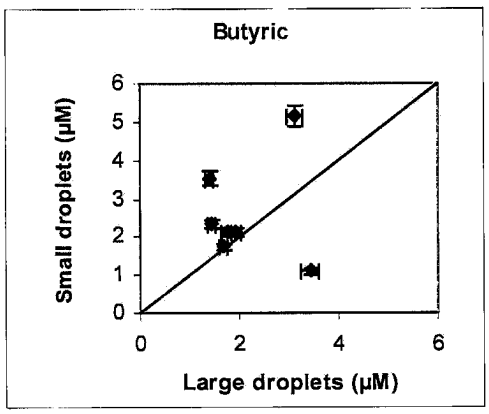

Figure 3-37. Drop size-dependence of butyric acid in large and small drops. Error bars represent analytical RSD as reported in Chapter 2.

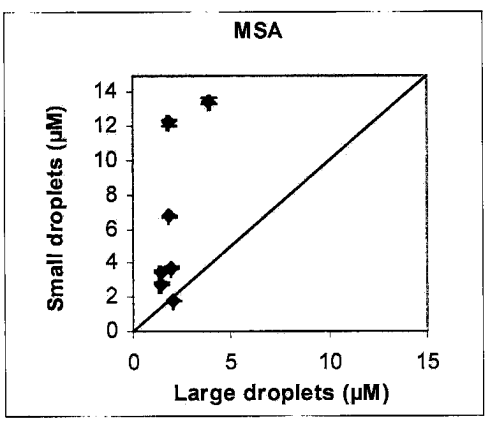

Figure 3-38. Drop size-dependence of MSA in large and small drops. Error bars represent analytical RSD as reported in Chapter 2.

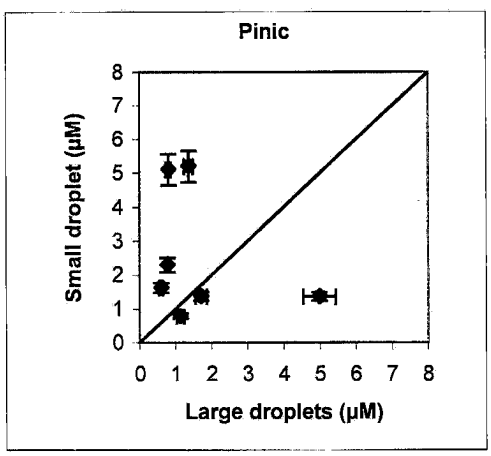

Figure 3-39. Drop size-dependence of pinic acid in large and small drops. Error bars represent analytical RSD as reported in Chapter 2.

Previous studies have shown oxalic acid and other dicarboxylic acids exist in accumulation mode aerosol, and hence were strongly enriched in small droplets (Ludwig and Klemm, 1988; Neusüβ et al., 2000). This explanation, also mentioned in section 3.3.2, cannot account for observations of formic or acetic acid. These low molecular weight organic compounds have high vapor pressures and are found predominantly in the gas phase rather than in particles. Therefore, it's important to study the gas-to-liquid partitioning of these gaseous acids, i.e., the uptake rate. As Ervens et al. (2003) showed, these weak acids are soluble enough at high pH that the time required to reach gas-liquid phase partitioning equilibrium can be quite long. Because smaller drops have a relatively higher surface area:volume ratio, uptake of highly soluble species tends to occur faster there leading to possible enrichment of such highly soluble species in smaller drop sizes. Due to the high solubility of these low molecular-weight acids, they may become "trapped" in the small droplets, requiring a long time to re-equilibrate across the drop size-spectrum.

Chemical reactions inside the droplets will also affect gas-particle partitioning. Both acetate and formate may be oxidized readily by hydroxyl radicals. As formate is oxidized in the large droplets, it cannot be replenished as quickly as in the small drops, because mass transport is much slower into the large drops. This may also lead to a depletion of formate in the small drops.

3.11 Charge balance

3.11.1 Bulk sample charge balance

To understand the extent to which the ionic component of fog solutes has been speciated, a charge balance is calculated. This consists of adding up the concentrations of all the anion species (including dissociated mono- and dicarboxylic acids, OH^-, HCO_3^-, and CO_3^{2-}) and the cation species (including inorganic and hydrogen ions), and computing the anion:cation ratio. A background concentration of 370 ppm was assumed for atmospheric CO_2 to determine equilibrium concentrations of carbonate and bicarbonate in solution. In nature, a zero charge must exist, which simply means there must be as many cationic charges as there are anionic charges. If the anion:cation ratio is larger than one that means that more anions have been accounted for in the sample than cations. If the ratio is less than one, than more cations have been accounted for than anions. The charge balance ratio is as follows:

$$[Acetate^{-1}] + [Formate^{-1}] + [Propionate^{-1}] + [Pyruvate^{-1}] + [Lactate^{-1}] + [Butyrate^{-1}] + [Glutarate^{-1}] + [Glutarate^{-2}] + [Succinate^{-1}] + [Succinate^{-2}] + [Malonate^{-1}] + [Malonate^{-2}] + [Oxalate^{-1}] + [Oxalate^{-2}] + [Cl^-] + [NO_3^-] + [NO_2^-] + [SO_4^{2-}] + [OH^-] + [HCO_3^-] + [CO_3^{2-}] = [Na^+] + [NH_4^+] + [K^+] + [Mg^{2+}] + [Ca^{2+}] + [H^+] \quad (3\text{-}3)$$

Hydrogen bisulfite (HSO_3^-) and sulfite (SO_3^{2-}) may be present, however they were not measured in the fog samples. It is believed that these concentrations would be very small due to low concentrations of SO_2 in the region and rapid

aqueous-phase oxidation to sulfate. Previous observations of S(IV) species in the SJV generally find them at low concentrations (Collett et al., 1999a; Reilly, 2000).

One could assume that all the acids would dissociate completely because the pH of the samples was well above the pKa values of the acids. However, this may not always be the case. Rather than assume that the acids had fully dissociated, it was assumed the concentrations measured were actually the undissociated acid plus its conjugate base ([Measured] = [Acid] + [Conjugate base]). Using the concentration of H^+ measured in each sample, the undissociated acid concentrations were calculated as follows:

$$[Acid] = \frac{[Measured][H^+]}{K_a + [H^+]} \tag{3-4}$$

The calculated acid concentration was then subtracted from the original measurement to determine the concentration of the conjugate base. In most cases, the undissociated acid only accounted for about 2% of the measured concentration. Table 3-4 reports the individual bulk anion:catio ratios taken on the two consecutive sampling periods.

	Anions (μN)	Cations (μN)	Anions/Cations
FSC01001	610.8	724.7	0.8
FSC01002	693.8	867.2	0.8
FSC01003	535.1	694.4	0.8
FSC01004	977.4	1156.8	0.8
FSC01101	2419.0	2460.7	1.0
FSC01102	1345.1	1762.5	0.8
FSC01103	1189.1	1561.5	0.8

Table 3-4. Bulk anion:catio ratios. Samples taken from ss-CASCC collector.

The average anion:cation ratio on the night of Jan. 10-11 was 0.82, while the ratio averaged 0.84 on the following night. This means that roughly 18% of the anions present in the samples have been unspeciated, if we assume that all the cation species have been accounted for. These results are consistent with those reported by Moore et al. (2004), in which they report an anion:cation ratio of 0.82 in radiation fogs collected in Davis, CA.

Collett et al. (1999b) reported higher concentrations of bicarbonate in fog samples than expected from equilibrium with typical atmospheric carbon dioxide concentrations. They attributed this disparity to possible exposure of the samples to indoor carbon dioxide concentrations, which are higher than outdoor concentrations. It is possible that some of the missing anions could be carbonate and bicarbonate, since an equilibrium concentration of 370 ppm CO_2 was assumed for the bicarbonate and carbonate concentration calculations.

3.11.2 Drop size-dependence

Charge balances were also calculated for the small and large size-fractionated samples. On the first night (Jan. 10-11), the average small drop anion:cation ratio was 1.0, and the large drop ratio was 0.70. On the second night, the small drop ratio was 0.98, and the large drop ratio was 0.70. Table 3-5 reports the anion:cation ratios for the individual drop size-fractionated samples.

These results are also similar to the results presented by Moore et al. (2004), who report an anion:cation ratio of 0.90 in the small drops and 0.75 in the large drops; however, the ratios of the small drops in these samples were slightly larger than reported by Moore, and the ratios of the large drops in these samples were slightly smaller than reported by Moore.

	Anions (μN)	Cations (μN)	Anions/Cations
FSCS01001	1828.9	1735.2	1.1
FSCL01001	474.4	580.3	0.8
FSCS01002	1616.4	1587.7	1.0
FSCL01002	391.5	551.4	0.7
FSCS01003	1131.4	1160.7	1.0
FSCL01003	351.8	519.7	0.7
FSCS01004	1331.3	1404.5	0.9
FSCL01004	522.6	888.7	0.6
FSCS01101	5152.5	5252.5	1.0
FSCL01101	1073.6	1316.0	0.8
FSCS01102	4818.4	5051.3	1.0
FSCL01102	668.9	1080.1	0.6
FSCS01103	2978.0	2931.9	1.0
FSCL01103	671.7	1024.1	0.7

Table 3-5. Drop size-fractionated anion:cation ratios for the two consecutive sampling nights.

3.5 Carbonyl concentrations

3.5.1 Analysis by HPLC method

Table 3-4 summarizes the two sampling periods for which carbonyl aliquots were taken. Aliquots were taken from the ss-CASCC collector. Acetone and acrolein are reported together because they coelute from the HPLC column

together, and are thereby indistinguishable by the detector. They are then seen as one inseparable peak on the chromatogram.

	Formaldehyde	Acetaldehyde	Acrolein/Acetone	Isovaleraldehyde	m-Tolualdehyde
Jan.10-11	17.80	3.64	1.40	1.87	0.08
Jan.11-12	34.35	4.23	3.25	3.18	0.15
	p-Tolualdehyde	Hexaldehyde	Glyoxal	Methyl Glyoxal	
Jan.10-11	0.12	0.27	11.84	10.13	
Jan.11-12	0.39	0.96	16.71	14.51	

Table 3-6. Summary of carbonyl concentrations (units: μM). Values were averaged over total sampling period for each event.

Figure 3-40 shows the composition of the carbonyl species for each fog event. Over both events, formaldehyde, glyoxal, methyl glyoxal and acetaldehyde were the dominant species, accounting for roughly 26%, 14%, 12% and 4% of the total carbonyl species, respectively.

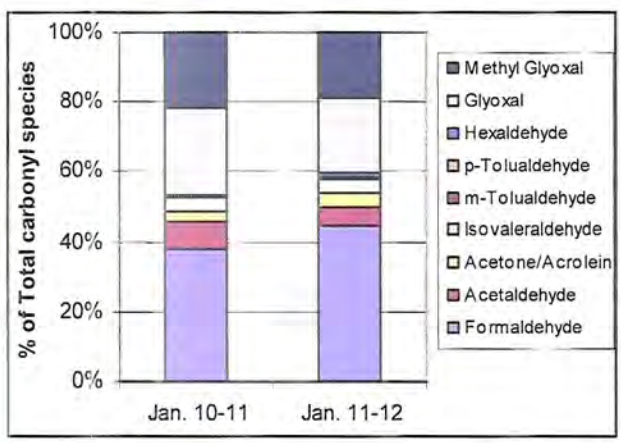

Figure 3-40. Composition of carbonyl compounds for both consecutive fog events. Values for each event averaged over total sampling period.

3.5.2 Formaldehyde analysis by fluorometry

This method measures formaldehyde differently than the HPLC method. HCHO can react with HSO_3^- in the fog drops to form hydroxymethanesulfonic acid (HMS),

$$HCHO\ (aq) + HSO_3^- \rightarrow HOCH_2SO_3H \qquad (3\text{-}5)$$

HMS is a strong acid, so it will readily dissociate completely in the droplets to form hydroxymethanesulfonate (HMSA). The reaction rate of HMSA increases exponentially with pH, due to increasing concentrations of HSO_3^-, and becomes appreciable above pH 5 (Seinfeld and Pandis, 1998). HMS formation acts to increase the solubility the HCHO (Munger et al., 1986). However, this reaction also depends on the availability of gaseous SO_2.

Chang (2004) found that different buffer solutions used in the HPLC procedure led to different amounts of HMS. He found that the citrate buffer used in the HPLC analyses significantly underestimated the HMS originally in the fog water. This means that the difference between the HCHO measured by the fluorescence and HPLC methods can approximate the HMS concentrations originally in the fog. Table 3-7 reports the HCHO concentrations per sample for each procedure and the approximate HMS concentrations (fluorescence – HPLC). In most samples, HMS accounted for roughly half of the HCHO measured by the fluorometer.

Sample	HCHO by HPLC (μM)	HCHO by fluorescence (μM)	HMS (μM)
FSC36401	24.59	37.85	13.26
FSC01001	13.47	23.17	9.70
FSC01002	17.40	38.12	20.72
FSC01003	16.76	28.84	12.08
FSC01003DUP	17.31	27.79	10.48
FSC01004	24.08	40.47	16.39
FSC01101	38.16	61.59	23.43
FSC01102	28.21	50.56	22.35
FSC01103	36.69	61.36	24.67
FSCL01001	18.27	26.95	8.68
FSCL01002	18.62	29.30	10.68
FSCL01003	16.20	26.40	10.20
FSCL01003DUP	16.05	25.44	9.39
FSCL01004	20.04	36.73	16.69
FSCL01101	40.80	62.07	21.27
FSCL01102	21.21	44.10	22.89
FSCL01103	36.51	58.12	21.61
FSCS01001	21.84	36.91	15.07
FSCS01002	17.25	41.88	24.63
FSCS01003	14.33	30.77	16.44
FSCS01003DUP	14.26	32.74	18.48
FSCS01101	30.72	89.47	58.75
FSCS01102	27.73	66.74	39.01
FSCS01103	27.98	57.13	29.15

Table 3-7. Formaldehyde concentrations, measured by the HPLC and fluorescence procedures, and HMS concentrations for each sample.

3.5.3. Temporal variations

Figures 3-41 and 3-42 show the temporal variations of the carbonyl species and LWC. As the LWC decreases, the concentration of the carbonyls tends to increase. This is most apparent with formaldehyde, glyoxal and methyl glyoxal.

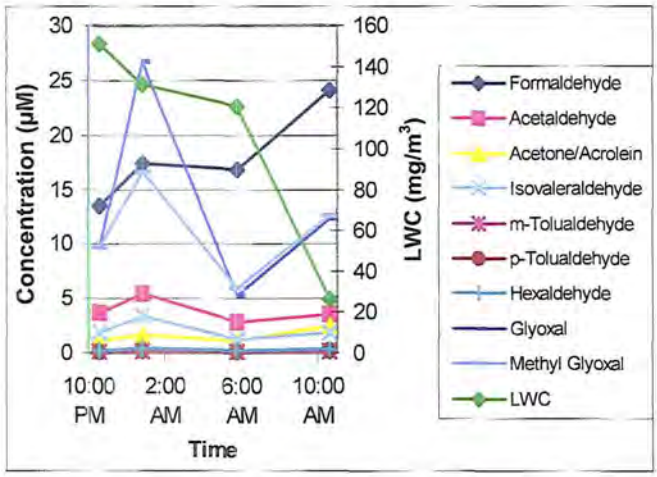

Figure 3-41. Temporal variation of carbonyl species on Jan. 10-11.

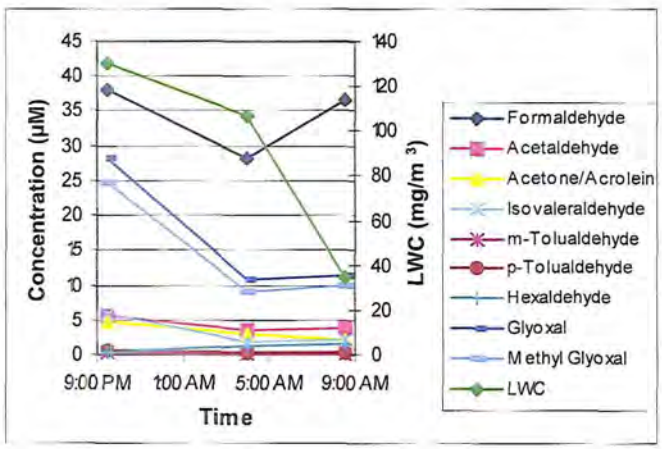

Figure 3-42. Temporal variation of carbonyl species on Jan. 11-12.

3.5.2 Drop size-dependence

Figures 3-43 to 3-51 show the drop size-dependence of the carbonyl species, measured from the sf-ss-CASCC collector. Most of the species show enrichment in the small drops, some more strongly than others. The formaldehyde plot is based on measurements made with the fluorescence method.

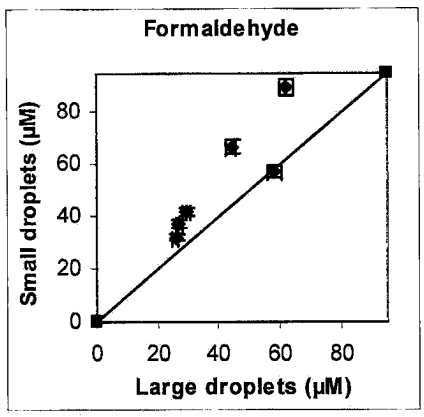

Figure 3-43. Drop size-dependence of formaldehyde in large and small drops. Error bars represent the analytical RSD value as reported in Chapter 2.

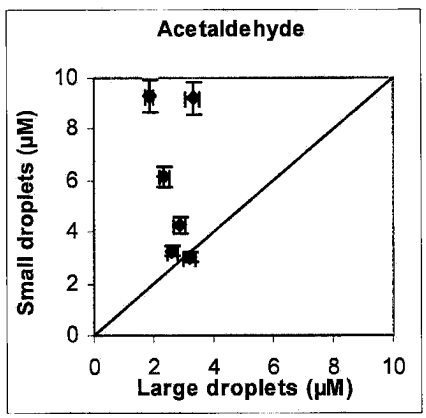

Figure 3-44. Drop size-dependence of acetaldehyde in large and small drops. Error bars represent the analytical RSD value as reported in Chapter 2.

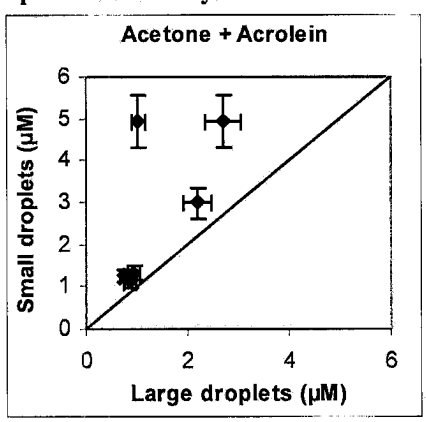

Figure 3-45. Drop size-dependence of acetone + acrolein in large and small drops. Error bars represent the analytical RSD value as reported in Chapter 2.

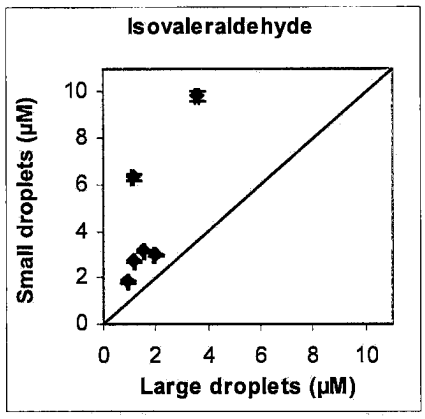

Figure 3-46. Drop size-dependence of isovaleraldehyde in large and small drops. Error bars represent the analytical RSD value as reported in Chapter 2.

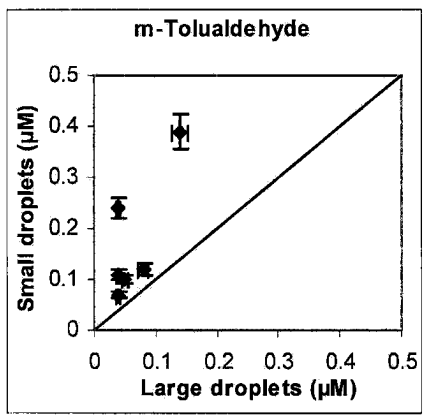

Figure 3-47. Drop size-dependence of m-tolualdehyde in large and small drops. Error bars represent the analytical RSD value as reported in Chapter 2.

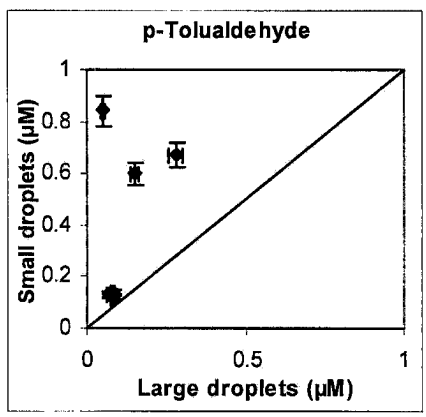

Figure 3-48. Drop size-dependence of p-tolualdehyde in large and small drops. Error bars represent the analytical RSD value as reported in Chapter 2.

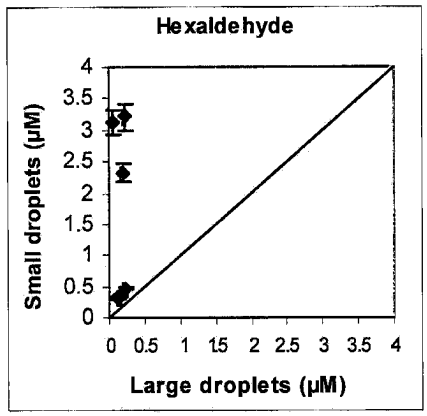

Figure 3-49. Drop size-dependence of hexaldehyde in large and small drops. Error bars represent the analytical RSD value as reported in Chapter 2.

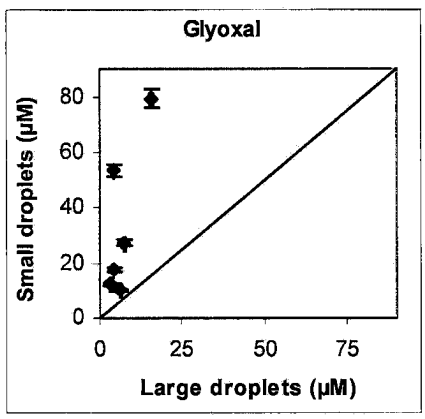

Figure 3-50. Drop size-dependence of glyoxal in large and small drops. Error bars represent the analytical RSD value as reported in Chapter 2.

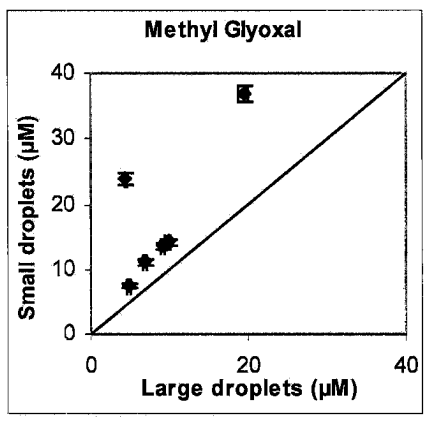

Figure 3-51. Drop size-dependence of methyl glyoxal in large and small drops. Error bars represent the analytical RSD value as reported in Chapter 2.

Gaseous formaldehyde reaches equilibrium with the fog droplets after about 10 seconds, so the equilibrium effects seen for formic and acetic acid are not applicable to the HCHO size-dependence (Ervens et al, 2003). HMS formation acts to increase the amount of HCHO dissolved in the droplets, and its formation rate increases at high pH values. Therefore, HMS may be formed faster in large drops, due to their higher pH. However, because mass transport to the larger drops is much slower, due to the smaller surface area:volume ratio, HCHO will partition more quickly to the small drops, leading to an enrichment in HCHO and HMS (shown in Figure 3-52). It is important to keep in mind, however, that these values are estimates and that error associated with the HMS concentrations has not been quantified.

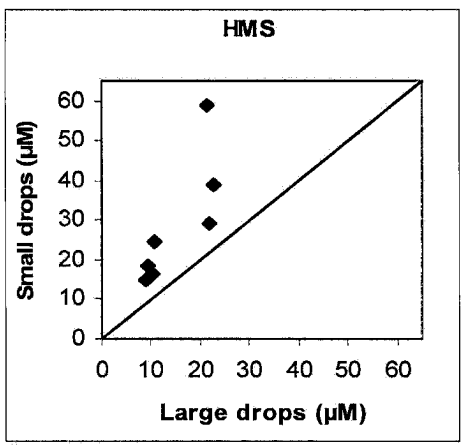

Figure 3-52. Drop size-dependence of HMS in large and small drops (see page 61).

3.6 Levoglucosan

Levoglucosan was measured from the first and second organic acid aliquots taken on Jan. 11. Table 3-8 reports the levoglucosan values of the samples

measured. The average concentration of the samples was 0.60 μg/mL. Levoglucosan was also measured from the organic acid aliquots taken from the size-fractionated collector. The average concentration in the small drops was 0.82 ug/mL and the average concentration in the large drops was 0.11 ug/mL, showing an obvious enrichment in the small drops.

	Sample	Levoglucosan (μg/mL)
Jan. 11-12	Bulk #1	0.67
	Bulk #2	0.53
	Small drops #1	1.9
	Small drops #2	1.8
	Large drops #1	0.29
	Large drops #2	0.20

Table 3-8. Levoglucosan values measured from samples taken Jan. 11-12.

3.7 Dissolved Organic Nitrogen (DON)

Table 3-9 shows the average NO_2^-, NO_3^-, NH_4^+, DON, and total dissolved inorganic nitrogen (TDIN).

	NO_2^-	NO_3^-	NH_4^+	DON	TDIN
Dec. 31	1.40	2.09	9.74	2.68	13.2
Jan. 10-11	0.90	4.12	11.2	1.74	16.3
Jan. 11-12	0.95	11.8	23.5	4.53	36.3

Table 3-9. Summary of ionic, TDIN (total dissolved inorganic nitrogen), and DON concentrations. Values given in mgN/L.

Nitrate and ammonium were the dominant ions in the dissolved inorganic nitrogen fraction, accounting for about 24% and 60% of the TDIN, respectively.

Figure 3-53 shows the percent composition of the total dissolved nitrogen in the samples from the three nights, measured from samples taken from the ss-CASCC collector. Averaged over the three nights, ammonium accounted for about 60% of the dissolved nitrogen in the samples, nitrate accounted for 21%, DON accounted for 13%, and nitrite accounted for 5%. These values coincide with values reported by Zhang and Anastasio (2001), who studied fog water in the Central Valley.

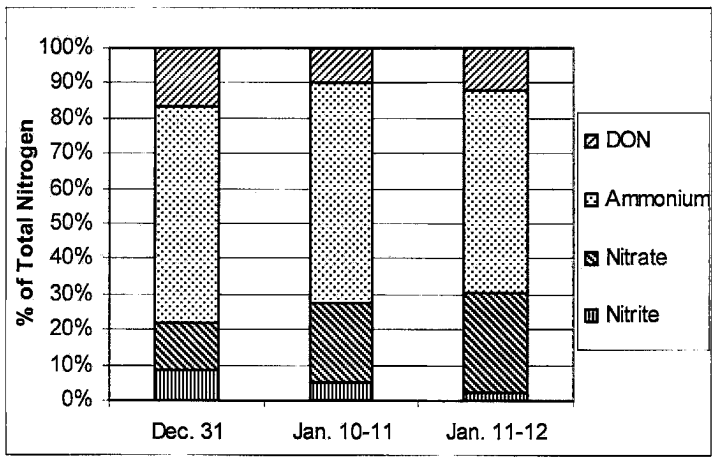

Figure 3-53. Percent composition of event-averaged total dissolved nitrogen species.

3.7.1 Temporal variations

Figure 3-54 shows the temporal variations of DON and LWC for the two consecutive sampling events. It has been shown with the other solute species that as the fog dissipates, the solute concentrations increase. This trend was not present in the dissolved organic nitrogen species.

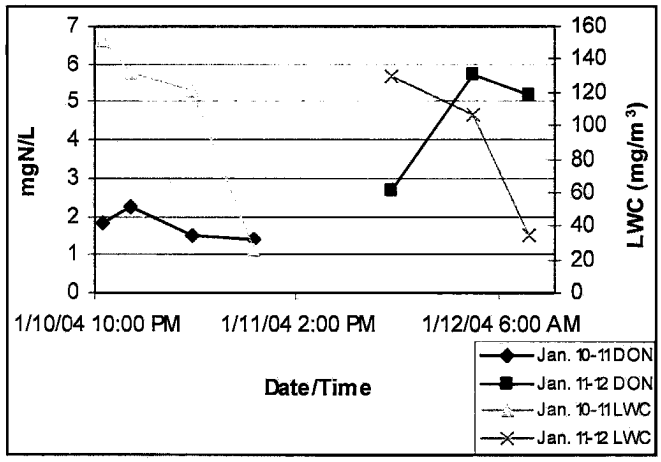

Figure 3-54. Temporal variations of DON over two consecutive sampling events.

3.7.2 Drop size-dependence

Figure 3-55 shows the drop size-dependence of DON, which was slightly enriched in the large droplets. This is somewhat surprising considering the DOC was enriched in the small droplets (shown in section 3.8).

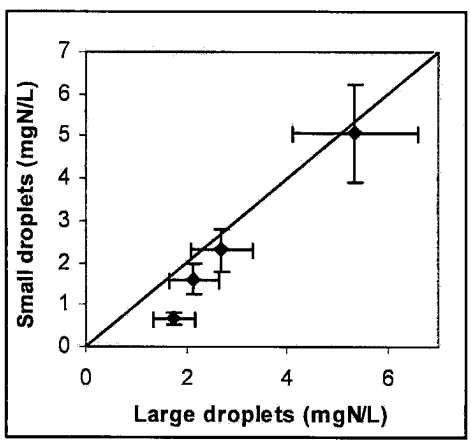

Figure 3-55. Drop size-dependence of dissolved organic nitrogen. Error bars represent the analytical RSD value as reported in Chapter 2.

3.8 Total Organic Carbon/ Dissolved Organic Carbon

Table 3-10 shows the average fog TOC and DOC concentrations measured the nights of Jan. 10-11 and Jan. 11-12. The insoluble carbon (TOC – DOC) makes up the fraction of the carbonaceous species that do not dissolve in the fog droplets. The TOC ranged from 9.2 to 41.0 ppmC, and the DOC ranged from 6.4 to 35.4 ppmC. These values are similar to TOC and DOC values reported by Herckes et al. (2002b). The DOC averaged to be about 74% of the TOC.

	TOC	DOC	Insoluble C	% DOC of TOC
Jan. 10-11	12.3	9.4	3.0	74.7
Jan. 11-12	28.5	21.4	7.1	72.0

Table 3-10. Summary of event-averaged TOC, DOC, and Insoluble C in fog drops. Values are in ppmC.

Figure 3-56 shows the percentage of the average bulk TOC (from the ss-CASCC) that is dissolved (DOC) and insoluble. The insoluble carbonaceous compounds likely include elemental carbon and various hydrophobic organics. Herckes et al. (2002a) speciated numerous organic compounds in the soluble and insoluble phases of fog water samples, including long chain *n*-alkanes, ranging from 14 to 36 carbon atoms, polycyclic aromatic hydrocarbons (PAH), and *n*-alkanoic acids ($C_9 - C_{28}$). They determined that more than 90% of the *n*-alkanes were associated with the insoluble fraction while less than 10% were found in the water-soluble fraction. Lower molecular weight PAH were found in both dissolved and insoluble fractions, while higher MW PAH were found predominantly in the insoluble phase. Lower MW *n*-alkanoic acids were also found predominantly in the dissolved phase, whereas higher MW acids were

enriched in the insoluble phase. Hence, we would expect the insoluble carbon compounds in the Fresno samples to be comprised mainly of higher molecular weight organic compounds.

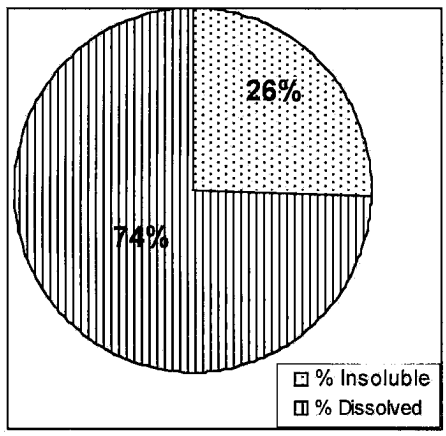

Figure 3-56. TOC composition by percentage.

3.8.1 Temporal variations

Figures 3-57 and 3-58 show the temporal variations (measured from the ss-CASCC collector) of TOC and DOC as well as LWC on the nights of Jan. 10-11 and Jan. 11-12. The same trend is observed for other species is very clear on the first night: as the LWC decreases at the end of the fog event, the TOC and DOC concentrations increase significantly. This trend is not as evident on the second night.

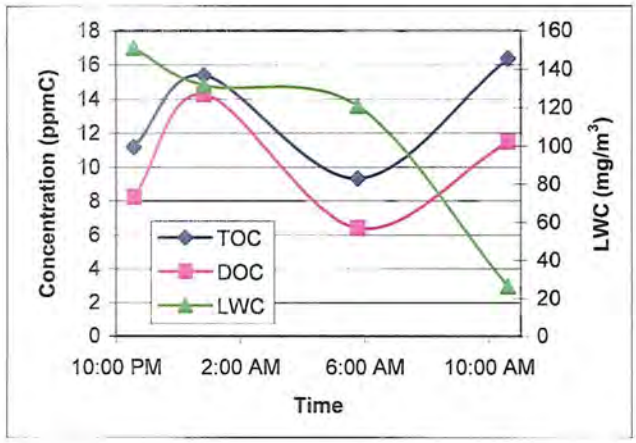

Figure 3-57. Temporal variations in TOC and DOC on Jan. 10-11.

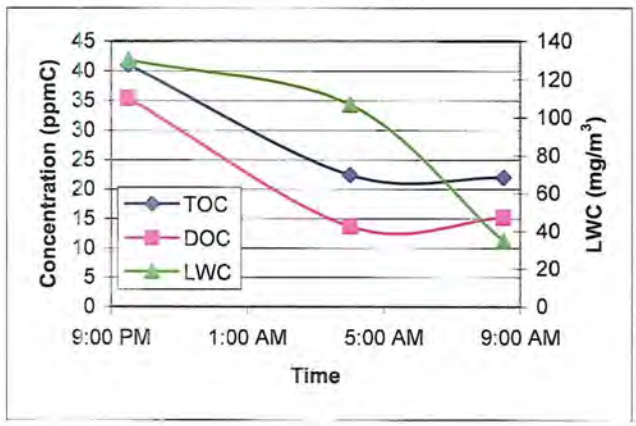

Figure 3-58. Temporal variations in TOC and DOC on Jan. 11-12.

3.8.2 Drop size-dependence

Figures 3-59 and 3-60 show the drop size-dependence of TOC and DOC of samples taken from the sf-ss-CASCC collector. Carbonaceous species are obviously enriched in the small droplets. On average, the TOC concentrations in the small droplets were about three times larger than those in the large droplets, similar to observations by Herckes et al. (2002a).

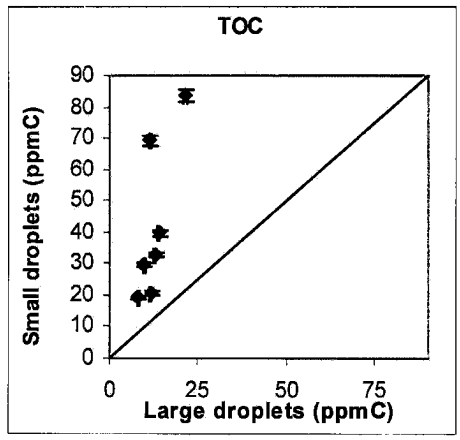

Figure 3-59. Drop size-dependence of TOC in large and small drops. Error bars represent the analytical RSD value as reported in Chapter 2.

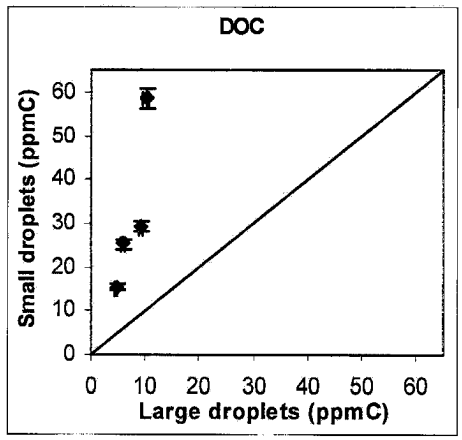

Figure 3-60. Drop size-dependence of DOC in large and small drops. Error bars represent the analytical RSD value as reported in Chapter 2.

3.8.3 Solute mass percentage

A main goal of this study was to speciate the organic matter present in the fog water. To make the argument that organic matter is an important fraction of the fog solutes, the contribution that each solute made to the total solute mass concentration was determined. The TOC analysis measures the mass concentration of carbon in the solute species, however, there may be other atoms and/or functional groups (e.g., H, S, amines, carboxylic acids, etc.) present in the solutes that contribute to a total organic mass concentration. To understand how

much organic matter may be present, a ratio to convert measured TOC to total organic matter (TOM) must be used. This ratio is essentially an average molecular weight:carbon weight. Previous studies of the TOM:TOC ratio in aerosol have shown that this ratio may vary anywhere from 1.2 to 2.1 (Turpin and Lim, 2001; Russell, 2003) depending on the species present, the type of emissions (anthropogenic or biogenic), and the age of the particles. Turpin and Lim (2001) determined that a ratio of 1.6 may be suitable for urban aerosol, while a ratio of 2.1 may be more suitable for nonurban aerosol. For the purposes of the current study, a TOM:TOC ratio of 1.8 was assumed. This ratio is thought to be appropriate based on the major solute species present in the fog water, specifically carbonyls and nitrogen-containing compounds, and the molecular weight per carbon weight of particle-phase organic compounds as reported by Turpin and Lim (2001). Also, wood smoke influence may have acted to increase the ratio.

Figure 3-61 shows the percentage of the solute mass of each of the major solutes, including total organic matter. As shown, the nitrate accounts for about 31% of the total solute mass, ammonium accounts for about 22%, and TOM accounts for about 35% of the total solute mass. In other words, organic matter accounts for a substantial fraction of the solutes present in the fog droplets.

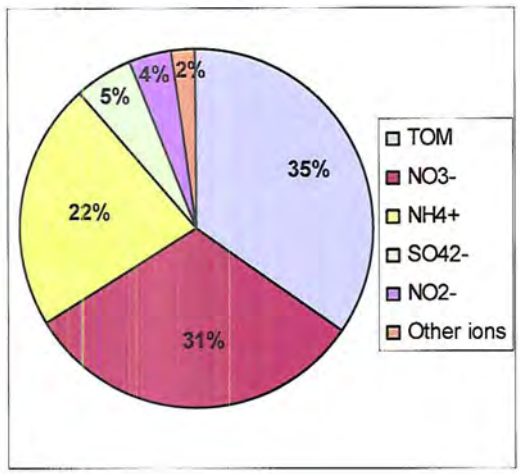

Figure 3-61. Percent of total measured solute mass concentration of major solute species. Other ions include Na^+, Cl^-, Mg^{2+}, Ca^{2+}, and K^+.

3.8.4 DOC Composition

One of the goals in the study of organic fog chemistry is to achieve mass closure; i.e., be able to account for every compound that adds to the total carbon mass.

Therefore, it is important to know what percentage of the carbon species we can account for that makes up the DOC. Species that we can account for specifically in the DOC fraction are the low molecular weight organic acids and carbonyls. DOC concentrations are measured in parts per million of carbon (ppmC), or mg/L of carbon, while the organic acids and carbonyls are measured in μmol/L. Therefore, the organic acid and carbonyl concentrations need to be converted to ppmC via this equation,

$$ppmC = \frac{mgC}{L} = \frac{mol_i}{L} * \frac{mol_C}{mol_i} * \frac{12gC}{mol} * 1000 \qquad (3\text{-}6)$$

where *i* refers to the specific compound of interest.

Of the speciated organic acids, acetate accounted for the largest percentage of the DOC (21-31%), followed by formate (6-7%), oxalate (3-4%) and propionate (2-3%). Formaldehyde was the most prevalent carbonyl compound (3-4%), followed by methyl glyoxal (2-4%) and glyoxal (2-3%). The remaining speciated organic acids (pyruvate, glutarate, succinate, malonate, lactic acid, butyric acid, and pinic acid) accounted for about 5% of the total DOC, and the remaining speciated carbonyls (acetaldehyde, acetone/acrolein, isovaleraldehyde, m-tolualdehyde, p-tolualdehyde, and hexaldehyde) accounted for about 3% of the total DOC. Levoglucosan accounted for about 1% of the DOC, but it was only measured on the night of Jan. 11-12. Roughly 43% of the DOC remains unspeciated. Figure 3-62 shows the total dissolved organic carbon species comprised of organic acids, carbonyls and levoglucosan.

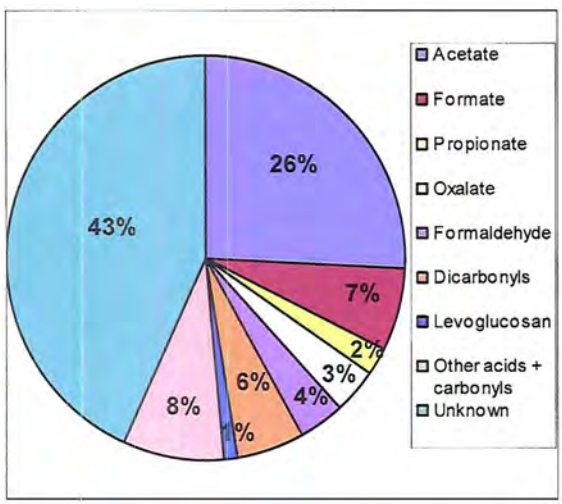

Figure 3-62. Percentage of DOC comprised of speciated organic acids and carbonyls. Values averaged over the two consecutive fog events. Unknown fraction represents unspeciated fraction of DOC.

In addition to formaldehyde, formate and acetate, Herckes et al. (2002a) also determined the contributions *n*-alkanes, PAH, and *n*-alkanoic acids made to the TOC. They determined that the *n*-alkanes accounted for an average 0.1% of the TOC, PAH accounted for less than 0.02%, and the *n*-alkanoic acids accounted for an average of 0.24% of the TOC. In total, these higher molecular weight compounds contributed to less than 1% on average to the organic matter.

Dissolved organic nitrogen compounds also comprise a fraction of the DOC species. The DON concentrations are measured in units of μmol (of N) L^{-1}, so they need to be converted into units of ppmC. The following equation is used:

$$ppmC = \frac{mgC}{L} = \frac{molN}{L} * \frac{molC}{molN} * \frac{12gC}{mol} * 1000 \qquad (3\text{-}7)$$

where the *C:N* ratio represents the intramolecular carbon-to-nitrogen ratio. A problem arises, however, with this C:N mole ratio. Because the organic nitrogen compounds are not individually speciated, an accurate C:N ratio is not known. A ratio must be estimated in order to convert the DON concentrations to DOC concentrations.

Zhang and Anastasio (2001,2003) characterized a fraction of the DON compounds found in Davis, Ca fog waters. They found an average of 531 μM N of DON in their samples, which they further speciated into two categories: free amino compounds (FACs; i.e., amino acids and alkyl amines) and combined amino compounds (CACs; i.e., proteins and peptides). 22 dissolved organic nitrogen species were measured in all. They determined that FAC accounted on average for 4% of the DON in the samples, and CACs accounted on average for 16% of the DON. Roughly 80% of the DON in the samples remained unspeciated.

They also determined that the total amino compounds speciated accounted for about 13% of the DOC in their fog water samples.

The average C:N ratio of the compounds speciated by Zhang and Anastasio was about 4 (i.e., four carbon atoms for every one nitrogen atom in a molecule). If this ratio had been used to equate DON to DOC in our Fresno samples, the DON would have accounted for more than 100% of the DOC in many of the samples, which is not physically possible. The average C:N ratio of the six most concentrated DON species in the samples analyzed by Zhang and Anastasio was about 3. This ratio would also give a very high DON percentage in our samples. Therefore, for the bulk fog water samples, a C:N ratio of 2 was assumed. The individual compounds that had been speciated in the DOC fractions were known to not contain nitrogen, so they were subtracted from the DOC of each sample to determine the percentage of DOC that the DON could possibly account for. With this estimated C:N ratio, DON accounted for about 32% of the DOC, averaged over the two consecutive fog events. This percentage is roughly three times larger than what Zhang and Anastasio reported. However, their DON concentrations were roughly 2.5 times larger than those measured in the samples from the current study.

Figure 3-63 shows the DOC composition of the samples taken on both nights with the DON accounted for also. Since DON has been accounted for as part of the DOC, 11% of the DOC remains unspeciated.

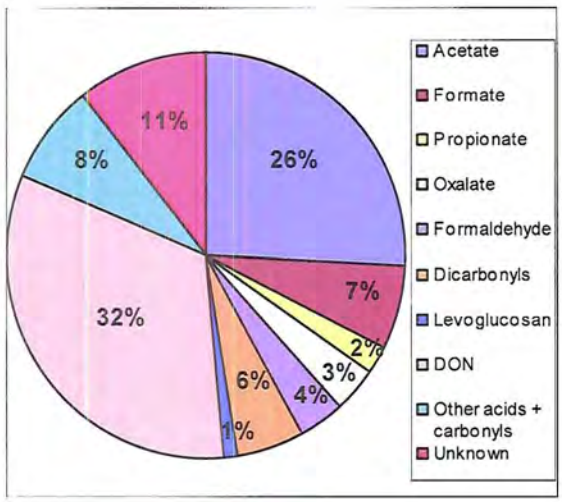

Figure 3-63. Percent composition of DOC. Values averaged over two consecutive fog events.

Of the speciated drop size-dependent organic acids, acetate accounted for the largest percentage of the DOC (30%: large drops, 12%: small drops), followed by formate (7%: large drops, 3%: small drops), propionate (2%: large drops, 1%: small drops) and oxalate (1%: large drops, 1%: small drops). These values were averaged over the two consecutive fog events. Formaldehyde was again the most prevalent carbonyl compound (5%: large drops, 2%: small drops), followed by methyl glyoxal (3%: large drops, 2%: small drops) and glyoxal (2%: large drops, 2%: small drops). The remaining speciated organic acids (pyruvate, glutarate, succinate, malonate, lactic acid, butyric acid, and pinic acid) accounted for about 4% of the total DOC in both drop size-fractions, and the remaining speciated carbonyls (acetaldehyde, acetone/acrolein, isovaleraldehyde, m-tolualdehyde, p-tolualdehyde, and hexaldehyde) accounted for about 2% of the total DOC in the large drops and 3% in the small drops. Levoglucosan accounted for about 3% of

the DOC in the large drops and 2% in the small drops, but it was only measured on the night of Jan. 11-12.

For the DON calculations, a C:N ratio of 1 was used for the large droplets and 2 for the small droplets. Again, these ratios are estimates and somewhat arbitrary. If a larger ratio had been used for large droplets, the DON concentrations would have been larger than the DOC concentrations, which couldn't be physically possible. With these ratios, DON accounted for about 38% of the DOC in the large droplets and about 13% of the DOC in the small drops. The 13% found in the small drops is similar to the value calculated by Zhang and Anastasio (2003). The C:N could theoretically be smaller than one, however, based on the major nitrogen species thought to be present (e.g., methylamine), a minimum ratio of one was considered appropriate for the large droplets.

Figure 3-64 shows the size dependence of the constituents that are accounted for in the DOC fraction. Roughly 56% of the DOC of the small droplets are still uncharacterized, while about 3% of the large droplets are uncharacterized. This number probably is not very accurate, though, because the DON contribution to the DOC is quite uncertain.

DON has been shown to possibly account for a significant fraction of the dissolved organic carbon compounds in fog water, however more work must be done to further speciate individual DON compounds. For example, HPLC may be used to speciate primary amino acids and alkyl amines, as explained by Zhang and Anastasio (2003).

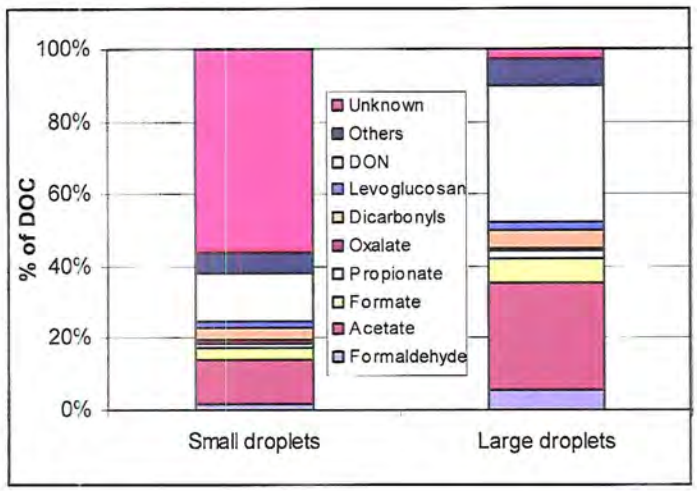

Figure 3-64. Percent composition of DOC based on drop size from sf-ss-CASCC. Values averaged over consecutive fog events. "Others" refers to remaining speciated organic acids and carbonyls.

3.8.3.1 Ultrafiltration

After all the aliquots were taken, there were three samples with enough volume left to conduct ultrafiltration measurements with: one from the night of Jan. 10-11, and two from the following night. All three were samples from the large fraction of the sf-ss-CASCC.

The efficiency of the filters was first determined. This was done by measuring the carbon concentrations of three standards, filtering them through the ultrafiltration filters, and then measuring the carbon concentration of the filtrate. The three standards used were oxalic acid (MW= 126.07 g mol^{-1}), naringin hydrate (MW= 580.55 g mol^{-1}), and β-cyclodextrin hydrate (MW= 1134.98 g mol^{-1}). For the 1000 Da filter to be 100% efficient, the carbon concentrations of the oxalic acid and naringin hydrate filtrates should both have been equal to their original concentrations when filtered through the 1000 Da filter, while the β-cyclodextrin hydrate concentration should have been zero. For the 500 Da filter to

be 100% efficient, the oxalic acid filtrate concentration should have been equal to the original concentration, while the naringin hydrate and β-cyclodextrin hydrate filtrate concentrations should have both been zero. Table 3-11 shows the efficiency measurements for both filters. The 500 Da filter performed well; it passed 80% of the low molecular weight oxalic acid, retained 82% of the 580 Da naringin hydrate, and retained 99% of the high molecular weight β-cyclodextrin hydrate. The 1000 Da filter passed 82% of the oxalic acid and retained 84% of the 1135 Da β-cyclodextrin hydrate. These performances indicate the filters do a reasonably good job making a broad separation of organic compounds by molecular weight.

Table 3-12 reports the carbon concentrations and the percentage of DOC of each molecular weight fraction for each sample, as well as their standard deviations based on replicate measurements. On average, when the pH of the samples was not modified, about 26% of the sample's carbon compounds had molecular weights greater than 1000 Da (Fraction 1), about 4% had molecular weights between 500 and 1000 Da (Fraction 2), and about 70% had molecular weights smaller than 500 Da (Fraction 3).

500 Da Filter					
	MW (g/mol)	*Total (ppmC)*	*Filter (ppmC)*	*Retention Efficiency (%)*	*Passing Efficiency (%)*
Oxalic acid	126.1	22.17	17.8	N/A	80.3
Naringin hydrate	580.6	22.3	3.9	82.3	N/A
β-cyclodextrin hydrate	1135.0	14.6	0.2	98.7	N/A
1000 Da Filter					
	MW (g/mol)	*Total (ppmC)*	*Filter (ppmC)*	*Retention Efficiency (%)*	*Passing Efficiency (%)*
Oxalic acid	126.1	22.2	18.1	N/A	81.8
β-cyclodextrin hydrate	1135.0	14.6	2.3	84.1	N/A

Table 3-11. Efficiency calculations for 500 and 1000 Da filters.

Herckes et al. (2002b) reported a retention efficiency for the 1000 Da filter of 48%, and a passing efficiency for the 500 Da filter of 71%. This 500 Da filter efficiency is similar to the efficiency reported above, but the retention efficiencies of the 1000 Da filters do not agree well at all. Herckes et al.'s results did show that the nominal membrane size-cuts provide only an approximate indication of the size of the organic matter retained. The effective separation also depends on molecular structure, in addition to its molecular weight. DOC fractionation using the membranes can provide an approximate indication of the molecular weight distribution of the organic solutes in the fog water, but a systematic tendency to underestimate the higher molecular weight fractions may exist.

Sample	pH	Total (ppm)	Fr. 1 (ppm)	Fr. 1 (%)	Fr. 2 (ppm)	Fr. 2 (%)	Fr. 3 (ppm)	Fr. 3 (%)
FSCL01001	~7	7.358	2.280	31	0.590	8	4.488	61
FSCL01001	~7	6.621	1.880	28.4	0.090	1.4	4.651	70.2
FSCL01001	~7	6.151	1.898	30.9	0.367	6	3.886	63.1
FSCL01001	~7	6.172	1.834	29.7	0.471	7.6	3.867	62.6
Stand. Dev.		0.56	0.21	1.22	0.21	3.03	0.41	4.08
FSCL01001	2	5.547	1.682	30.3	0.579	10.4	3.286	59.2
FSCL01001	2	5.597	1.687	30.1	1.025	18.3	2.705	48.3
FSCL01001	2	5.766	1.163	20.2	0.951	16.5	3.652	63.3
FSCL01001	2	5.186	1.341	25.9	0.383	7.4	3.462	66.8
Stand. Dev.		0.24	0.26	4.74	0.30	5.11	0.41	8.03
FSCL01101	~7	10.460	3.184	30.4	0.635	6.1	6.641	63.5
FSCL01101	~7	10.600	3.121	29.4	0.670	6.3	6.809	64.2
Stand. Dev.		0.10	0.04	0.71	0.02	0.14	0.12	0.49
FSCL01101	2	10.680	2.286	21.4	0.527	4.9	7.867	73.7
FSCL01101	2	10.070	1.747	17.35	1.021	10.14	7.302	72.15
Stand. Dev.		0.43	0.38	2.86	0.35	3.71	0.40	1.10
FSCL01102	~7	8.052	0.601	7.5	0.796	9.8	6.655	82.7
FSCL01102	~7	8.340	1.310	15.7	0.138	1.7	6.891	82.6
FSCL01102	~7	8.488	1.53	18	0.261	3.1	6.697	78.9
Stand. Dev.		0.22	0.49	5.52	0.35	4.33	0.13	2.17
FSCL01102	2	8.470	2.636	31.1	1.057	12.5	4.777	56.4
FSCL01102	2	8.291	2.586	34.4	0.364	4.4	5.341	64.4
FSCL01102	2	7.702	2.589	33.6	0.312	4.1	4.801	62.3
FSCL01102	2	7.018	2.147	30.6	0.146	2.1	4.725	67.3
FSCL01102	2	7.211	2.102	18	0.022	3.1	5.087	78.9
Stand. Dev.		0.64	0.26	6.65	0.40	4.16	0.26	8.31

Table 3-12. Ultrafiltration results of original and acidified samples. Fr. 1 refers to the Da > 1000 fraction, Fr. 2 refers to the 1000 > Da > 500 Da fraction, and Fr. 3 refers to the 500 > Da fraction.

Table 3-13 reports the calculated relative standard deviation of the total organic carbon the samples, as well as the individual molecular weight fractions.

The extremely low carbon concentrations in Fraction 2 of the samples led to very high RSD values. In many of the samples, the carbon concentrations in Fraction 2 were actually below the minimum detection limit of the instrument, defined in section 2.4.2.4.

	Total RSD (%)	*Fr. 1 RSD (%)*	*Fr. 2 RSD (%)*	*Fr. 3 RSD (%)*
pH ≈ 7	4.2	7.1	33.2	4.7
pH = 2	6.4	15.0	55.7	7.7

Table 3-13. RSD summary of molecular weight fractions.

It has been shown that organic ligands may be capable of binding with trace metals in precipitation (Spokes et al., 1996). If this is the case in our fog water samples, then at least part of Fraction 1 may be comprised of these organic complexes. By acidifying the samples sufficiently, these complexes are likely to fall apart, and therefore Fraction 1 might decrease. Acidification to pH 2 was used to determine whether metal-organic ligand complexes were artificially inflating the apparent contribution of high molecular weight organics.

Figures 3-65 to 3-67 compare the molecular weight fractions of the individual samples determined for the original fog sample and the acidified aliquot. In sample FSCL01001, there was a slight decrease in Fraction 1 and an increase in Fraction 2, which could be explained by the breakup of organic complexes. However, if one takes the measurement precision into account, then there is no significant difference between the original and acidified sample. In sample FSCL01101, there was a more significant decrease in Fraction 1, and a significant

increase in Fraction 3. Again, this could be explained by the breakdown of the organic complexes. In sample FSCL01102, however, the trend was not the same. Fraction 1 significantly increased, while Fraction 3 decreased. This may be due to acid-catalyzed polymerization reactions forming organic macromolecules. Several studies have shown evidence that acid-catalyzed oligomerization reactions form macromolecular compounds in secondary organic aerosol (e.g., Gao et al, 2004; Tolocka et al, 2004); these reactions may also possibly occur in the aqueous samples.

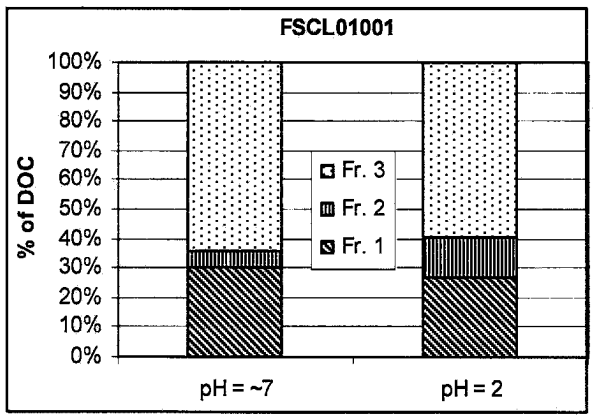

Figure 3-65. Ultrafiltration fractions of sample FSCL01001.

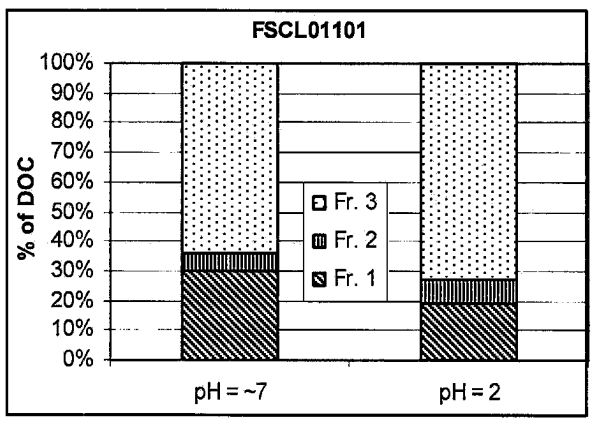

Figure 3-66. Ultrafiltration fractions of sample FSCL01101.

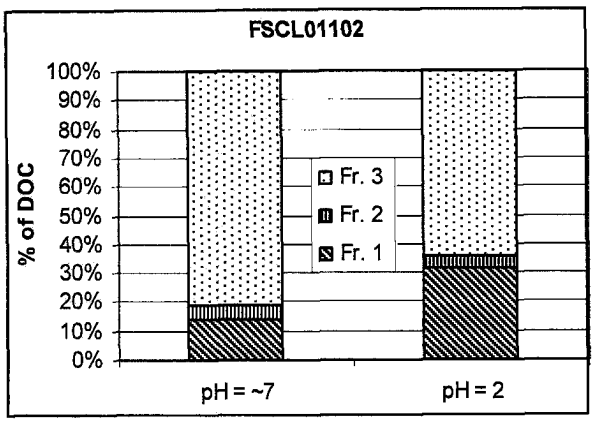

Figure 3-67. Ultrafiltration fractions of sample FSCL01102.

Overall, the general distribution of organic compound molecular weights was not affected very much by the acidification tests. Accordingly, we judge it best for samples similar to those examined here to conduct ultrafiltration tests at the original sample pH and avoid possible sample modification from acidification.

3.9 Fog scavenging efficiencies

To study how the fog water scavenged organic carbon, a Hi-Vol sampler was attached to the ss-CASCC downstream of the stainless steel strands, to collect aerosol particles not scavenged by the fog water and impacted on the strands. This aerosol is referred to as interstitial aerosol. The same sampler was also used to collect pre-fog aerosol. The interstitial aerosol and pre-fog aerosol samples were then extracted with deionized water, filtered through a pre-fired quartz filter, and analyzed with the TOC analyzer, as explained in section 2.3.2.2. This sample contains the water-soluble fraction of the aerosol filter samples, or the DOC fraction.

The efficiency of fog scavenging of WSOC is calculated with the following equation:

$$\eta_{DOC} = 1 - \left(\frac{DOC_{IA}}{DOC_{PFA}} \right) \times 100 \qquad (3\text{-}8)$$

where η_{DOC} is the fog scavenging efficiency (reported as a percent), DOC_{IA} is the DOC of the interstitial aerosol, and DOC_{PFA} is the DOC of the pre-fog aerosol. This efficiency calculation is best applied only in the first few hours of a fog episode since droplet scavenging of carbonaceous material followed by droplet deposition on the ground could appreciably decrease the total boundary layer concentration of these compounds during an extended fog event. Fog scavenging efficiency calculations were completed for the events on Jan. 10-11 and Jan. 11-12. Table 3-14 lists the start date and time and end date and time of the four filter samples analyzed, the volume of air sampled for each, the airborne DOC concentration, and the WSOC scavenging efficiency calculated from both pairs of samples.

	Start date/time	End date/time	Air volume sampled (m^3)	DOC (mg/m^3_{air})	Efficiency (%)
FOG011002 (PFA)	1/10/04 1:10 PM	1/10/04 9:00 PM	531.1	3.58E-03	
FOG011003 (IA)	1/10/04 9:30 PM	1/11/04 12:00 AM	169.5	6.80E-03	-90.1
FOG011103 (PFA)	1/11/04 12:30 PM	1/11/04 5:10 PM	316.4	6.76E-03	
FOG011201 (IA)	1/11/04 5:10 PM	1/12/04 12:45 AM	514.15	4.71E-03	30.4

Table 3-14. WSOC scavenging efficiency calculations for consecutive fog events.

This efficiency calculation is subject to the assumption made that the boundary layer composition, and hence the fog layer composition, does not change in the first few hours of the fog episode. This assumption does not always hold true since differences in air masses can also invalidate the assumption, although this is usually not a major issue in the low wind speed environments under which these radiation fogs form. The boundary layer typically grows with the onset of fog, but this assumption needs to be made nonetheless.

The scavenging efficiencies determined for the two nights were about -90% and 30%, respectively. The -90% efficiency arises from the fact that there was more DOC in the interstitial aerosol than in the pre-fog aerosol; in other words, there was an increase in airborne WSOC between the pre-fog and foggy periods. This increase may be due to increased carbonaceous emissions near the site, secondary organic aerosol production, or entrainment from above the boundary layer. This increase may also be partly due to uptake of soluble volatile organic compounds (VOCs) onto the wet interstitial aerosol filter. The filter becomes wet because some of the fog drops make it through the collection strands and impact on the filter, and the sampled air is at 100% relative humidity.

A more easily explicable scavenging efficiency was calculated on the second night. The 30% scavenging efficiency suggests that the fog water was able to scavenge about 30% of the particulate WSOC in the air. The interstitial aerosol DOC may be higher (and the scavenging efficiency lower) due to adsorption/absorption of VOCs onto the wet filter in this case as well. Much more work needs to be done to study the extent of the processes that affect the fog

scavenging efficiency calculations. Focusing on individual chemical species also might facilitate interpretation of scavenging observations.

It would be ideal to directly compare fog DOC with pre-fog DOC to determine a scavenging efficiency, but this is not possible because fog DOC is comprised of both scavenged pre-fog aerosol and soluble organic gases that have partitioned to the drops. It is possible to sum the DOC measured in the fog and the interstitial aerosol for use as a consistency check. This sum should equal or exceed the pre-fog or below-cloud aerosol DOC concentration. This check will indicate whether a large decrease in aerosol (perhaps due to entrainment of cleaner air from about the boundary layer) or the removal of aerosol (due to drop deposition or drizzle) would render a comparison of pre-fog and interstitial aerosol concentrations inappropriate. In both fog episodes, it was found that the DOC_{IA} + DOC_{fog} concentrations exceeded the concentrations of DOC_{PFA}, although the fog and interstitial aerosol filter sampling times did not line up perfectly. Table 3-15 lists the start and end times, the airborne DOC concentrations, and the DOC_{fog}+ DOC_{IA} values for the pre-fog and interstitial aerosol samples, and fog water samples for both events.

	Start time	End time	DOC in air (mg/m^3_{air})	DOC_{fog} + DOC_{IA}
FOG011002 (PFA)	1:10 PM	9:00 PM	3.58E-03	
FOG011003 (IA)	9:30 PM	12:00 AM	6.80E-03	
FSC01001 (Fog)	9:30 PM	11:37 PM	8.04E-03	1.48E-02
FOG011103 (PFA)	12:30 PM	5:10 PM	6.76E-03	
FOG011201 (IA)	5:10 PM	12:45 AM	4.71E-03	
FSC01101 (Fog)	6:00 PM	1:00 AM	9.31E-03	1.40E-02

Table 3-15. Consistency scavenging check for both fog events.

It was also noted that post-fog aerosol DOC concentrations were greater than pre-fog DOC concentrations for the first fog event, suggesting that aqueous reactions in the fog droplets may be transforming soluble VOCs into lower volatility SOA species. Reactions of this type have been discussed in the literature (e.g., Blando and Turpin, 2000), but the importance of aqueous phase SOA production is still a matter of speculation. Data reported by Herckes et al. (2005) showed that fog water scavenged organic carbon more efficiently than elemental carbon in Fresno aerosol samples. They calculated scavenging efficiencies for OC that varied between 33 and 90%, while scavenging efficiencies for EC varied between 5 and 12%.

Herckes et al. (2005) also determined a fog water scavenging efficiency of 95% for levoglucosan on the night of Jan. 11-12. A scavenging efficiency was not calculated for the previous night because the interstitial aerosol sample was larger than the pre-fog aerosol sample, analogous to values reported in Table 3-16.

3.10 Deposition plates

3.10.1 Deposition concentrations and fluxes

Deposition fluxes of fog water and fog solutes were measured with two Teflon deposition plates laying side-by-side on the two consecutive nights of sampling. Thirteen samples were collected during the two consecutive fog events. Figures 3-

68 to 3-89 show a comparison of water mass, solute concentrations, and species fluxes observed on the replicate plates.

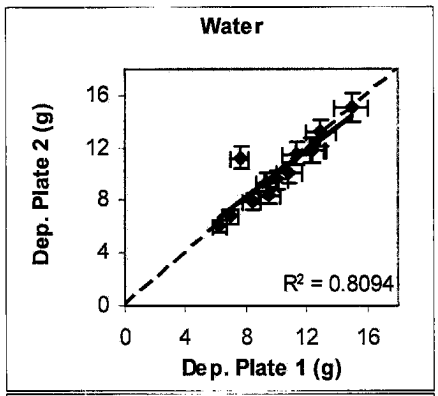

Figure 3-68. Comparison of fog water masses collected by two deposition plates. The solid line is the data trend line; the dashed line is the 1:1 line. Error bars represent the pooled standard deviation of replicate samples from the 2 collocated deposition plates.

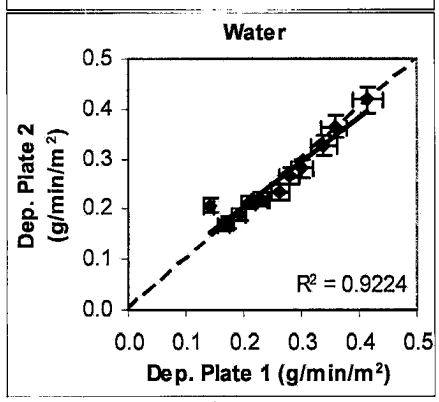

Figure 3-69. Comparison of fog water fluxes collected by two deposition plates. The solid line is the data trend line; the dashed line is the 1:1 line. Error bars represent the pooled standard deviation of replicate samples from the 2 collocated deposition plates.

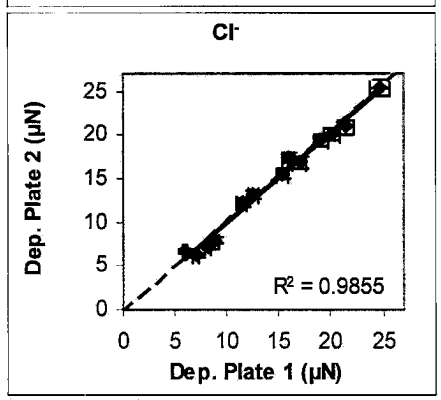

Figure 3-70. Comparison of Cl- concentrations collected by two deposition plates. The solid line is the data trend line; the dashed line is the 1:1 line. Error bars represent the pooled standard deviation of replicate samples from the 2 collocated deposition plates.

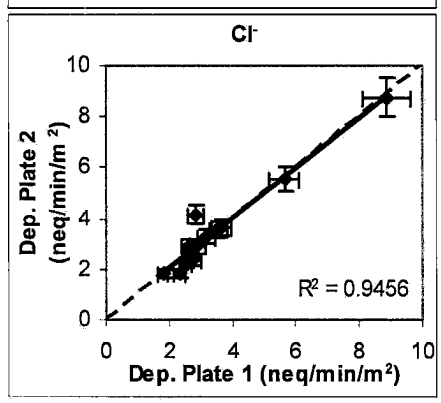

Figure 3-71. Comparison of Cl- fluxes collected by two deposition plates. The solid line is the data trend line; the dashed line is the 1:1 line. Error bars represent the pooled standard deviation of replicate samples from the 2 collocated deposition plates.

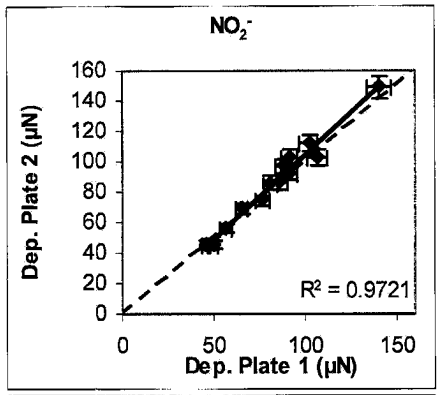

Figure 3-72. Comparison of NO2- concentrations collected by two deposition plates. The solid line is the data trend line; the dashed line is the 1:1 line. Error bars represent the pooled standard deviation of replicate samples from the 2 collocated deposition plates.

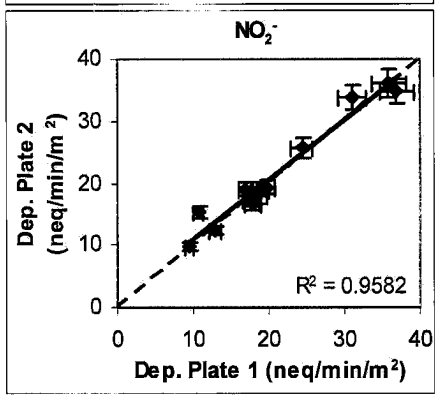

Figure 3-73. Comparison of NO2- fluxes collected by two deposition plates. The solid line is the data trend line; the dashed line is the 1:1 line. Error bars represent the pooled standard deviation of replicate samples from the 2 collocated deposition plates.

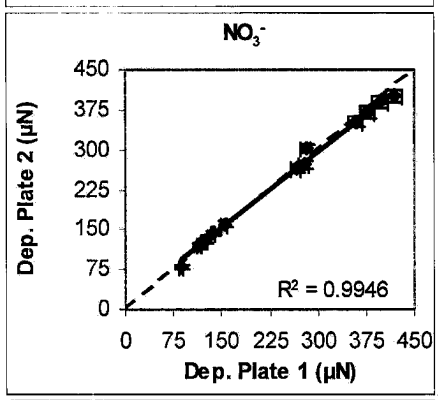

Figure 3-74. Comparison of NO3- concentrations collected by two deposition plates. The solid line is the data trend line; the dashed line is the 1:1 line. Error bars represent the pooled standard deviation of replicate samples from the 2 collocated deposition plates.

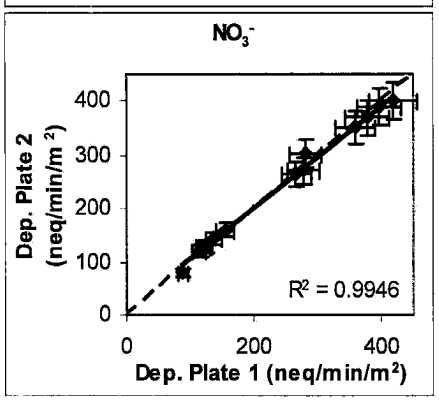

Figure 3-75. Comparison of NO3- fluxes collected by two deposition plates. The solid line is the data trend line; the dashed line is the 1:1 line. Error bars represent the pooled standard deviation of replicate samples from the 2 collocated deposition plates.

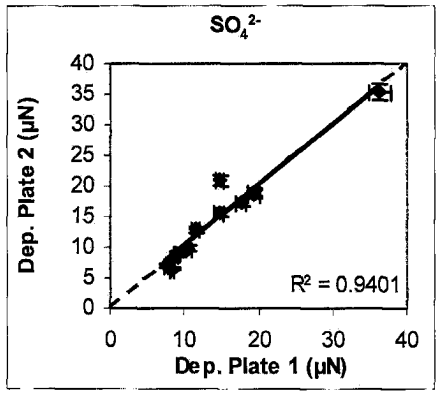

Figure 3-76. Comparison of SO42- concentrations collected by two deposition plates. The solid line is the data trend line; the dashed line is the 1:1 line. Error bars represent the pooled standard deviation of replicate samples from the 2 collocated deposition plates.

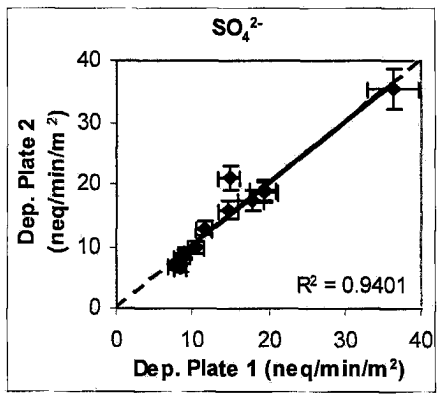

Figure 3-77. Comparison of SO42- fluxes collected by two deposition plates. The solid line is the data trend line; the dashed line is the 1:1 line. Error bars represent the pooled standard deviation of replicate samples from the 2 collocated deposition plates.

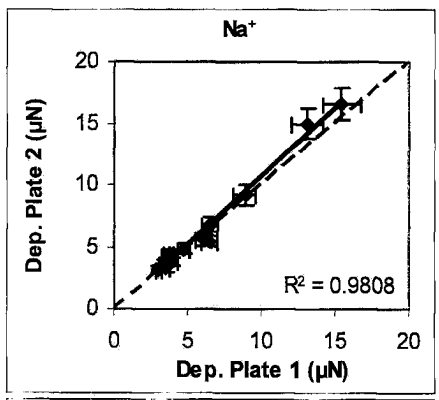

Figure 3-78. Comparison of Na+ concentrations collected by two deposition plates. The solid line is the data trend line; the dashed line is the 1:1 line. Error bars represent the pooled standard deviation of replicate samples from the 2 collocated deposition plates.

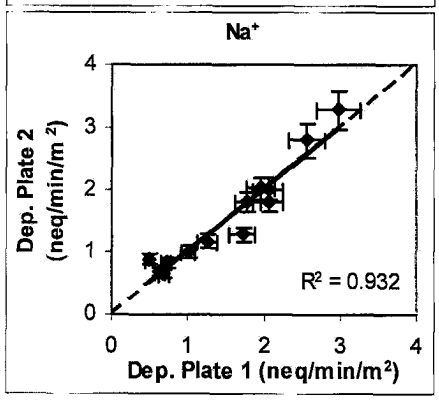

Figure 3-79. Comparison of Na+ fluxes collected by two deposition plates. The solid line is the data trend line; the dashed line is the 1:1 line. Error bars represent the pooled standard deviation of replicate samples from the 2 collocated deposition plates.

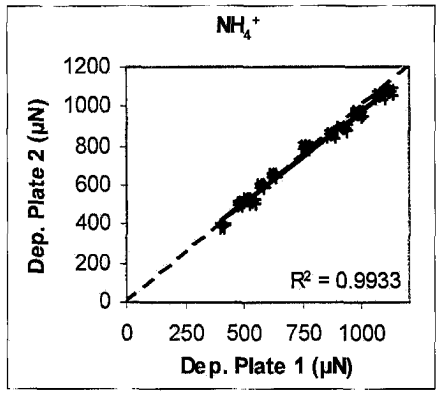

Figure 3-80. Comparison of NH4+ concentrations collected by two deposition plates. The solid line is the data trend line; the dashed line is the 1:1 line. Error bars represent the pooled standard deviation of replicate samples from the 2 collocated deposition plates.

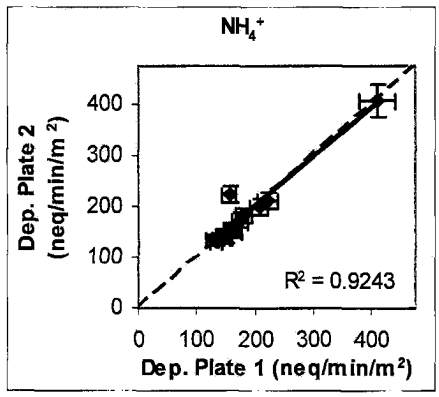

Figure 3-81. Comparison of NH4+ fluxes collected by two deposition plates. The solid line is the data trend line; the dashed line is the 1:1 line. Error bars represent the pooled standard deviation of replicate samples from the 2 collocated deposition plates.

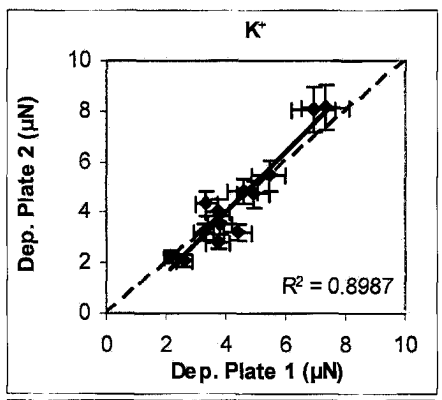

Figure 3-82. Comparison of K+ concentrations collected by two deposition plates. The solid line is the data trend line; the dashed line is the 1:1 line. Error bars represent the pooled standard deviation of replicate samples from the 2 collocated deposition plates.

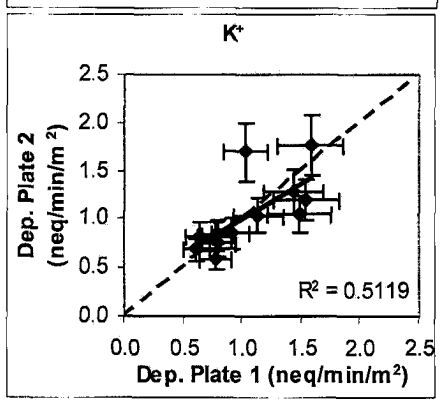

Figure 3-83. Comparison of K+ fluxes collected by two deposition plates. The solid line is the data trend line; the dashed line is the 1:1 line. Error bars represent the pooled standard deviation of replicate samples from the 2 collocated deposition plates.

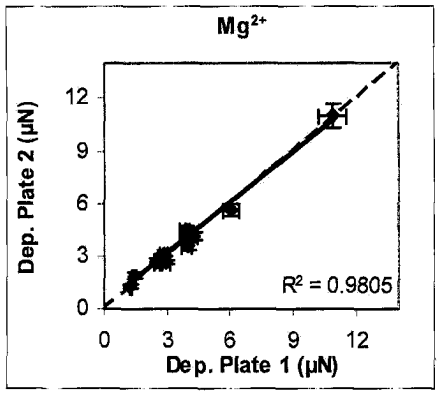

Figure 3-84. Comparison of Mg2+ concentrations collected by two deposition plates. The solid line is the data trend line; the dashed line is the 1:1 line. Error bars represent the pooled standard deviation of replicate samples from the 2 collocated deposition plates.

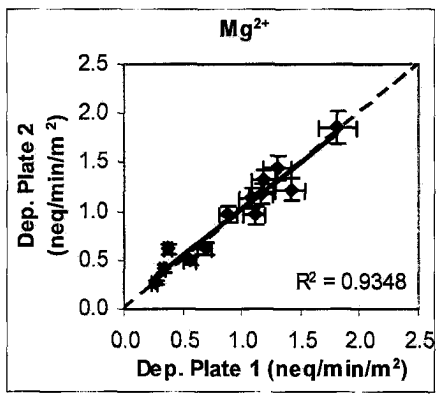

Figure 3-85. Comparison of Mg2+ fluxes collected by two deposition plates. The solid line is the data trend line; the dashed line is the 1:1 line. Error bars represent the pooled standard deviation of replicate samples from the 2 collocated deposition plates.

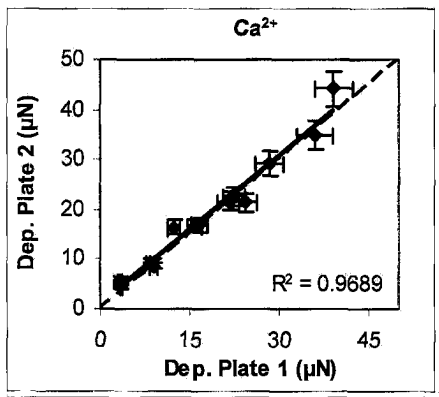

Figure 3-86. Comparison of Ca2+ concentrations collected by two deposition plates. The solid line is the data trend line; the dashed line is the 1:1 line. Error bars represent the pooled standard deviation of replicate samples from the 2 collocated deposition plates.

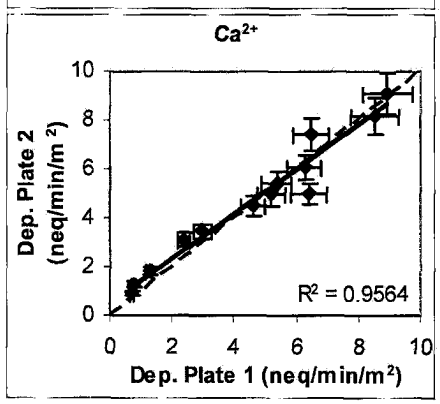

Figure 3-87. Comparison of Ca2+ fluxes collected by two deposition plates. The solid line is the data trend line; the dashed line is the 1:1 line. Error bars represent the pooled standard deviation of replicate samples from the 2 collocated deposition plates.

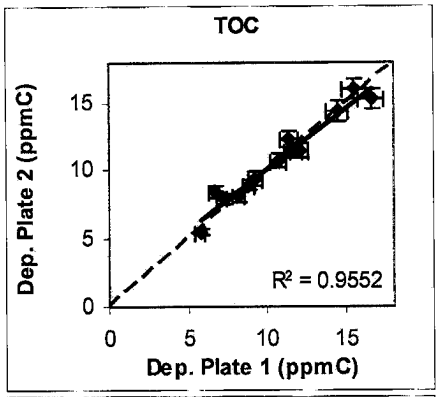

Figure 3-88. Comparison of TOC concentrations collected by two deposition plates. The solid line is the data trend line; the dashed line is the 1:1 line. Error bars represent the pooled standard deviation of replicate samples from the 2 collocated deposition plates.

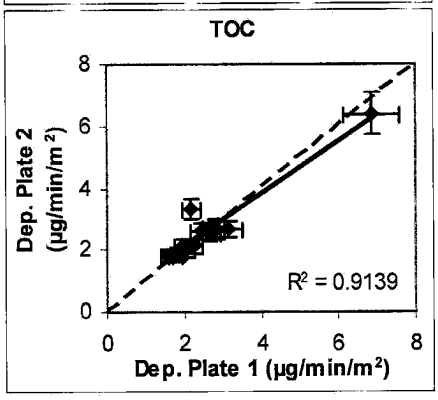

Figure 3-89. Comparison of TOC fluxes collected by two deposition plates. The solid line is the data trend line; the dashed line is the 1:1 line. Error bars represent the pooled standard deviation of replicate samples from the 2 collocated deposition plates.

The results reveal that the two plates agree well. Agreement between the two plates is good for the solute concentrations. Agreement is also good for fog water mass with the exception of one sample. Correlation coefficients (R^2) between the two deposition plates for fluxes of water, Cl^-, NO_2^-, NO_3^-, SO_4^{2-}, Na^+, NH_4^+, Mg^{2+}, Ca^{2+}, and TOC are higher than 0.9, while the correlation coefficient for K^+ is only 0.51. This may be because the concentrations of K^+ were relatively low and could be more easily affected by contamination either from the ground (i.e., dust) or sample handling.

Table 3-16 lists the precision estimates of concentration and flux measurements, as determined from the replicate deposition plate measurements. The results indicate that the deposition measurements are relatively precise for the

major solute species. The relative standard deviation of the water mass, sulfate, nitrite, nitrate, ammonium, and TOC concentrations ranged from 2.9% to 7.6%, while their fluxes ranged from 6.0% to 10.5%. The trace species measurements were also relatively precise, with the exception of K^+.

Solute	Concentration RSD (%)	Flux RSD (%)
Water	7.61	6.19
Cl^-	3.66	8.53
NO_2^-	4.99	6.02
NO_3^-	2.89	8.79
SO_4^{2-}	4.04	9.33
Na^+	8.31	9.50
NH_4^+	2.18	7.59
K^+	10.67	17.93
Mg^{2+}	6.26	8.80
Ca^{2+}	8.09	8.88
TOC	4.84	10.46

Table 3-16. Relative standard deviations of fog solute concentrations and fluxes as derived from two collocated deposition plates.

A summary of the range of water, ion and TOC fluxes is shown in Table 3-17 averaged over the two consecutive nights. Fog water flux rates averaged 0.25 g/min/m^2 during the two episodes. The nitrate, ammonium, and TOC fluxes were the highest of the chemical species, averaging 57.3 neq/min/m^2, 183.5 neq/min/m^2, and 2.7 μg/min/m^2, respectively. The deposition fluxes of Cl^-, NO_3^-, SO_4^{2-}, K^+, NH_4^+, and TOC increased on the second night, while the fluxes of NO_2^-, Na^+, Mg^{2+}, Ca^{2+}, and fog water decreased on the second night.

Solute		*Minimum*	*Maximum*	*Average*
Water	g/min/m^2	0.14	0.42	0.25
Cl^-	neq/min/m^2	1.80	8.88	3.50
NO_2^-	neq/min/m^2	9.53	36.95	21.06
NO_3^-	neq/min/m^2	29.00	156.89	57.30
SO_4^{2-}	neq/min/m^2	6.47	36.32	14.42
Na^+	neq/min/m^2	0.50	3.28	1.54
NH_4^+	neq/min/m^2	126.60	408.76	183.49
K^+	neq/min/m^2	0.59	1.77	1.04
Mg^{2+}	neq/min/m^2	0.27	1.86	0.95
Ca^{2+}	neq/min/m^2	0.73	9.08	4.66
TOC	µg/min/m^2	1.54	6.87	2.65

Table 3-17. Summary of observed deposition fluxes.

3.10.2 Deposition Velocities

The deposition fluxes can be used to calculate deposition velocities of the fog water solutes with the following equation,

$$v_i = \frac{Flux_i}{LWC \times Concentration_i} \tag{3-9}$$

where v_i is the deposition velocity of species i (units: cm/s), $Flux_i$ is the measured flux of species i to the deposition plates, LWC is the fog liquid water content, and $Concentration_i$ is the aqueous concentration of species i in the simultaneously measured bulk fogwater samples.

Several assumptions have been made in calculating deposition velocities: no evaporation/condensation, the deposition plates represent a "realistic" surface, the measured composition is not affected by drop mixing prior to collection, and no ground sources exist for the species of interest. The assumption that all deposition

is via sedimentation may not always be true. Studies have shown, though, that sedimentation dominates turbulent deposition for radiation fogs for Fresno-type conditions with low wind speeds, larger drops, and low surface roughness (Dollard and Unsworth, 1983; Thalmann et al., 2002).

Table 3-18 shows the ranges of deposition velocities of fog water and solute species averaged over the two consecutive sampling periods, as well as the measurement precision (RSD) for each species determined from the replicate plate measurements. The average deposition velocity trend of the major solute species is NO_2^- > water > NH_4^+ > TOC > SO_4^{2-} > NO_3^-.

Figure 3-90 shows the average fog water and solute deposition velocities plotted from smallest to largest velocity. As mentioned above, there is a clear trend in the deposition velocities of the major solute species: NO_2^- > water > NH_4^+ > TOC > SO_4^{2-} > NO_3^-. Mg^{2+} and Ca^{2+} had the largest deposition velocities averaged over the two nights; however, they were both smaller than the fog water velocity on the second night.

Dry deposition velocities for particles ranging from about 0.1 – 0.5 μm (accumulation mode particles) are roughly 0.01 – 0.02 cm s^{-1} (Seinfeld and Pandis, 1998). Therefore, solute species deposited via wet deposition (fog droplets) may have deposition velocities roughly 10 to 100 times greater than dry deposition alone.

Solute	Deposition Velocity (cm/s)			RSD (%)
	Minimum	Maximum	Average	
Na^+	0.23	5.87	1.61	9.54
NO_3^-	0.50	8.18	2.34	6.26
SO_4^{2-}	0.65	9.26	2.62	9.10
TOC	0.61	7.02	2.93	6.02
Cl^-	0.57	10.05	3.06	9.29
NH_4^+	0.75	7.93	3.08	4.43
K^+	0.83	8.14	3.08	17.40
Water	1.61	10.78	4.73	4.07
Mg^{2+}	0.96	18.62	5.97	7.53
NO_2^-	1.39	16.76	6.12	7.20
Ca^{2+}	0.62	16.60	6.28	8.74

Table 3-18. Measured ranges of deposition velocities and relative standard deviations.

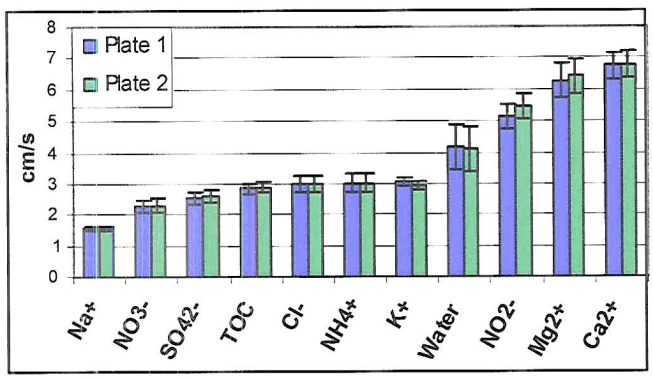

Figure 3-90. Fog water and solute deposition velocities averaged over two consecutive fog events. Error bars represent pooled standard deviation as reported in Table 3-18.

Moore et al. (2004) found that fog solute deposition velocities depend on the species distribution across the drop size spectrum. Enrichment of solutes in smaller drops leads to lower deposition velocities, due to the dependence of settling velocity on drop size. Similarly, solutes enriched in large drops tend to exhibit higher deposition velocities. Therefore, the tendency for the fog water

deposition velocities to exceed that of solutes enriched in the small drops (e.g., nitrate, sulfate, TOC) is expected. Also, the deposition velocity of fog water should be smaller than that of NO_2^-. NO_2^- deposition is weighted more heavily by the larger drops, which sediment faster. Theoretically, then, the Mg^{2+} and Ca^{2+} might be expected to have deposition velocities smaller than that of the fog water, but this was not the case on the night of Jan. 10-11; Mg^{2+} and Ca^{2+} actually had larger deposition velocities than fog water. This may be the result of sample contamination, either by dust settling on the plates or during sample handling. It might also reflect a vertical concentration gradient in fog Ca^{2+} and Mg^{2+} concentrations arising from the surface source of these species.

High deposition velocities lead to rapid removal of air pollutants during extended fog episodes. Jacob et al. (1984) proposed that enhanced aerosol deposition in fogs efficiently limits pollutant accumulation during stagnation episodes. During their study in the San Joaquin Valley, they found that the amount of solute decreased substantially over the course of each fog event. They attributed this behavior, in part, to the removal of aerosols during these stagnation episodes. Herckes et al. (2005) estimated fog deposition fluxes were capable of reducing boundary layer atmospheric concentrations of major species (e.g., nitrate, ammonium, and organic carbon) at a rate on the order of 0.5-1 $\mu g/m^3$ hr. However, some of the deposited water-soluble material may be volatile and subject to partial emission back into the atmosphere if the wetted ground dries following fog evaporation. Also, new aerosol mass may be formed in the droplets (e.g., SO_2 oxidation) which will act to compete with deposition.

4. Conclusions and future work

Radiation fogs are common events in California's Central Valley during the wintertime. These fogs can play two main roles in the atmosphere as processors of aerosol particles and trace gases: they promote new particle formation (e.g., via aqueous oxidation of sulfur dioxide to sulfate) and they promote particle removal (e.g., via scavenging followed by direct deposition). This thesis detailed the steps taken to better understand the processing of inorganic and, especially, organic compounds by radiation fogs observed in Fresno, CA in winter 2003-2004. As a result of the data analyses conducted during this study, some conclusions have been reached and some recommendations for future work are made.

4.1 Conclusions

- The fog water samples were more alkaline than pure water. The pH ranged from 6.41 to 6.66 (average 6.56) during the first fog event, 6.52 to 7.1 (average 6.73) during the second event, and 6.38 to 7.23 (average 6.95) during the third event. Ammonia can neutralize strong acids and make fog water alkaline. Consistent with previous studies, ammonium was the most dominant inorganic compound, followed by nitrate, sulfate and nitrite.

- Organic compounds comprise an important fraction of the fog solutes. The majority of the organic carbon in the fog droplets was dissolved, accounting for roughly 74% of the total organic carbon. The dominant organic acids (acetate, formate, oxalate and propionate) accounted for roughly 38% of the DOC. The dominant carbonyl species (formaldehyde, glyoxal and methyl glyoxal) accounted for roughly 10% of the DOC.
- A significant fraction of the dissolved organic matter in the fogs appeared to have high molecular weights, similar to findings reported in other recent studies of SJV fog composition. Roughly 26% of the carbon compounds were determined to have molecular weights greater than 1000 Da.
- Dissolved organic nitrogen compounds were calculated to comprise approximately 23% of the DOC in the bulk fog water samples. This estimate is fairly uncertain, however, since the appropriate C:N ratio needed to convert moles of N to moles of carbon had to be estimated. The DON:DOC ratio in small fog droplets was similar to the ratio in bulk fog water, but this ratio was much higher in large fog drops.
- Droplet composition was observed to vary with droplet size. The pH of the large (roughly > 20 μm diameter) droplets was approximately 1.0 – 1.2 units higher than the pH of small (< 20 μm diameter) droplets, possibly due in part to preferential uptake of HNO_3 into small drops. Most of the inorganic species were enriched in the small drops, a pattern observed before in SJV radiation fogs. Nitrite, however, was enriched in the large drops, likely as a consequence of increased nitrous acid solubility at higher pH. Organic carbon

and most measured organic species also showed an enrichment in the small droplets.

- Anion:cation charge balances determined in most samples were less than 100%. Approximately 10-20% of the anion species in the fog water samples remain unspeciated, assuming that all the cation species present have been accounted for and there is no significant bias in measured species concentrations. Bicarbonate may make up part of the missing anion fraction. Previous studies have reported *in situ* bicarbonate concentrations greater than those expected from equilibrium with background northern hemisphere CO_2 mixing ratios. Unmeasured anionic organic compounds may also be important contributors to the sample charge balance.
- The deposition velocities of the fog solutes were governed by their drop size-dependence. Nitrite, found to be enriched in the large drops, had a deposition velocity greater than the fog water. Species enriched in the small drops had deposition velocities smaller than the water. The average deposition velocity trend for the major inorganic species was found to be NO_2^- > water > NH_4^+ > TOC > SO_4^{2-} > NO_3^-. This trend is consistent with previous studies.
- Deposition velocities of fog water and fog solutes were typically of the order of 2 to 6 cm/s, much higher than typical deposition velocities for accumulation mode aerosol species. The rapid deposition of pollutants scavenged by SJV fogs probably plays an important role in limiting pollutant buildup during wintertime regional stagnation episodes.

4.2 Recommendations for future work

- Additional work is needed to more fully speciate organic matter in fog drops, including developing a better understanding of the composition of the high molecular weight organic fractions identified in this study. One goal of such work should be to develop improved models of the composition of organic molecules present in cloud condensation nuclei. Examples of promising techniques to be applied to this problem include H-NMR, ^{13}C-NMR, LC/MS, and various fractionation/detection schemes (e.g., size-exclusions/TOC, acidity/NMR). Anticipated addition of a new, high resolution time-of-flight LC/MS system in our laboratory should greatly enhance future efforts to identify unknown organic constituents, including those high in molecular weight.
- With respect to speciation of OC in fog drops, additional work needs to be done to better understand the composition of organic nitrogen present in the fog water. Compounds worth targeting include amines (likely emissions from animal husbandry operations in the SJV), proteins, and amino acids. ON speciation will also lead to better estimations of carbon:nitrogen ratios, which are important in understanding the fraction of DOC comprised of DON.
- Size distribution studies of fog water composition have a trade off between sampling time/sample volume and the sharpness of collector size cuts. The current 2-stage sf-ss-CASCC collector permits sufficient fog water collections within a short time, but only yields composition information for two drop size classes. The CSU 5-stage collector used in previous studies often yields

insufficient sample volumes for detailed chemical composition analysis. Newly developed 3-stage plastic collectors, designed at CSU, will increase understanding of drop size-dependence without compromising sample volume.

- Few studies of the organic composition of fogs and clouds have been done in relatively pristine sampling conditions, e.g., marine and remote continental environments. Consequently, we know little about the types of organic particles actively scavenged by clouds/fogs in most regions of the globe. An upcoming study at Storm Peak Lab in Steamboat Springs, CO (July-August 2005) will help us better understand the organic content and organic composition of orographic clouds in one fairly clean environment. Of particular interest are contributions to DOC in these clouds by low molecular weight organic acids and carbonyls as well as other compounds including cellulose, sugars, and tetrols.

References

Bator, A. and Collett, Jr., J. L., 1997. Cloud chemistry varies with drop size. *J. of Geophys. Res.*, **102(D23)**: 28071-28078.

Blando, J. D., Porcja, R. J., Li, T.-H., Bowman, D., Lioy, P. J., Turpin, B. J., 1998. Secondary formation and the Smoky Mountain organic aerosol : An examination of aerosol polarity and functional group composition during SEAVS. *Environ. Sci. Tech.*, **32**: 604-613

Blando, J. D. and Turpin, B. J., 2000. Secondary organic aerosol formation in cloud and fog droplets: a literature evaluation of plausibility. *Atmos. Environ.*, **34**: 1623-1632.

Chang, H., 2004. The processing of aerosol particles and soluble trace gases by chemically heterogeneous radiation fogs. Ph.D. dissertation, Colorado State University, Fort Collins, CO.

Collett, Jr., J. L., Bator, A., Rao, X., Demoz, B. B., 1994. Acidity variations across the cloud drop size spectrum and their influence on rates of atmospheric sulfate production. *Geophys. Res. Letts.*, **21(22)**: 2393-2396.

Collett, Jr., J. L., Hoag, K. J., Sherman, D. E., Bator, A., Richards, L. W., 1999a. Spatial and temporal variations in San Joaquin Valley fog chemistry. *Atmos. Environ.*, **33**: 129-140.

Collett, Jr., J. L., Hoag, K. J., Rao, X., Pandis, S. N., 1999b. Internal acid buffering in San Joaquin Valley fog drops and its influence on aerosol processing. *Atmos. Environ.*, **33**: 4833-4847.

Collett, Jr., J. L., Sherman, D. E., Moore, K. F., Hannigan, M. P., Lee, T., 2001. Aerosol particle processing and removal by fogs: Observations in chemically heterogeneous central California radiation fogs. *Water, Air and Soil Pollution: Focus*, **1**: 303-312.

Collett, Jr., J. L., Bator, A., Sherman, D. E., Moore, K. F., Hoag, K. J., Demoz, B. B., Rao, X., Reilly, J. E., 2002. The chemical composition of fogs and intercepted clouds in the United States. *Atmos. Res.*, **64**: 29-40.

Demoz, B. B., Collett, Jr., J. L., Daube, Jr., B. C., 1996. On the Caltech Active Strand Cloudwater Collectors. *Atmos. Res.*, **41**: 47-62.

Dollard, G. J. and Unsworth, M. H., 1983. Field measurements of turbulent fluxes of wind-driven fog drops to a grass surface. *Atmos. Environ.*, **17(4)**: 775-780.

Ervens, B., Herckes, P., Feingold, G., Lee, T., Collett, Jr., J. L., Kreidenweis, S. M., 2003. On the drop-size dependence of organic acid and formaldehyde concentrations in fog. *J. of Atmos. Chem.*, **46**: 239-269.

Facchini, M. C., Fuzzi, S. Zappoli, S. Andracchio, A., Gelencsér, A., Kiss, G., Krivácsy, Z., Mészáros, E., Hansson, H.-C., Alsberg, T., Zebühr, Y., 1999. Partitioning of the organic aerosol component between fog droplets and interstitial air. *J. of Geophys. Res.*, **104(D21)**: 26821-26832.

Gao, S., Melita, K., Ng, N. L., Surratt, J., Varutbangkul, V., Bahreini, R., Flagan, R. C., Seinfeld, J. H., 2004. Low-molecular-weight and oligomeric components in secondary organic aerosol from the ozonolysis of cycloalkenes and α-pinene. *J. of Phys. Chem. A*, **108(46)**: 10147-10164.

Herckes, P., Hannigan, M. P., Trenary, L., Lee, T., Collett, Jr., J. L., 2002a. Organic compounds in radiation fogs in Davis (California). *Atmos. Res.*, **64**: 99-108.

Herckes, P., Lee, T., Trenary, L., Kang, G., Chang, H., Collett, Jr., J. L., 2002b. Organic matter in central California radiation fogs. *Environ. Sci. Tech.*, **36**: 4777-4782.

Herckes, P., Youngster, S., Lee, T., Collett, Jr., J. L., 2005. Fog processing of atmospheric organic matter. *Atmos. Environ.* (submitted).

Holets, S., and Swanson, R. N., 1981. High-inversion fog episodes in central California. *J. of App. Met.*, **20**: 890-899.

Jacob, D. J., Waldman, J. M., Munger, J. W., Hoffmann, M. R., 1984. A field investigation of physical and chemical mechanisms affecting pollutant concentrations in fog droplets. *Tellus*, **36B**: 272-285.

Jacob, D. J., 1986. Chemistry of OH in remote clouds and its role in the production of formic acid and peroxymonosulfate. *J. of Geophys. Res.*, **91(D9)**: 9807-9826.

Jacob, D. J., Munger, J. W., Waldman, J. M., Hoffmann, M. R., 1986. The H_2SO_4-HNO_3-NH_3 system at high humidities and in fogs 1. Spatial and temporal patterns in the San Joaquin Valley of California. *J. of Geophys. Res.*, **91(D1)**: 1073-1088.

Laj, P., Fuzzi, S., Facchini, M. C., Lind, J. A., Orsi, G., Preiss, M., Maser, R., Jaeschke, W., Seyffer, E., Helas, G., Acher, K., Wieprecht, W., Möller, D., Arends, B. G., Mölls, J. J., Colvile, R. N., Gallagher, M. W., Beswick, K. M., Hargreaves, K. J., Storeton-West, R. L., Sutton, M. A., 1997. Cloud processing of soluble gases. *Atmos. Environ.*, **31(16)**: 2589-2598.

Likens, G. E., Edgerton, E. S., Galloway, J. N., 1983. The composition and deposition of organic-carbon in precipitation. *Tellus*, **35B**: 16-24.

Ludwig, J. and Klemm, O., 1988. Organic acids in different size classes of atmospheric particulate material, *TellusI,* **40B**, 340–347.

Moore, K. F., 2002. Drop size-dependent chemical composition in clouds and fogs. Ph.D. dissertation, Colorado State University, Fort Collins, CO.

Moore, K. F., Sherman, D. E., Reilly, J. E., Collett, Jr., J. L., 2004. Drop size-dependent chemical composition in clouds and fogs. Part I. Observations. *Atmos. Environ.*, **38**: 1389-1402.

Munger, J. W., Jacob, D. J., Waldman, J. M., Hoffmann, M. R., 1983. Fogwater chemistry in an urban atmosphere. *J. of Geophys. Res.*, **88(C9)**: 5109-5121.

Munger, J. W., Tiller, C., Hoffmann, M. R., 1986. Identification of hydroxymethanesulfonate in fog water. *Science*, **231**: 247-249.

Munger, J. W., Collett, Jr., J. Daube, Jr., B., Hoffmann, M. R., 1989. Chemical composition of coastal stratus clouds: dependence on droplet size and distance from the coast. *Atmos. Environ.*, **23(10)**: 2305-2320.

Neusüß, C. Pelzing, M., Plewka, A., Herrmann, H., 2000. A new analytical approach for size-resolved speciation of organic compounds in

atmospheric aerosol particles: Methods and first results, *J. of Geophys. Res.*, **105:** 4513–4527.

Ogren, J. A. and Charlson, R. J., 1992. Implications for models and measurements of chemical inhomogeneities among cloud droplets. *Tellus*, **44B**: 208-225.

Rao, X. and Collett, Jr., J. L., 1998. The drop size-dependence of iron and manganese concentrations in clouds and fogs: Implications for sulfate production. *J. of Atmos. Chem.*, **30**: 273-289.

Reilly, J. E., Rattigan, O. V., Moore, K. F., Judd, C., Sherman, D. E., Dutkiewicz, V. A., Kreidenweis, S. M., Husain, L., Collett, Jr., J. L., 2001. Drop size-dependent S(IV) oxidation in chemically heterogeneous radiation fogs. *Atmos. Environ.*, **35**: 5717-5728.

Russell, L. M., 2003. Aerosol organic-mass-to-organic-carbon ratio measurements. *Environ. Sci. Tech.*, **37**: 2982-2987.

Schell, D., Wobrock, W., Maser, R., Preiss, M., Jaeschke, W., Georgii, H.-W., Gallagher, M. W., Bower, K. N., Beswick, K. M., Pahl, S., Facchini, M. C., Fuzzi, S., Wiedensohler, A., Hansson, H.-C., Wendisch, M., 1996. The size-dependent chemical composition of cloud droplets. *Atmos. Environ.*, **31(16)**: 2561-2276.

Seinfeld, J. H. and Pandis, S. N., 1998. Atmospheric Chemistry and Physics. *John Wiley and Sons, Inc.* New York.

Spokes, L. J., Campos, M. L. A. M., Jickells, T. D., 1996. The role of organic matter in controlling copper speciation in precipitation. *Atmos. Environ.*, **30(23)**: 3959-3966.

Strader, R., Lurmann, F., Pandis, S. N., 1999. Evaluation of secondary organic aerosol formation in winter. *Atmos. Environ.*, **33**: 4849-4863.

Tolocka, M. P., Jang, M., Ginter, J. M., Kamens, R. M., Johnston, M. V., 2004. Formation of oligomers in secondary organic aerosol. *Eviron. Sci. Tech.*, **38**: 1428-1434.

Thalmann, E., Burkhard, R., Wrzesinsky, T., Eugster, W., Klemm, O., 2002. Ion fluxes from fog and rain to an agricultural and a forest ecosystem in Europe. *Atmos. Res.*, **64(1-4)**: 147-158.

Turpin, B. J. and Lim, H-J., 2001. Species Contributions to PM2.5 Mass Concentrations: Revisiting Common Assumptions for Estimating Organic Mass. *Aerosol Sci. and Tech.*, **35**: 602-610.

Vong, R. J., Baker, B. M., Brechtel, F. J., Collier, R. T., Harris, J. M., Kowalski, A. S., McDonald, N. C., McInnes, L. M., 1996. Ionic and trace element composition of cloud water collected on the Olympic Peninsula of Washington State. *Atmos. Environ.*, **31(13)**: 1991-2001.

Zhang, Q. and Anastasio, C., 2001. Chemistry of fog waters in California's Central Valley- Part 3: concentrations and speciation of organic and inorganic nitrogen. *Atmos. Environ.*, **35**: 5629-5643.

Zhang, Q. and Anastasio, C., 2003. Free and combined amino compounds in atmospheric fine particles ($PM_{2.5}$) and fog waters from northern California. *Atmos. Eviron.* **37**: 2247–2258.

A. Appendix: Formaldehyde preservation solution preparation

Preparation of the preservation solution is as follows:

0.08 g NaOH

0.3644 g CDTA (Fluka Scientific)

0.0294 g $NaHSO_3$ (Sigma Chemical Co.)

Dilute to 100 mL with DI water

The solution pH should be measured to ensure that it is approximately 4.8 ± 0.1.

B. Appendix: Recrystallization of 2,4-Dinitrophenylhydrazine (DNPH)

B1. Prepare a saturated solution of DNPH by boiling excess DNPH in 200 mL of acetonitrile for approximately 1 hour.

B2. After 1 hour, remove and transfer the supernatant to a covered beaker on a hot plate and allow gradual cooling to 40 to 60°C. Maintain this temperature range until 95% of the solvent has evaporated, leaving crystals.

B3. Decant the solution to waste and rinse the remaining crystals twice with three times their apparent volume of acetonitrile.

B4. Transfer the crystals to a clean beaker, add 200 mL of acetonitrile, heat to boiling, and again let the crystals grow slowly at 40 to 60°C until 95% of the solvent has evaporated. Repeat the rinsing process as in Section B3.

B5. Take an aliquot of the second rinse, dilute 10 times with acetonitrile, acidify with 1 mL of 3.8 M perchloric acid per 100 mL of DNPH solution, and analyze with HPLC.

B6. If the impurity level is not satisfactory, pipet off the solution to waste, repeat the recrystallization as in Section B4 but rinse with two 25 mL portions of acetonitrile. Prepare and analyze the second rinse as in Section B5.

B7. When the impurity level is satisfactory, place the crystals in an all-glass reagent bottle, add another 25 mL of acetonitrile, stopper, and shake the bottle. Use clean pipets when removing the saturated DNPH stock solution to reduce the possibility of contamination of the solution. Maintain only a minimum volume of

the saturated solution adequate for day to day operation to minimize waste of the purified reagent.

C. Appendix: Data tables

Samples are labeled according to collector, event date, and number of sample during the event. Collector codes are as follows: FCC = CASCC, FSC = ss-CASCC, FSCS = small fraction of ss-sf-CASCC, FSCL = large fraction of ss-sf-CASCC, FD0 = first deposition plate, FD1 = second deposition plate. In all the tables, "ND" refers to "not detected".

Table C-1. Sample start date, start time, end time, pH, and LWC.

Sample Name	Start Date	Start Time	End Time	Sample Weight (g)	pH	LWC (mg/m^3)
FCC360BLK	12/26/2003					
FCC36401	12/31/2003	2:30:00 AM	3:30:00 AM	52.07	6.41	117.65
FCC36402	12/31/2003	3:30:00 AM	4:30:00 AM	42.25	6.58	101.32
FCC36403	12/31/2003	4:30:00 AM	5:30:00 AM	22.19	6.66	126.05
FCC36404	12/31/2003	5:30:00 AM	6:33:00 AM	24.47	6.6	100.65
FCC365BLK	12/31/2003	4:25:00 PM		499.1		
FCC365DI	12/31/2003	4:25:00 PM		519.08		
FCC01001	1/10/2004	9:30:00 PM	11:30:00 PM	218.82	6.65	149.25
FCC01002	1/10/2004	11:30:00 PM	1:30:00 AM	179.84	6.69	146.13
FCC01003	1/11/2004	1:30:00 AM	3:30:00 AM	197.06	6.52	69.33
FCC01004	1/11/2004	3:30:00 AM	5:30:00 AM	176.65	6.79	93.36
FCC01005	1/11/2004	5:30:00 AM	7:30:00 AM	165.28	6.56	164.90
FCC01005DUP	1/11/2004	5:30:00 AM	7:30:00 AM	165.28	6.56	164.90
FCC01006	1/11/2004	7:30:00 AM	9:30:00 AM	134.56	6.89	146.62
FCC01007	1/11/2004	9:30:00 AM	11:40:00 AM	73.41	6.68	26.07
FCC01101	1/11/2004	6:00:00 PM	8:00:00 PM	83.13	6.65	126.35
FCC01102	1/11/2004	8:00:00 PM	10:00:00 PM	62.67	6379	111.05
FCC01103	1/11/2004	10:00:00 PM	1:00:00 AM	72.55	6.92	145.17
FCC01104	1/12/2004	1:00:00 AM	4:00:00 AM	107.5	7.01	117.28
FCC01105	1/12/2004	4:00:00 AM	7:00:00 AM	146.73	7.15	96.40
FCC01106	1/12/2004	7:00:00 AM	10:00:00 AM	104.4	7.1	34.73
FCC012BLK	1/12/2004					
FCC01301	1/13/2004	4:20:00 AM	4:53:00 AM	2.64		32.32
FCC01302	1/13/2004	4:53:00 AM	5:08:00 AM	3.13		22.54
FCC01303	1/13/2004	5:08:00 AM	5:23:00 AM	4.21		21.13
FCC01303DUP	1/13/2004					21.13
FCC01304	1/13/2004	5:23:00 AM	5:38:00 AM	5.02		19.41
FCC01305	1/13/2004	5:38:00 AM	5:53:00 AM	3.89		17.87

FCC01306	1/13/2004	5:53:00 AM	6:08:00 AM	2.46		17.00
FCC01306DUP	1/13/2003					17.00
FCC01307	1/13/2004	6:08:00 AM	6:23:00 AM	1.62		18.28
FCC01308	1/13/2004	6:23:00 AM	6:38:00 AM	1.35		17.15
FCC01309	1/13/2004	6:38:00 AM	6:53:00 AM	0.28		16.83
FCC01310	1/13/2004	6:53:00 AM	7:53:00 AM			14.26
FCC013BLK	1/13/2004					
FSC01001	1/10/2004	9:30:00 PM	11:37:00 PM	255.38	6.71	150.88
FSC01002	1/10/2004	11:38:00 PM	2:00:00 AM	238.04	6.58	131.33
FSC01003	1/10/2004	2:00:00 AM	9:30:00 AM	760.1	6.89	120.60
FSC01003DUP	1/11/2004	2:00:00 AM	9:30:00 AM	760.1		120.60
FSC01004	1/11/2004	9:30:00 AM	11:40:00 AM	96.9	7.1	26.07
FSC01101	1/11/2004	6:00:00 PM	1:00:00 AM	183.7	6.91	130.07
FSC01102	1/11/2004	1:00:00 AM	7:00:00 AM	213.15	7.18	106.75
FSC01103	1/11/2004	7:00:00 AM	10:00:00 AM	83.5	7.23	34.73
FSC012BLK	1/12/2004			726.02		
FSC01301	1/13/2004	4:53:00 AM				17.22
FSCS360BLK	12/26/2003			432.61		
FSCS01001	1/10/2004	9:30:00 PM	1:30:00 AM	65.01	6.6	147.78
FSCS01002	1/10/2004	1:30:00 AM	5:30:00 AM	81.11	6.61	81.44
FSCS01003	1/10/2004	5:30:00 AM	9:30:00 AM	100.12	6.76	154.83
FSCS01003DUP	1/11/2004	5:30:00 AM	9:30:00 AM	100.12		154.83
FSCS01004	1/11/2004	9:30:00 AM	11:40:00 AM	10.9	7.22	26.07
FSCS01101	1/11/2004	6:00:00 PM	1:00:00 AM	44.1	5.95	130.07
FSCS01102	1/11/2004	1:00:00 AM	7:05:00 AM	65.66	6.81	106.14
FSCS01103	1/11/2004	7:05:00 AM	10:05:00 AM	32.01	7	33.49
FSCS012BLK	1/12/2004			510.69		
FSCL360BLK	12/26/2003			491.14		
FSCL01001	1/10/2004	9:30:00 PM	1:30:00 AM	849.17	6.72	147.78
FSCL01002	1/10/2004	1:30:00 AM	5:30:00 AM	897.42	6.8	81.44
FSCL01003	1/10/2004	5:30:00 AM	9:30:00 AM	759.4	6.92	154.83
FSCL01003DUP	1/11/2004	5:30:00 AM	9:30:00 AM	759.4		154.83
FSCL01004	1/11/2004	9:30:00 AM	11:40:00 AM	215.2	7.05	26.07
FSCL01101	1/11/2004	6:00:00 PM	1:00:00 AM	559.75	7.02	130.07
FSCL01102	1/11/2004	1:00:00 AM	7:05:00 AM	574.42	7.13	106.14
FSCL01103	1/1/1104	7:05:00 AM	10:05:00 AM	264.37	7.06	33.49
FSCL012BLK	1/12/2004			667.14		
FD0364BLK	12/30/2003					
FD001001	1/10/2004	9:30:00 PM	11:30:00 PM	10.82		149.25
FD001002	1/10/2004	11:30:00 PM	1:30:00 AM	9.47		146.13
FD001003	1/10/2004	1:30:00 AM	3:30:00 AM	12.22		69.33
FD001004	1/11/2004	3:30:00 AM	5:30:00 AM	10.02		93.36
FD001005	1/11/2004	5:30:00 AM	7:30:00 AM	12.9		164.90
FD001005DUP	1/11/2004	5:30:00 AM	7:30:00 AM	12.9		164.90
FD001006	1/11/2004	7:30:00 AM	9:30:00 AM	8.35		146.62
FD001007	1/11/2004	9:30:00 AM	11:40:00 AM	6.23		26.07
FD0011BLK	1/11/2004					
FD001101	1/11/2004	6:00:00 PM	8:00:00 PM	14.94		126.35

FD001102	1/11/2004	8:00:00 PM	10:00:00 PM	6.94		111.05
FD001103	1/11/2004	10:00:00 PM	1:00:00 AM	7.59		145.17
FD001104	1/12/2004	1:00:00 AM	4:00:00 AM	12.3		117.28
FD001105	1/12/2004	4:00:00 AM	7:00:00 AM	11.3		96.40
FD001106	1/12/2004	7:00:00 AM	10:04:00 AM	9.38		34.34
FD0012BLK	1/12/2004					
FD1364BLK	12/30/2003					
FD101001	1/10/2004	9:30:00 PM	11:30:00 PM	10.09		149.25
FD101002	1/10/2004	11:30:00 PM	1:30:00 AM	8.41		146.13
FD101003	1/10/2004	1:30:00 AM	3:30:00 AM	11.79		69.34
FD101004	1/11/2004	3:30:00 AM	5:30:00 AM	9.56		93.36
FD101005	1/11/2004	5:30:00 AM	7:30:00 AM	13.13		164.90
FD101005DUP	1/11/2004	5:30:00 AM	7:30:00 AM	13.13		164.90
FD101006	1/11/2004	7:30:00 AM	9:30:00 AM	7.91		146.62
FD101007	1/11/2004	9:30:00 AM	11:30:00 AM	6.07		26.07
FD1011BLK	1/11/2004					
FD101101	1/11/2004	6:00:00 PM	8:00:00 PM	15.06		126.35
FD101102	1/11/2004	8:00:00 PM	10:00:00 PM	6.8		111.05
FD101103	1/11/2004	10:00:00 PM	1:00:00 AM	11.2		145.17
FD101104	1/12/2004	1:00:00 AM	4:00:00 AM	11.83		117.28
FD101105	1/12/2004	4:00:00 AM	7:00:00 AM	11.52		96.40
FD101106	1/12/2004	7:00:00 AM	10:03:00 AM	9.35		34.34
FD1012BLK	1/12/2004					

Table C-2. Concentrations of inorganic ion species. Units in μN.

Sample	Cl^-	NO_2^-	NO_3^-	SO_4^{2-}	Na^+	NH_4^+	K^+	Mg^{2+}	Ca^{2+}
FCC360BLK	0.74	0.21	0.39	ND	1.11	2.72	0.40	1.39	1.70
FCC36401	10.85	172.07	245.57	47.72	5.25	752.89	6.55	2.93	9.26
FCC36402	10.62	134.82	168.09	43.05	4.27	683.72	5.33	2.18	7.78
FCC36403	12.61	121.70	211.57	65.27	5.23	783.66	6.60	3.85	15.52
FCC36404	15.99	94.90	300.32	86.49	6.73	825.06	8.40	3.85	19.63
FCC01001	8.57	50.46	295.34	68.95	3.15	709.99	3.10	2.34	6.23
FCC01002	9.10	101.39	304.56	68.24	4.17	828.15	4.11	3.29	11.62
FCC01003	8.90	67.79	260.73	55.76	4.17	664.77	3.35	2.70	7.63
FCC01004	13.53	64.79	246.87	54.89	3.96	667.28	2.93	2.58	5.64
FCC01005	8.37	33.18	178.87	39.65	2.86	511.45	2.49	1.24	3.90
FCC01005DUP	8.58	33.79	182.88	40.56	4.50	506.36	2.50	1.61	4.26
FCC01006	13.89	65.80	261.32	62.35	6.08	780.02	5.10	3.10	11.75
FCC01007	16.47	72.91	389.69	94.37	11.75	992.04	4.71	5.93	24.72
FCC01101	53.79	98.44	1124.43	246.56	9.59	2025.88	9.35	5.63	27.29
FCC01102	44.90	90.48	1206.72	234.80	6.98	2159.02	9.51	3.65	16.25
FCC01103	47.82	88.16	1278.29	267.36	6.70	2322.15	12.80	2.83	10.28
FCC01104	35.88	60.56	1120.67	234.20	6.56	2036.65	9.72	1.74	5.85
FCC01105	29.44	41.43	676.91	194.54	5.85	1518.87	7.99	1.68	5.56
FCC01106	22.12	84.25	519.34	152.68	3.99	1350.59	6.60	3.23	31.72

FCC012BLK	0.61	0.80	8.11	2.46	0.68	18.78	0.36	1.34	2.42
FCC01301	19.73	135.68	405.15	113.70	9.45	1019.70	9.74	7.24	42.98
FCC01302	34.97	207.53	693.35	182.52	17.97	1568.22	17.74	9.70	59.71
FCC01303	37.94	239.12	758.77	194.76	18.68	1692.28	18.53	10.02	57.38
FCC01303DUP	38.64	244.25	779.79	201.55	17.55	1729.10	17.04	9.92	53.96
FCC01304	39.76	241.82	877.03	223.78	16.20	1824.94	17.19	9.45	55.02
FCC01305	36.93	241.73	820.19	205.28	14.78	1755.60	15.34	7.49	44.07
FCC01306	34.52	225.33	750.22	192.73	15.50	1619.72	15.44	7.86	45.14
FCC01306DUP	34.55	224.77	750.79	192.05	15.69	1625.70	16.06	7.60	45.58
FCC01307	36.31	231.25	784.39	199.42	16.33	1665.62	15.45	8.86	47.34
FCC01308	37.34	230.70	791.68	197.11	19.35	1649.05	17.24	9.41	51.50
FCC013BLK	1.87	0.39	0.32	ND	2.96	4.90	1.58	1.13	4.87
FSC01001	9.90	50.00	285.62	61.22	14.62	694.98	3.61	2.87	8.60
FSC01002	9.59	100.21	281.92	53.21	13.99	834.13	3.70	2.91	12.50
FSC01003	13.29	58.12	232.32	52.30	12.56	665.29	4.46	2.42	9.72
FSC01003DUP	13.12	58.01	231.33	51.96	11.37	666.42	4.22	2.16	9.19
FSC01004	18.68	72.09	398.07	89.37	30.38	1085.99	5.37	6.39	28.65
FSC01101	57.34	88.69	1360.50	259.79	25.63	2395.59	11.60	4.53	23.31
FSC01102	34.66	47.96	772.03	196.82	32.34	1706.61	11.82	2.40	9.31
FSC01103	28.03	85.74	573.81	152.08	44.49	1467.12	9.67	3.97	36.20
FSC012BLK	0.66	0.37	3.01	1.36	5.22	8.30	0.37	0.71	3.52
FSCS360BLK	7.11	0.09	9.27	5.37	1.70	7.90	2.34	3.31	8.73
FSCS01001	42.33	60.77	1101.04	211.76	54.16	1587.56	15.22	9.66	68.59
FSCS01002	41.04	66.35	982.86	169.07	47.11	1449.90	14.59	9.11	66.95
FSCS01003	30.82	48.21	681.22	120.58	26.27	1089.19	7.63	4.83	32.78
FSCS01003DUP	30.55	47.73	675.54	119.88	27.59	1096.21	8.52	5.26	33.34
FSCS01004	36.95	67.76	675.66	125.69	111.82	1210.97	10.06	8.31	63.31
FSCS01101	148.34	59.40	3257.07	701.75	62.32	5062.49	12.34	12.16	103.18
FSCS01102	125.27	50.32	2986.97	740.25	49.18	4932.13	11.79	6.85	51.32
FSCS01103	73.20	54.07	1893.46	430.93	66.92	2794.54	21.21	5.64	43.59
FSCS012BLK	1.46	0.64	13.85	3.81	2.71	2.14	0.71	1.77	7.27
FSCL360BLK	1.20	ND	1.67	1.12	6.45	5.85	0.42	1.22	5.11
FSCL01001	5.61	76.23	148.14	31.88	31.13	532.50	2.48	2.82	11.36
FSCL01002	6.93	70.29	130.44	26.17	7.54	530.73	2.54	2.10	8.48
FSCL01003	6.97	47.41	118.74	25.71	9.27	498.07	2.75	2.24	7.35
FSCL01003DUP	7.07	47.17	119.50	25.67	9.64	491.60	2.68	2.27	8.35
FSCL01004	10.56	75.14	239.82	57.53	16.51	842.21	3.61	5.01	21.34
FSCL01101	19.47	91.90	413.72	95.42	15.45	1280.27	4.39	3.04	12.81
FSCL01102	14.29	49.60	299.67	84.74	8.91	1062.70	3.91	1.19	3.37
FSCL01103	11.41	90.10	239.60	71.95	15.52	976.09	4.11	3.26	25.09
FSCL012BLK	0.81	0.77	8.78	2.40	1.25	1.87	0.40	1.16	4.15
FD0364BLK	0.17	ND	ND	0.23	0.22	5.11	ND	0.98	1.93
FD001001	5.98	65.50	114.18	27.52	3.37	483.03	2.58	3.86	28.39
FD001002	8.79	140.47	123.91	31.86	6.53	623.28	5.44	4.22	24.30
FD001003	8.20	91.59	121.07	26.40	6.06	513.63	4.39	3.85	15.85
FD001004	11.40	87.78	136.68	31.83	6.43	536.11	3.25	3.86	16.59
FD001005	7.01	49.81	87.64	21.19	3.51	405.08	2.15	2.47	8.32
FD001005DUP	6.99	49.95	87.52	22.02	3.56	407.34	2.22	2.78	9.21

FD001006	12.51	81.03	154.82	45.30	8.87	572.39	4.91	6.09	22.42
FD001007	15.81	102.03	281.60	69.25	15.45	762.05	3.71	10.89	39.07
FD001101	21.40	86.48	378.05	87.52	4.73	984.97	3.72	2.85	21.54
FD001102	19.05	91.73	396.64	91.56	3.73	1077.12	3.35	2.93	12.32
FD001103	20.12	76.20	418.32	105.37	3.59	1111.31	7.33	2.69	8.95
FD001104	24.72	56.56	358.88	85.04	13.06	979.91	6.94	1.46	3.39
FD001105	16.96	45.55	266.29	91.93	3.04	871.62	3.83	1.27	3.50
FD001106	15.32	106.72	278.80	84.55	3.94	918.45	4.57	3.96	36.02
FD0011BLK	0.10	0.11	0.38	ND	0.17	3.08	ND	1.02	0.78
FD0012BLK	2.78	1.15	0.76	0.90	2.58	4.05	1.63	1.07	2.86
FD101001	6.60	69.02	120.86	28.72	3.61	505.30	2.11	4.23	29.17
FD101002	7.96	148.89	128.68	27.70	5.48	651.50	5.46	4.11	21.40
FD101003	7.25	103.15	129.34	27.37	5.56	529.63	3.23	4.42	16.66
FD101004	12.27	96.75	144.22	32.13	6.79	519.63	3.22	4.30	16.90
FD101005	6.12	45.31	79.50	19.06	3.21	397.49	2.26	2.68	9.51
FD101005DUP	6.25	46.32	81.26	20.80	3.05	393.66	2.32	2.32	6.72
FD101006	13.20	85.97	160.11	44.68	9.17	601.47	4.72	5.58	22.58
FD101007	17.41	112.06	302.21	76.77	16.55	798.55	4.05	11.04	44.13
FD101101	20.93	86.26	369.67	84.43	4.82	975.12	2.85	3.14	21.71
FD101102	19.32	92.00	389.93	91.33	4.41	1055.84	4.35	2.63	16.42
FD101103	20.01	74.05	400.71	100.89	4.26	1074.80	8.15	2.96	8.69
FD101104	25.34	56.30	352.45	85.15	14.95	961.26	8.06	1.89	5.86
FD101105	16.83	45.76	264.69	89.16	3.14	858.27	3.51	1.28	4.36
FD101106	15.54	102.72	270.65	91.03	3.73	894.41	4.83	3.57	35.13
FD1011BLK	0.09	0.29	0.21	ND	0.19	7.77	ND	0.97	4.54
FD1012BLK	ND	ND	ND	ND	0.16	7.56	ND	1.17	1.20
FD1364BLK	0.11	ND	0.19	ND	2.40	6.77	0.62	0.94	3.01

Table C-3. Concentrations of carbonyl species. Units in μM. Formaldehyde values from fluorescence analysis.

Sample	Formaldehyde	Acetaldehyde	Acetone/Acrolein	Butyraldehyde	Isovaleraldehyde
FCC36401	34.13				
FCC36402	38.53				
FCC36403	38.93				
FCC36404	40.41				
FCC365BLK	1.06				
FCC365DI	1.14				
FCC01001	23.95				
FCC01002	34.79				
FCC01003	32.24				
FCC01004	28.13				
FCC01005	22.31				
FCC01005DUP	20.90				
FCC01006	34.19				
FCC01007	40.23				
FCC01101	65.34				
FCC01102	72.71				

FCC01103	65.94				
FCC01104	56.23				
FCC01105	45.20				
FCC01106	57.88				
FCC012BLK	1.58				
FCC013BLK	1.47				
FSC360BLK	1.37				
FSC365BLK	1.59				
FSC365DI	1.12				
FSC36401	37.85				
FSC01001	23.17	3.64	1.1	ND	1.82
FSC01002	38.12	5.42	1.62	ND	3.34
FSC01003	28.84	2.83	1.05	ND	1.16
FSC01003DUP	27.79	2.78	0.77	ND	1.19
FSC01004	40.47	3.51	2.45	ND	1.83
FSC01101	61.59	5.49	4.6	ND	5.75
FSC01102	50.56	3.34	3.03	ND	1.81
FSC01103	61.36	3.87	2.13	ND	1.97
FSC012BLK	3.10				
FSCS360BLK	1.50	2.05	0.22		0.48
FSCS01001	36.91	3.03	1.13	ND	2.96
FSCS01002	41.88	4.25	1.33	ND	2.69
FSCS01003	30.77	3.25	1.26	ND	1.83
FSCS01003DUP	32.74	3.73	1.27	ND	1.77
FSCS01004	17.24				
FSCS01101	89.47	9.22	4.94	3.16	9.83
FSCS01102	66.74	9.28	4.94	2.04	6.32
FSCS01103	57.13	6.16	2.98	ND	3.14
FSCS012BLK	1.88				
FSCL360BLK	1.55	2.18	0.22		
FSCL01001	26.95	3.18	0.87	ND	1.96
FSCL01002	29.30	2.88	0.94	ND	1.15
FSCL01003	26.40	2.61	0.75	ND	0.94
FSCL01003DUP	25.44	2.57	0.88	ND	0.93
FSCL01004	36.73	2.50	2.54	ND	1.42
FSCL01101	62.07	3.32	2.70	ND	3.55
FSCL01102	44.10	1.86	1.03	ND	1.11
FSCL01103	58.12	2.36	2.21	ND	1.55
FSCL012BLK	1.95				

Sample	o-Tolualdehyde	m-Tolualdehyde	p-Tolualdehyde	Hexaldehyde	Glyoxal	Methyl Glyoxal
FSC01001	ND	0.07	0.08	0.17	9.64	9.63
FSC01002	ND	0.14	0.17	0.42	26.65	16.59
FSC01003	ND	0.05	0.08	0.2	5.19	5.87
FSC01003DUP	ND	0.044	0.073	0.2	5.37	6.01
FSC01004	ND	0.1	0.21	0.34	12.33	12.53
FSC01101	ND	0.28	0.45	0.38	28.02	24.6
FSC01102	ND	0.08	0.34	1.18	10.82	8.94

FSC01103	ND	0.09	0.37	1.31	11.29	10
FSCS360BLK						0.18
FSCS01001	0.31	0.11	0.12	0.31	10.11	14.18
FSCS01002	ND	0.10	0.14	0.47	17.36	11.01
FSCS01003	ND	0.07	0.13	0.33	12.19	7.43
FSCS01003DUP	ND	0.06	0.13	0.30	11.56	6.95
FSCS01101	ND	0.39	0.60	3.21	79.19	36.91
FSCS01102		0.24	0.84	3.12	53.15	23.94
FSCS01103	ND	0.12	0.67	2.31	27.25	13.60
FSCL360BLK						0.18
FSCL01001	ND	0.04	0.08	0.12	6.32	9.81
FSCL01002	ND	0.05	0.08	0.22	4.18	6.83
FSCL01003	ND	0.04	0.07	0.15	3.26	4.77
FSCL01003DUP	ND	0.05	0.08	0.16	3.06	4.95
FSCL01004	ND	0.09	0.13	0.28	8.21	11.33
FSCL01101	ND	0.14	0.15	0.21	15.86	19.39
FSCL01102	ND	0.04	0.05	0.06	4.23	4.42
FSCL01103	ND	0.08	0.28	0.19	7.40	9.16

Table C-4. Concentrations of organic acid species. Units in µM.

Sample	Acetate (µM)	Propionate	Formate	Pyruvate	Glutarate
FCC36401	205.45	12.95	61.53	ND	1.82
FCC36402	142.95	9.81	48.72	ND	1.72
FCC36403	161.36	9.98	51.11	0.17	1.53
FCC36404	119.95	8.39	47.87	0.41	2.02
FCC365BLK	4.41	ND	8.11	ND	ND
FCC365DI	5.21	ND	8.47	ND	ND
FCC01001	106.46	5.87	39.24	0.30	1.72
FCC01002	159.03	9.05	51.70	0.40	2.05
FCC01003	84.51	4.95	41.21	0.64	1.22
FCC01004	78.65	5.47	39.92	0.60	1.30
FCC01005	49.86	3.34	27.76	0.37	1.10
FCC01005DUP	48.70	3.13	27.33	0.34	1.37
FCC01006	104.78	7.58	41.78	0.49	1.35
FCC01007	202.10	14.15	90.52	0.78	2.07
FCC01101	356.16	19.09	155.46	0.46	5.79
FCC01102	325.82	18.28	141.84	0.33	6.01
FCC01103	312.89	17.18	122.13	0.57	5.66
FCC01104	164.04	9.65	77.22	1.15	4.48
FCC01105	79.83	5.04	45.67	1.01	2.82
FCC01106	138.79	7.50	70.00	0.34	2.58
FCC012BLK	1.44	ND	1.27	ND	ND
FCC013BLK	0.92	ND	0.63	ND	ND
FSC01001	106.57	5.77	39.76	0.42	0.36
FSC01002	143.13	7.57	56.84	0.57	0.65
FSC01003	77.92	5.14	45.75	0.50	0.21
FSC01003DUP	77.67	5.21	44.30	0.54	0.25
FSC01004	196.38	14.31	100.11	0.38	1.16

FSC01101	310.65	16.67	165.80	1.02	5.57
FSC01102	100.02	5.86	67.75	1.08	2.39
FSC01103	143.26	7.88	85.68	0.47	2.21
FSC012BLK	1.13	ND	1.24	ND	ND
FSCS360BLK	0.83	ND	1.57	ND	ND
FSCS01001	138.64	6.97	62.55	3.29	4.43
FSCS01002	124.94	8.25	66.29	2.99	3.30
FSCS01003	86.58	5.69	53.33	1.71	2.24
FSCS01003DUP	84.60	5.37	50.34	1.84	1.53
FSCS01004	180.13	12.13	84.64	0.27	2.02
FSCS01101	328.20	11.42	247.78	14.41	21.69
FSCS01102	292.92	18.53	184.09	15.13	17.63
FSCS01103	154.03	9.03	102.07	4.59	8.01
FSCS012BLK	1.43	ND	0.99	ND	ND
FSCL360BLK	0.59	ND	0.96	ND	ND
FSCL01001	122.85	1.74	43.66	0.14	0.90
FSCL01002	77.75	4.83	35.96	0.42	0.14
FSCL01003	67.19	4.67	31.78	0.24	ND
FSCL01003DUP	68.45	4.79	33.41	0.28	ND
FSCL01004	12.77	3.36	53.50	0.22	ND
FSCL01101	243.72	10.80	108.90	0.16	2.43
FSCL01102	92.10	5.32	43.96	0.58	1.44
FSCL01103	125.96	6.87	59.16	1.23	ND
FSCL012BLK	4.55	ND	2.99	ND	ND

Sample	Succinate	Malonate	Oxalate	Lactic	Butyric	MSA	Pinic
FCC36401	1.94	0.60	6.95	2.65	2.36	1.81	0.92
FCC36402	1.48	0.46	9.52	1.90	1.82	1.13	1.24
FCC36403	1.87	0.50	10.16	2.57	2.24	0.97	0.76
FCC36404	1.74	0.52	12.38	3.61	1.63	1.18	0.86
FCC365BLK	ND	ND	0.38	0.38			
FCC365DI	ND	ND	ND	0.22			
FCC01001	2.03	0.35	12.03	0.53	1.44	1.08	0.60
FCC01002	1.62	0.34	11.07	1.33	2.51	1.21	0.92
FCC01003	1.09	0.22	10.02	0.87	1.29	1.13	0.33
FCC01004	0.93	0.18	9.23	0.86	1.41	1.06	0.18
FCC01005	0.54	4.01	8.05	0.53	1.08	0.91	ND
FCC01005DUP	0.65	3.76	7.95	0.51	0.94	0.91	ND
FCC01006	1.00	0.16	9.78	2.03	2.60	1.40	0.07
FCC01007	3.09	0.44	14.66	0.54	3.42	0.91	0.91
FCC01101	8.82	6.78	35.40	0.84	3.71	4.54	5.36
FCC01102	8.26	8.13	35.81	0.88	3.27	6.32	4.55
FCC01103	7.13	8.02	37.06	2.16	2.57	4.27	4.55
FCC01104	5.81	0.96	33.00	2.77	1.91	3.97	
FCC01105	3.71	1.63	24.07	5.45	1.05	2.58	1.84
FCC01106	3.23	1.66	20.42	1.19	1.56	2.50	1.09
FCC012BLK	ND	ND	0.42				
FCC013BLK	ND	ND	ND				

FSC01001	2.23	0.72	14.77	1.40	1.61	1.85	2.14
FSC01002	2.16	1.09	10.86	1.56	2.51	1.60	2.10
FSC01003	1.59	0.95	9.97	1.94	1.69	1.60	1.32
FSC01003DUP	1.72	1.03	9.40	1.93	1.71	1.59	1.09
FSC01004	4.10	2.41	17.33	1.62	3.63	2.65	2.09
FSC01101	8.73	10.65	44.31	2.63	3.77	5.99	6.18
FSC01102	4.63	1.56	28.59	3.77	1.50	3.25	3.13
FSC01103	3.78	1.70	23.48	3.30	1.91	3.18	2.38
FSC012BLK	ND	ND	0.97				
FSCS360BLK	ND	ND	1.06	1.69			
FSCS01001	6.66	9.80	73.38	4.23	2.10	3.75	5.19
FSCS01002	5.28	8.12	53.12	4.99	2.32	3.49	5.10
FSCS01003	2.70	0.59	36.50	2.77	1.73	2.76	2.30
FSCS01003DUP	2.74	0.61	35.53	2.76	1.73	2.83	2.16
FSCS01004	5.69	2.50	39.35	2.40	1.09	1.79	0.79
FSCS01101	29.34	31.57	137.38	4.01	5.14	13.48	1.37
FSCS01102	25.54	30.12	127.00	7.32	3.52	12.21	1.63
FSCS01103	13.26	20.07	73.80	6.85	2.14	6.74	1.38
FSCS012BLK	ND	ND	1.49				
FSCL360BLK	ND	ND	1.38	0.52			
FSCL01001	1.52	1.60	10.51	1.12	1.93	1.93	1.36
FSCL01002	ND	1.89	7.78	1.13	1.45	1.38	0.80
FSCL01003	ND	3.72	8.25	1.07	1.69	1.38	0.78
FSCL01003DUP	ND	3.18	8.12	1.08	1.53	1.38	0.83
FSCL01004	3.69	1.75	12.18		3.42	2.02	1.14
FSCL01101	6.27	2.29	19.70		3.13	3.88	4.99
FSCL01102	3.95	ND	14.69	1.36	1.41	1.79	0.60
FSCL01103	2.90	ND	12.75	1.11	1.74	1.84	1.71
FSCL012BLK	ND	ND	1.02				

Table C-5. Concentrations of TOC, DOC, and DON. Units of TOC and DOC are in ppmC, units of DON are in μM of N.

Sample	TOC	DOC	DON
FCC01001	11.80		
FCC01002	16.12		
FCC01003	10.89		
FCC01004	8.87		
FCC01005	6.68		
FCC01005DUP	6.77		
FCC01006	10.79		
FCC01007	14.95		
FCC01101	34.33		
FCC01102	34.94		
FCC01103	31.36		
FCC01104	25.52		
FCC01105	17.05		

FCC01106	18.02		
FCC012BLK	0.47		
FCC013BLK	0.16		
FCC360BLK	0.38		
FCC36401	17.77		
FCC36402	14.38		
FCC36403	15.23		
FCC36404	14.62		
FCC365BLK	0.17		
FCC365DI	ND		
FSC01001	11.16	8.22	128.53
FSC01002	15.38	14.26	160.81
FSC01003	9.42	6.38	106.44
FSC01003DUP	9.21	6.36	155.20
FSC01004	16.36	11.48	100.80
FSC01101	41.04	35.38	191.40
FSC01102	22.47	13.69	408.84
FSC01103	21.99	15.17	370.97
FSC012BLK	0.33		13.59
FSCS360BLK	1.80	1.55	16.27
FSCS01001	32.58	29.23	114.82
FSCS01002	29.53	25.18	48.13
FSCS01003	18.95	15.34	159.21
FSCS01003DUP	19.40		168.28
FSCS01004	20.53		
FSCS01101	83.43		
FSCS01102	69.28	58.57	
FSCS01103	39.71		
FSCS012BLK	0.89		9.89
FSCL360BLK	1.14	0.77	10.16
FSCL01001	12.84	9.33	152.69
FSCL01002	9.68	5.84	125.32
FSCL01003	8.47	4.65	231.32
FSCL01003DUP	7.74	5.10	154.46
FSCL01004	11.76	15.00	191.45
FSCL01101	21.31	20.40	168.48
FSCL01102	11.34	10.10	382.30
FSCL01103	13.95	12.88	217.66
FSCL012BLK	0.83		16.92

Table C-6. Deposition flux calculations. Units of water flux in g $min^{-1}m^{-2}$, units of TOC in µg C $min^{-1}m^{-2}$, and units of ionic species in neq $min^{-1}m^{-2}$.

Sample	Water	Cl^-	NO_2^-	NO_3^-	SO_4^{2-}	Na^+	NH_4^+	K^+	Mg^{2+}	Ca^{2+}	TOC
FD001001	0.30	1.80	19.69	34.32	8.27	1.01	145.18	0.78	1.16	8.53	2.77
FD001002	0.26	2.31	36.95	32.59	8.38	1.72	163.96	1.43	1.11	6.39	3.16
FD001003	0.34	2.78	31.09	41.10	8.96	2.06	174.35	1.49	1.31	5.38	2.42
FD001004	0.28	3.17	24.43	38.04	8.86	1.79	149.22	0.90	1.07	4.62	2.27

FD001005	0.36	2.51	17.85	31.40	7.59	1.26	145.15	0.77	0.89	2.98	2.06
FD001006	0.23	2.90	18.79	35.91	10.51	2.06	132.76	1.14	1.41	5.20	1.54
FD001007	0.17	2.63	16.95	46.78	11.51	2.57	126.60	0.62	1.81	6.49	1.77
FD101001	0.28	1.85	19.34	33.87	8.05	1.01	141.62	0.59	1.18	8.18	2.63
FD101002	0.23	1.86	34.78	30.06	6.47	1.28	152.20	1.27	0.96	5.00	2.67
FD101003	0.33	2.37	33.78	42.36	8.97	1.82	173.45	1.06	1.45	5.46	2.59
FD101004	0.27	3.26	25.69	38.30	8.53	1.80	137.99	0.86	1.14	4.49	2.13
FD101005	0.36	2.23	16.52	29.00	6.95	1.17	144.98	0.82	0.98	3.47	2.00
FD101006	0.22	2.90	18.89	35.18	9.82	2.02	132.16	1.04	1.23	4.96	1.85
FD101007	0.17	2.94	18.89	50.96	12.94	2.79	134.64	0.68	1.86	7.44	1.80
FD001101	0.42	8.88	35.89	156.89	36.32	1.96	408.76	1.54	1.18	8.94	6.87
FD001102	0.19	3.67	17.68	76.46	17.65	0.72	207.65	0.64	0.56	2.38	2.78
FD001103	0.14	2.83	10.71	58.80	14.81	0.50	156.20	1.03	0.38	1.26	2.18
FD001104	0.23	5.63	12.88	81.74	19.37	2.97	223.20	1.58	0.33	0.77	2.65
FD001105	0.21	3.55	9.53	55.72	19.24	0.64	182.40	0.80	0.27	0.73	1.84
FD001106	0.17	2.66	18.54	48.43	14.69	0.68	159.54	0.79	0.69	6.26	1.97
FD101101	0.42	8.76	36.08	154.65	35.32	2.02	407.93	1.19	1.31	9.08	6.40
FD101102	0.19	3.65	17.38	73.65	17.25	0.83	199.44	0.82	0.50	3.10	2.72
FD101103	0.21	4.15	15.36	83.11	20.92	0.88	222.92	1.69	0.61	1.80	3.32
FD101104	0.22	5.55	12.33	77.21	18.65	3.28	210.59	1.77	0.41	1.28	2.51
FD101105	0.21	3.59	9.76	56.47	19.02	0.67	183.10	0.75	0.27	0.93	1.90
FD101106	0.17	2.69	17.79	46.86	15.76	0.65	154.87	0.84	0.62	6.08	2.13

Table C-7. Deposition velocity calculations. Units given in cm s^{-1}.

Sample	Water	Cl^-	NO_2^-	NO_3^-	SO_4^{2-}	Na^+	NH_4^+	K^+	Mg^{2+}	Ca^{2+}	TOC
FD001001	3.36	2.03	4.40	1.34	1.51	0.77	2.33	2.40	4.52	11.08	2.78
FD001002	3.00	2.75	4.21	1.32	1.80	1.40	2.24	4.41	4.35	5.83	2.35
FD001003	8.16	5.03	12.86	4.25	4.12	3.94	6.30	8.03	12.96	13.31	6.19
FD001004	4.97	4.26	7.50	2.92	3.02	2.54	4.00	3.62	7.91	8.48	4.30
FD001005	3.62	1.91	3.10	1.37	1.47	1.01	2.21	1.75	3.70	3.10	2.21
FD001006	2.64	2.48	3.68	1.76	2.28	1.86	2.27	2.90	6.63	6.08	1.86
FD001007	10.62	8.99	15.03	7.51	8.23	5.40	7.45	7.33	18.10	14.48	6.92
FD101001	3.13	2.09	4.32	1.32	1.47	0.77	2.28	1.83	4.61	10.62	2.63
FD101002	2.66	2.21	3.96	1.22	1.39	1.04	2.08	3.93	3.77	4.56	1.98
FD101003	7.87	4.30	13.97	4.38	4.12	3.48	6.27	5.71	14.36	13.50	6.62
FD101004	4.74	4.38	7.89	2.94	2.91	2.56	3.70	3.42	8.42	8.25	4.04
FD101005	3.69	1.70	2.87	1.26	1.34	0.94	2.20	1.87	4.08	3.61	2.14
FD101006	2.50	2.48	3.69	1.72	2.13	1.83	2.26	2.64	5.75	5.80	2.23
FD101007	10.78	10.05	16.76	8.18	9.26	5.87	7.93	8.14	18.62	16.60	7.02
FD001101	5.47	2.04	5.34	1.52	1.84	1.01	2.25	1.75	3.44	5.06	2.21
FD001102	2.89	0.96	2.99	0.84	1.02	0.42	1.30	0.83	1.87	1.53	1.02
FD001103	1.61	0.57	1.39	0.50	0.65	0.23	0.75	1.02	0.96	0.62	0.61
FD001104	3.24	2.31	3.82	1.50	1.40	1.31	1.86	1.90	1.97	1.18	1.67
FD001105	3.62	1.77	3.44	1.25	1.69	0.34	1.85	1.17	1.91	1.36	1.42
FD001106	8.43	4.61	10.49	4.10	4.69	0.75	5.28	3.99	8.40	8.39	4.35
FD101101	5.52	2.01	5.37	1.50	1.79	1.04	2.25	1.36	3.82	5.14	2.06

FD101102	2.83	0.96	2.94	0.81	1.00	0.49	1.25	1.06	1.65	2.00	1.00
FD101103	2.38	0.83	1.99	0.70	0.92	0.40	1.07	1.67	1.55	0.89	0.93
FD101104	3.11	2.28	3.66	1.42	1.35	1.44	1.75	2.12	2.45	1.96	1.59
FD101105	3.69	1.79	3.52	1.26	1.67	0.36	1.85	1.09	1.97	1.72	1.46
FD101106	8.40	4.66	10.07	3.96	5.03	0.71	5.12	4.20	7.56	8.15	4.69